PERFORMANCE ANALYSIS OF DIRECTION-OF-ARRIVAL ESTIMATION ALGORITHMS IN THE PRESENCE OF ARRAY IMPERFECTIONS AND MULTIPATH FOR DIFFERENT ANTENNA ARRAY GEOMETRIES

A THESIS SUBMITTED TO
THE GRADUATE SCHOOL OF NATURAL AND APPLIED SCIENCES
OF
MIDDLE EAST TECHNICAL UNIVERSITY

BY

MUSTAFA ÇALIŞKAN

IN PARTIAL FULFILLMENT OF THE REQUIREMENTS
FOR
THE DEGREE OF MASTER OF SCIENCE
IN
ELECTRICAL AND ELECTRONICS ENGINEERING

AUGUST 2014

Approval of the thesis:

PERFORMANCE ANALYSIS OF DIRECTION-OF-ARRIVAL ESTIMATION ALGORITHMS IN THE PRESENCE OF ARRAY IMPERFECTIONS AND MULTIPATH FOR DIFFERENT ANTENNA ARRAY GEOMETRIES

submitted by **MUSTAFA ÇALIŞKAN** in partial fulfillment of the requirements for the degree of **Master of Science in Electrical and Electronics Engineering Department, Middle East Technical University** by,

Prof. Dr. Canan Özgen
Dean, Graduate School of **Natural and Applied Sciences** _____

Prof. Dr. Gönül Turhan Sayan
Head of Department, **Electrical and Electronics Engineering** _____

Prof. Dr. T. Engin Tuncer
Supervisor, **Electrical and Electronics Engineering Dept., METU** _____

Examining Committee Members:

Prof. Dr. Kemal Leblebicioğlu
Electrical and Electronics Engineering Dept., METU _____

Prof. Dr. T. Engin Tuncer
Electrical and Electronics Engineering Dept., METU _____

Prof. Dr. Buyurman Baykal
Electrical and Electronics Engineering Dept., METU _____

Assoc. Prof. Dr. Çağatay Candan
Electrical and Electronics Engineering Dept., METU _____

M.Sc. Onur Çulha
TÜBİTAK SAGE _____

Date: _____

I hereby declare that all information in this document has been obtained and presented in accordance with academic rules and ethical conduct. I also declare that, as required by these rules and conduct, I have fully cited and referenced all material and results that are not original to this work.

Name, Last Name: MUSTAFA ÇALIŞKAN

Signature :

ABSTRACT

PERFORMANCE ANALYSIS OF DIRECTION-OF-ARRIVAL ESTIMATION ALGORITHMS IN THE PRESENCE OF ARRAY IMPERFECTIONS AND MULTIPATH FOR DIFFERENT ANTENNA ARRAY GEOMETRIES

Çalışkan, Mustafa
M.S., Department of Electrical and Electronics Engineering
Supervisor : Prof. Dr. T. Engin Tuncer

August 2014, 104 pages

Direction of Arrival (DOA) Estimation is an important topic in signal processing. In this thesis, DOA estimation is considered when there are gain/phase mismatches, mutual coupling for the antennas and multipath signals are observed. In the first part, DOA estimation for uniform linear array (ULA) in the presence of mutual coupling is considered. Different methods in the literature are investigated and a promising solution for this case [1] is implemented. Auxiliary sensors are used and MUSIC algorithm is employed for both DOA and mutual coupling coefficient estimation. This method has extensions for two dimensional case and hence the same problem is considered for uniform rectangular (URA) array. The simulation results show that DOA estimation in 2D array can be effectively done in case of mutual coupling. In case of both gain/phase mismatch and mutual coupling, a self-calibration method is implemented where gain/phase mismatch and mutual coupling are estimated iteratively for DOA estimation. Different array geometries are considered for the performance evaluation. The benefit of exploiting prior-knowledge for DOA estimation is considered. In this case, there are some known sources as well as unknown ones. In addition, source signals are correlated. Constrained-MUSIC (C-MUSIC) [2] , Prior-knowledge based DOA estimation (PLEDGE) [3], Prior-Exploiting Orthogonally Weighted Direction Estimator(POWDER) [4], and Forward-backward spatial smoothing and MUSIC (FBSS-MUSIC) [5] algorithms are implemented and compared. The scenario is

also extended to include mutual coupling and multipath.

Keywords: direction-of-arrival estimation, mutual coupling, gain-phase mismatch, multipath, antenna arrays, sensor array signal processing,

ÖZ

GELİŞ-AÇISI KESTİRİM ALGORİTMALARININ FARKLI ANTEN DİZİNİ GEOMETRİLERİ, ÇOKYOLLULUK VE İDEALDEN UZAK ANTEN DİZİLERİ DURUMUNDA PERFORMANS ANALİZİ

Çalışkan, Mustafa
Yüksek Lisans, Elektrik ve Elektronik Mühendisliği Bölümü
Tez Yöneticisi : Prof. Dr. T. Engin Tuncer

Ağustos 2014 , 104 sayfa

Geliş-açısı(GA) kestirimi sinyal işleme alanında önemli bir konudur. Bu tezde, anten dizileri için kazanç/faz uyuşmazlığı ve müşterek bağlaşım varlığında çokyollu sinyal kaynaklarının geliş açısı kestirimi incelenmiştir. Birinci bölümde, müşterek bağlaşım durumunda düzenli doğrusal dizilim (ULA) için geliş açısı kestirimi ele alınmıştır. Literatürdeki farklı yöntemler araştırılmıştır ve bu durum için iyi bir çözüm [1] uygulanmıştır. Geliş açılarının ve müşterek bağlaşım katsayılarının kestirimi için yardımcı sensörler ile MUSIC algoritması çalıştırılmıştır. Bu yöntem iki boyutlu durum için genişletilmiştir ve aynı problem düzenli dikdörtgen dizilimi(URA) için ele alınmıştır. Simülasyon sonuçları müşterek bağlaşım durumunda iki boyutlu dizilim için geliş açısı kestiriminin etkin olarak yapılabildiğini göstermektedir. Kazanç/faz uyumsuzluğu ve müşterek bağlaşım durumunda, geliş açılarının kestirimi için müşterek bağlaşım ve kazanç/faz uyumsuzluğu katsayılarını yinelemeli olarak kestiren bir otomatik kalibrasyon metodu uygulanmıştır. Performans değerlendirmesi için farklı dizi geometrileri ele alınmıştır. Geliş açısı kestiriminde ön bilgi kullanımının yararı incelenmiştir. Bu durumda, bazı bilinen kaynakların yanı sıra bilinmeyen kaynaklar vardır. Bu duruma ek olarak, sinyal kaynakları ilişkilidir. Kısıtlı-MUSIC (Constrained-MUSIC) [2], Ön Bilgi Tabanlı Geliş Açısı Kestirimi (PLEDGE) [3], Ön-Bilgi Tabanlı Dik Ağırlıklı Yön Kestirici(POWDER) [4] ve Ön-arka uzaysal dü-

zeltme MUSIC(FBSS-MUSIC) [5] algoritmaları uygulanarak karşılaştırılmıştır. Senaryo ayrıca çokyolluluk ve müşterek bağlaşım durumu içerecek şekilde genişletilmiştir.

Anahtar Kelimeler: geliş açısı kestirimi, müşterek bağlaşım, kazanç-faz uyuşmazlığı, çokyolluluk, anten dizileri, sensör dizilimi sinyal işleme

To my family

ACKNOWLEDGMENTS

I would like to express my sincere gratitude to my supervisor Prof. Dr. Engin Tuncer for his guidance, advice and insight that he provided throughout this study.

I am grateful to TÜBİTAK SAGE throughout the production of my thesis.

Finally, I want to thank to my family for their support and encouragement to finish my thesis work.

TABLE OF CONTENTS

LIST OF TABLES

TABLES

LIST OF FIGURES

FIGURES

LIST OF ABBREVIATIONS

DOA	Direction-Of-Arrival
AOA	Angle-Of-Arrival
ML	Maximum Likelihood
ULA	Uniform Linear Array
NLA	Nonuniform Linear Array
URA	Uniform Rectangular Array
UHA	Uniform Hexagonal Array
SNR	Signal to Noise Ratio
RMSE	Root Mean Square Error
MCM	Mutual Coupling Matrix
MUSIC	Multiple Signal Classification
ESPRIT	Estimation of Signal Parameter via Rotational Invariance Techniques
MODE	Method of Direction Estimation
PLEDGE	Optimal Prior Knowledge Algorithm
POWDER	Prior Orthogonally Weighted Direction Estimator
FBSS	Forward Backward Spatial Smoothing
C-MUSIC	Constrained-Multiple Signal Classification
SVD	Singular Value Decomposition
MVDR	Minimum Variance Distortionless Response
PDF	Probability Density Function

CHAPTER 1

INTRODUCTION

1.1 Motivation and Previous Works

Direction-of-arrival (DOA) estimation has received considerable amount of interest in the field of wireless communications during the last few decades. There are many commercial and military applications in this field such as cellular communication, radar, sonar, astronomy and seismic explorations. The objective of the DOA estimation methods is to obtain high resolution in the DOA estimates by using the collected data from an antenna array. In practice, the collected data can be distorted due to the factors such as mutual coupling between antennas, gain/phase mismatches due to antenna radiation patterns.

Direction of arrival estimation in the presence of unknown mutual coupling is a challenging topic in array signal processing. Closely spaced antenna array elements unavoidably causes mutual coupling [6]-[7]. Mutual coupling means that current induced on one of the array element produces voltage at the receiver of nearby elements [8]. This serious effect leads to uncertainties in the array response and degrades the performance of the estimators.

High resolution eigendecomposition methods such as multiple signal classification (MUSIC)[9] and estimation of signal parameter via rotational invariance techniques (ESPRIT)[10] assume that the steering vector is exactly known which depends on the array geometry and the signal location. However, in real systems the steering vector may be easily distorted by mutual coupling effect [11]. Therefore, the performance of these high resolution methods will be greatly degraded when we have some dis-

turbances in the arrays manifold [12]-[13]-[14] and the practical applications of these methods are limited [15]. To solve this problem, many calibration algorithms are proposed in [16]-[17]-[18] to mitigate the mutual coupling effect. Two algorithms are presented in [16] which require calibration sources to eliminate mutual coupling effect. Maximum-Likelihood based algorithm in [17] also needs calibration sources at known positions for mutual coupling compensation. Iterative procedure is given in [18] to reduce the coupling effect and gain/phase mismatch. However, computational complexity of the algorithm is high and the algorithm converges slowly. It is described in [19]-[20] that, the negative effect of unknown sensor coupling can be diminished by using auxiliary sensors. The estimation accuracy of ESPRIT method with auxiliary elements is illustrated in [19] in the presence of mutual coupling. Many auxiliary sensors are used in [20] to estimate DOAs in mutual coupling. It is observed in [19]-[20] that, using auxiliary sensors increased the estimation accuracy of the algorithms in the presence of unknown sensor coupling.

In the literature, several methods have been proposed to solve the same problem in two dimensional DOA estimation. As previously stated, subspace based algorithms such as 2-D MUSIC is suboptimal in the presence of mutual coupling [21]-[22]-[23]. One-dimensional DOA estimation methods are expanded in [24]-[25] to solve two-dimensional DOAs. However, these methods are insufficient in the presence of mutual coupling or any other array imperfections. [26] presented a solution to estimate 2-D DOAs for uniform circular array in the presence of mutual coupling. However, the computational complexity of this method for URA is higher than ULA and UCA. So, extra improvements are required for this method.

In [16]-[27], DOA estimation methods in unknown sensor coupling are presented. These algorithms need calibration sources for mutual coupling compensation. In [28], DOA estimation with integer minimization approach in the presence of gain/phase mismatch is presented. However, these algorithms can only be applicable if there is only mutual coupling or gain/phase mismatch presented in the system model. If more than one disruptive effect happen, these algorithms may fail to estimate the DOA angles. By the way, some methods in [17]-[18] have been proposed to estimate DOA angles in the presence of more than one type of error is presented. In [17], maximum-likelihood based calibration algorithm is developed to estimate DOA an-

gles in unknown sensor coupling, sensor gain/phase error and sensor location error. This method also needs extra calibration sources in known positions. In [18], recurrent method is proposed to estimate DOA angles in mutual coupling and gain/phase mismatch. However, the method's computational complexity is high and convergence rate is slow. In [29], a promising solution is presented to handle both mutual coupling and gain/phase errors optimally. In chapter 5, the DOA estimation performance of this method is compared to another popular auto-calibration method proposed in [30] for ULA and NLA to see the performance of the former method in different scenarios.

In practical DOA estimation applications, we may have prior knowledge of signal directions such as in a radar application where the emitted signal is reflected from stationary objects. It is important to use this prior knowledge to estimate the unknown DOA angles as accurately as possible. Several methods have been proposed to use the prior information in an estimation algorithm.

In Constrained-MUSIC method [2]-[31], the noisy array output data is orthogonally projected to the noise subspace spanned by the steering vectors of known DOA angles. The known signal subspace is removed from the array manifold and unknown DOA angles are estimated from reduced-dimension samples.

In [3], optimal prior knowledge algorithm (PLEDGE) algorithm is proposed. PLEDGE is the extension of method of direction estimation (MODE) [32] algorithm which is a Maximum Likelihood based method and estimate the DOA angles with polynomial rooting. The MODE estimator cannot use prior information about known sources and estimates whole elements of AOA vector which contains unknown and known DOA angles, respectively. PLEDGE method, however, uses the prior DOA knowledge information in polynomial rooting approach. Using the a priori information gives good estimation results for PLEDGE algorithm as compared to MODE algorithm shown in [3]-[33].

The correlation state between the unknown and known signals can also be given as prior information in the applications. Using prior knowledge about known source location and correlation state between signal sources is also useful. A new prior knowledge based DOA estimation algorithm expressed as Prior Orthogonally Weighted Direction Estimator(POWDER) is proposed in [4] recently. In this algorithm, it is

assumed that known and unknown DOAs are uncorrelated. There is no assumption made on the correlation state between the signals in the subsets of known and unknown signals. In this context, it is proposed that POWDER method shows good accuracy for resolving closely separated multipath signals.

The objective of this thesis study is to examine the performance of direction of arrival estimation algorithms in the presence of array imperfections and multipath for different array geometries. Four main types of direction of arrival estimation approaches are investigated. In the first part, DOA estimation for ULA in the presence of mutual coupling is analyzed. A solution described in [1] is implemented. Auxiliary sensors are used for both DOA and mutual coupling coefficient estimation. DOA estimates are improved by using estimated mutual coupling coefficients and extended antenna array output. In the second part, the same problem is considered for uniform rectangular (URA) array. 2-D DOA estimation algorithm described in [34] is employed for URA in the presence of unknown sensor coupling. The DOA angles are accurately estimated with mutual coupling coefficient estimates and full URA array output. In the third part, DOA estimation in the presence of gain/phase mismatches and unknown mutual coupling is performed with a self-calibration method described in [29]. The gain-phase mismatches and mutual coupling coefficients are estimated iteratively for DOA estimation. The estimation performance of the algorithm is presented with ULA and NLA. In the fourth part, prior knowledge based DOA estimation algorithms are implemented and compared with classical subspace based methods to show the benefit of using a-priori knowledge in the estimator. Different scenarios are handled for performance evaluation of the algorithms. Mutual coupling and multipath effect are also presented in the simulations.

1.2 Organization of Thesis

The presentation of this thesis is organized into the following chapters.

In Chapter 2, background information about direction of arrival estimation is reviewed.

Chapter 3 describes the problem formulation and solution for DOA estimation in the presence of mutual coupling for uniform linear array. In addition, simulation results of the implementation is presented.

Chapter 4 analyzes 2-D DOA estimation for uniform rectangular array in the presence of unknown sensor coupling. The algorithms steps are explained and the simulation results are provided at the end of chapter.

Chapter 5 explains detailed steps a self-calibration method for DOAs, gain/phase mismatches and mutual coupling coefficients estimation. At the end of the chapter, the simulation results are performed for different scenarios.

Chapter 6 presents performance analysis of prior knowledge based DOA estimation algorithms. The detailed information about the algorithms is expressed. The simulation results are presented for different scenarios at the end of the chapter.

Chapter 7 provides a summary and conclusions of this thesis along with further research.

CHAPTER 2

DOA MODEL AND ESTIMATION METHODS

In this chapter, common DOA estimation methods in the literature and DOA model used in the estimators are briefly explained. More detailed information about the subjects can be found in [21]-[35]-[36].

2.1 DOA Model

Most of the modern DOA estimation methods are model-based and they rely on assumptions on the data obtained from antenna array in the real world. The ideal data model [21] used in the DOA estimation methods will be shortly described in this section. Consider the impinging signal on the m^{th} array element with sample index *n* is shown as $x_m(n)$, for $m = 1, \cdots, M$. The collected *N* sample data in the array output vector can be written as $\mathbf{x(n)} = [x_{\mathbf{1}}(\mathbf{n}), \cdots, x_{\mathbf{M}}(\mathbf{n})]^{\mathbf{T}}, n = \mathbf{1}, \cdots, N$. Then, the ideal array output without additive noise for a single signal source from the DOA θ can be written as,

$$\mathbf{x}(n) = \mathbf{a}(\theta)s(n) \tag{2.1}$$

where $\mathbf{a}(\theta)$ and $s(n)$ are the array manifold vector and the signal vector, respectively. The array manifold vector is defined as

$$\mathbf{a}(\theta) = [e^{jw_c\tau_1(\theta)}, \cdots, e^{jw_c\tau_M(\theta)}]^T \tag{2.2}$$

where w_c is the carrier frequency and $\tau_M(\theta)$ is the time delay of signal from the DOA θ at m^{th} array element. By using the linearity and super-position properties of the

impinging signals, the array output for Q far-field signals can be presented as,

$$\mathbf{x}(n) = \sum_{\mathbf{q=1}}^{\mathbf{Q}} \mathbf{a}(\theta_{\mathbf{q}})\mathbf{s}_{\mathbf{q}}(n) + n(\mathbf{n}) \tag{2.3}$$

where θ_q, $s_q(n)$ and $n(n)$ denote DOAs of sources, signals and additive noises, respectively. The data model in (2.3) can be written as a matrix form by defining array steering matrix $\mathbf{A}(\theta) = [\mathbf{a}(\theta_{\mathbf{1}}), \cdots, \mathbf{a}(\theta_{\mathbf{Q}})]$, where $\theta = [\theta_1, \cdots, \theta_Q]$ is the vector of DOAs and the signal vector $\mathbf{S} = [\mathbf{s_1}(n), \cdots, \mathbf{s_Q}(n)]$. Then, the array output can be written as,

$$\mathbf{x}(\mathbf{n}) = \mathbf{A}(\theta)\mathbf{s}(n) + \mathbf{n}(n), n = \mathbf{1}, \cdots, N \tag{2.4}$$

or, equivalently,

$$\mathbf{X} = [\mathbf{x}(\mathbf{1}), \cdots, \mathbf{x}(N)] = \mathbf{A}(\theta)\mathbf{S} + \mathbf{N} \tag{2.5}$$

The DOA estimation algorithms use the second-order statistics of the collected data from array output. The array output covariance matrix is written as

$$\mathbf{R} = \mathbf{A}(\theta)\mathbf{P}\mathbf{A}^{\mathbf{H}}(\theta) + \sigma^{\mathbf{2}}\mathbf{I} \tag{2.6}$$

where the signals are stationary and zero-mean random process uncorrelated with the noise. $\mathbf{P} = E[\mathbf{s}(n)\mathbf{s}^{\mathbf{H}}(n)]$ denotes the signal covariance matrix. It is also assumed that the noise is both spatially and temporally white with variance σ^2. The sample covariance matrix is constructed by the collected data from the array output to estimate the array covariance matrix as,

$$\hat{\mathbf{R}}_{\mathbf{x}} = \frac{1}{N}\sum_{n=1}^{N} \mathbf{x}(n)\mathbf{x}^H(n) = \frac{1}{N}\mathbf{X}\mathbf{X}^{\mathbf{H}}. \tag{2.7}$$

Hence, The DOA estimation can be summarized as given an array output data $\mathbf{X}$ formulated in 2.5, estimate the DOA angles θ with using the array manifold and signal correlation matrix defined in 2.7 in the estimator.

The following topics are assumed for the narrowband DOA estimation algorithms [37].

- *Homogeneous Transmission Media*: The transmission media is considered to be homogeneous and linear. The signal waveforms show the same characteristics for all DOA angles and the signals can be linearly added by using linearity and superposition principles.
- *Far-field assumption*: The sensor array is positioned in the far-field zone of the signal sources. The array elements receive equal power signal waveforms with the same DOA angles incoming from different sources.
- *Narrow-band assumption*: In the narrow-band signal model, it is considered that time-bandwidth production is small $(B\tau \ll 1)$, where B denotes bandwidth of signal and τ is time that the signal waveform propagates the antenna array. The array elements are assumed to capture the signals at the same time.
- *Noise assumption*: The sensor noises are zero-mean, i.i.d, white Gaussian processes with common variance σ^2, and uncorrelated with the signals.

2.2 Review of DOA Estimation Algorithms

In this section, a brief review of the classical direction-of-arrival estimation techniques such as beamforming, maximum likelihood based DOA estimation and subspace-based DOA estimation is presented.

2.2.1 Beamforming Techniques

Beamforming is defined as the antenna array is steered in one direction at a time and the output power is measured [36]. The maximum output power will be monitored, if the DOA angle is captured in the direction of the antenna array. DOA estimation algorithms are proposed to construct the appropriate form of output power to estimate the DOA angles. Capon's Beamformer and Linear Prediction are two common beamforming methods which will be summarized in the following sections.

2.2.1.1 Capon's Beamformer

Capon's Beamformer is a DOA estimation method which is developed to enhance the performance of the classical beamformers when multiple narrowband signal sources impinging on the array from different DOAs. This beamforming technique finds the maximum-likelihood estimate of power which is incoming from signal of interest and the other signal sources are assumed to be interference. The objective of this method is to estimate the signal of interest with good accuracy in terms of phase and amplitude. The estimation performance of Capon's Beamformer depends on the number of array elements and the SNR. When the signal sources are highly correlated, this method is suboptimal. The advantage of Capon's Beamformer is that this method provides nonparametric solution and there is no need for a prior knowledge about the specific statistical properties [38].

2.2.1.2 Linear Prediction

The prediction error between the output of m^{th} sensor and real output is minimized in Linear Prediction method [38]. The purpose of this DOA estimation technique is to find the weights to minimize the prediction error. Choosing the m^{th} array element output for prediction is random. The choice for prediction may degrade the accuracy of the estimation. If we choose the central array element for prediction, superposition of the other array elements can offer better estimation performance because the other array elements are positioned from the phase center of array. Thus, the performance of the Linear Prediction method relies on the chosen array element and the weights which minimize the prediction error. Linear prediction method shows good results when SNR is low or number of snapshots is limited.

2.2.2 Maximum Likelihood Method

The log-likelihood function is maximized to estimate the DOA angles in Maximum Likelihood method. The joint PDF of the sampled data given DOA angles is named as log-likelihood function. The true DOA angles parameterize the log-likelihood function and this method searches the directions which maximize the log of the likelihood

function. Maximum Likelihood method shows good estimation accuracy at low SNR and small snapshots of data or the signal sources are highly correlated or coherent [39].

2.2.3 Subspace-Based Methods

Subspace based algorithms depend on the eigenstructure of antenna array output correlation matrix. The orthogonal signal and noise subspaces are constructed by the eigenvectors of the estimated correlation matrix. The signal subspace is spanned by the steering vectors and the noise subspace is spanned by the eigenvectors corresponding to the remaining smaller eigenvalues of sample correlation matrix. MUSIC(Multiple Signal Classification) and ESPRIT(Estimation of Signal Parameters via Rotational Invariance Techniques) are the most common subspace-based algorithms. Brief information about these algorithms will be given in the upcoming sections [36].

2.2.3.1 MUSIC Method

Multiple Signal Classification (MUSIC) is an eigenstructure based high resolution direction of arrival estimation method. MUSIC method estimates DOA of signal sources, number of signals and the strength of the signals. In this method, the signal sources and additive noise are assumed to be uncorrelated. The DOA angles are estimated by using the orthogonality between the array steering vectors and the noise subspace eigenvectors of the array output correlation matrix. Hence, placing the Frobenius norm of this orthogonality in the denominator results in sharp peaks at the direction of arrival angles. If the source signals are highly correlated or coherent, MUSIC method becomes suboptimal [38].

2.2.3.2 ESPRIT Method

ESPRIT(Estimation of Signal Parameter via Rotational Invariance Techniques) method is the another subspace based, high resolution direction of arrival estimation method. In this method, two identical subarrays are formed by the same number of array el-

ements. The matched pair of the sensors with the same separation interval is named as doublet. The objective of ESPRIT method is to exploit the rotational invariance in the signal subspace which is composed of two arrays with a translational invariance model. ESPRIT method is implemented in three steps for DOA estimation. Firstly, a basis matrix is computed for the estimated signal subspace. Then, the solution of an invariance equation is computed from the basis matrix. Finally, the DOA angles are estimated by the eigenvalues of the solution of the invariance equation. This method is also extended for two dimensional DOA estimation with different antenna array geometries whose geometry is shift invariant [36].

CHAPTER 3

DIRECTION OF ARRIVAL ESTIMATION WITH UNIFORM LINEAR ARRAY IN THE PRESENCE OF UNKNOWN SENSOR COUPLING

In this chapter, DOA estimation for ULA in the presence of mutual coupling is examined. To eliminate the mutual coupling effect, the algorithm proposed in [1] is implemented. Firstly, MUSIC algorithm is directly applied for DOA estimation by using sufficient number of auxiliary sensors in the presence of unknown mutual coupling. Then, mutual coupling coefficients are estimated with the DOA estimates found in the first step. With the estimated mutual coupling coefficients, the entire antenna array output vector is used to improve the DOA estimation. The simulation results show that the DOA estimation accuracy is increased with the estimated mutual coupling coefficients. The problem formulation and the performance analysis of the algorithm in [1] are shown in the following sections. The algorithm [1] which is implemented in this section is also extended for planar arrays such as URA and UHA for two-dimensional DOA estimation presented in [34] and [40], respectively.

3.1 Problem Statement

Consider a uniform linear array composed of N sensors with half wavelength,$(\lambda/2)$, inter element spacing. We assume that there are M narrow-band signals impinging on the array from directions $\theta_1, \theta_2, ..., \theta_M$ respectively. The antennas are assumed to be identical and omnidirectional. Far-field assumption is made. The array output can be

written as,

$$\mathbf{x}(k) = \mathbf{CAs}(k) + \mathbf{n}(k) \tag{3.1}$$

where **s**(k) is a $\mathrm{M} \times 1$ signal vector which represents a stationary, zero-mean random process uncorrelated with the noise. It is assumed that the noise **n**(k), is both spatially and temporally white with variance σ^2. $\mathbf{A} = [\mathbf{a}(\theta_\mathbf{1}), \mathbf{a}(\theta_\mathbf{2}), ..., \mathbf{a}(\theta_\mathbf{M})]$ is the steering matrix for ULA and the steering vector is given as $\mathbf{a}(\theta_i) = [1, \beta(\theta_i), ..., \beta^{N-1}(\theta_i)]^T$ with $\beta(\theta_i) = \exp\{j\frac{2\pi d}{\lambda}\sin\theta_i\}$. $\mathbf{C}$ denotes the $\mathrm{N} \times \mathrm{N}$ banded symmetric Toeplitz mutual coupling matrix(MCM) for the antenna array. It is assumed that the main diagonal of the MCM is normalized to unity and coupling coefficient vector which is used to construct $\mathbf{C}$ is $\mathbf{c} = [1, c_1, \ldots, c_{P-1}]$ where *P* is the number of significant mutual coupling coefficients. The mutual coupling matrix in (3.1) can be written as a banded Toeplitz matrix for ULA,i.e.,

$$\mathbf{C} = \begin{bmatrix} 1 & c_1 & \cdots & c_{P-1} & \cdots & 0 \\ c_1 & 1 & c_1 & \cdots & \ddots & 0 \\ \vdots & c_1 & 1 & \ddots & \cdots & c_{P-1} \\ c_{P-1} & \cdots & \ddots & \ddots & c_1 & \vdots \\ 0 & \ddots & \cdots & c_1 & 1 & c_1 \\ 0 & \cdots & c_{P-1} & \cdots & c_1 & 1 \end{bmatrix} \tag{3.2}$$

The array output covariance matrix $\mathbf{R_x}$ is

$$\mathbf{R_x} = E\left\{\mathbf{x}(t)\mathbf{x}^H(t)\right\} = \mathbf{CAR_sA}^H\mathbf{C}^H + \sigma^2\mathbf{I}_N \tag{3.3}$$

where $\mathbf{R_s}$ is the source correlation matrix, and $\mathbf{I_N}$ is the identity matrix. Following the standard subspace approach we can partition the eigenvectors of array output covariance matrix as $\mathbf{E_s}$ and $\mathbf{E_n}$ which span signal and noise subspace respectively. The manifold matrix becomes $\mathbf{Ca}(\theta)$ in case of known mutual coupling. The manifold matrix is orthogonal to the noise subspace spanned by $\mathbf{E_n}$. Hence,

$$\left\|\mathbf{E}_\mathbf{n}^H\mathbf{Ca}(\theta_i)\right\| = 0 \quad \text{for} \quad i = 1, \cdots, M. \tag{3.4}$$

Therefore, MUSIC algorithm can be directly applied as $P_{\mathrm{MU}}(\theta) = 1/\left\|\mathbf{E}_\mathbf{n}^H\mathbf{Ca}(\theta)\right\|^2$ in known mutual coupling case. When the mutual coupling coefficients are not known, we can not estimate the DOA angles by using this method. In unknown mutual coupling case, auxiliary sensors will be used to estimate the true DOA angles.

3.1.1 Direction Finding in Unknown Mutual Coupling

To reduce the mutual coupling effect, *P*-1 auxiliary array elements are added on both sides of the N element ULA. N element middle array output of $(N+2P-2)$-element ULA can be written as,

$$\mathbf{x}(k) = \tilde{\mathbf{C}}\tilde{\mathbf{A}}\mathbf{s}(k) + \mathbf{n}(k) \tag{3.5}$$

where $\tilde{\mathbf{A}} = [\tilde{\mathbf{a}}(\theta_1), \tilde{\mathbf{a}}(\theta_2), ..., \tilde{\mathbf{a}}(\theta_M)]$

$$\tilde{\mathbf{a}}(\theta_i) = [\beta(\theta_i)^{1-P}, \beta(\theta_i)^{2-P}, ..., \beta(\theta_i)^{-1}, 1, \beta(\theta_i), ..., \beta(\theta_i)^{N-1}, \beta(\theta_i)^{N}, ..., \beta(\theta_i)^{N+P-2}]^T$$

$\mathrm{N} \times (\mathrm{N} + 2P - 2)$ mutual coupling matrix in (3.5) can be written as in (3.6).

$$\tilde{\mathbf{C}} = \begin{bmatrix} c_{P-1} & \cdots & c_1 & 1 & c_1 & \cdots & c_{P-1} & 0 & 0 & \cdots & 0 \\ 0 & c_{P-1} & \cdots & c_1 & 1 & c_1 & \cdots & c_{P-1} & 0 & \cdots & 0 \\ \vdots & \ddots & \ddots & \cdots & \ddots & \ddots & \ddots & \cdots & \ddots & \ddots & \vdots \\ 0 & \cdots & 0 & c_{P-1} & \cdots & c_1 & 1 & c_1 & \cdots & c_{P-1} & 0 \\ 0 & \cdots & 0 & 0 & c_{P-1} & \cdots & c_1 & 1 & c_1 & \cdots & c_{P-1} \end{bmatrix} \tag{3.6}$$

The covariance matrix of the array output with auxiliary sensors is

$$\tilde{\mathbf{R}}_{\mathbf{x}} = E\left\{\mathbf{x}(t)\mathbf{x}^H(t)\right\} = \tilde{\mathbf{C}}\tilde{\mathbf{A}}\mathbf{R}_{\mathbf{s}}\tilde{\mathbf{A}}^H\tilde{\mathbf{C}}^H + \sigma^2\mathbf{I}_N. \tag{3.7}$$

According to the subspace theory we can find $\tilde{\mathbf{E}}_{\mathbf{s}}$ and $\tilde{\mathbf{E}}_{\mathbf{n}}$, the eigenvectors which span the signal and noise subspace of $\tilde{\mathbf{R}}_{\mathbf{x}}$, respectively. Adding *P*-1 auxiliary sensors on both side of the ULA, the MUSIC method is applicable in unknown sensor coupling which will be shown in the following. The steering vector of middle ULA, $\tilde{\mathbf{C}}\tilde{\mathbf{a}}$, can be expressed in terms of the manifold vector of *N*-element ULA, $c(\theta)\mathbf{a}(\theta)$, as in [1].

$$\begin{aligned} \tilde{\mathbf{C}}\tilde{\mathbf{a}}(\theta) &= (c_{p-1}\beta(\theta)^{1-P} + \cdots + 1 + c_1\beta(\theta) + \cdots + c_{P-1}\beta(\theta)^{P-1}) \begin{bmatrix} 1 \\ \beta(\theta) \\ \vdots \\ \beta(\theta)^{N-1} \end{bmatrix} \\ &= (2\sum_{n=1}^{P-1} c_n \cos(2n\pi \sin(\theta)d/\lambda) + 1)\mathbf{a}(\theta) \\ &= c(\theta)\mathbf{a}(\theta) \end{aligned} \tag{3.8}$$

where $c(\theta)$ indicates the mutual coupling which is scalar and different from zero. Then, the DOA angles can be estimated directly by using the orthogonality between $\tilde{\mathbf{E}}_{\mathbf{n}}^{H}$ and $\mathbf{a}(\theta)$ [1] as,

$$\tilde{\mathbf{E}}_{\mathbf{n}}^{H}\tilde{\mathbf{C}}\tilde{\mathbf{a}}(\theta)=0 \;\Rightarrow\; \mathrm{c}(\theta)\tilde{\mathbf{E}}_{\mathbf{n}}^{H}\mathbf{a}(\theta)=0 \Rightarrow \tilde{\mathbf{E}}_{\mathbf{n}}^{H}\mathbf{a}(\theta)=0, \quad \theta=\theta_i,\; i=1,\cdots,M \tag{3.9}$$

where *M* is the number of DOAs. Finally, by using the smaller noise subspace matrix of extended ULA and the real steering vector of *N*-element ULA, we can estimate the DOA angles with MUSIC algorithm,

$$P_{\mathrm{MUSIC}}(\theta)=\frac{1}{\left\|\tilde{\mathbf{E}}_{\mathbf{n}}^{H}\mathbf{a}(\theta)\right\|^{2}}. \tag{3.10}$$

3.1.2 Mutual Coupling Coefficient Estimation

The mutual coupling coefficients are estimated by using array output of all sensors(including auxiliary sensors) and the DOA angle estimates of MUSIC algorithm in(3.10). The covariance matrix of the array output(including auxiliary elements) is shown as $\overline{\mathbf{R}}_x$. The eigenvectors of covariance matrix are $\mathbf{e}_1, \mathbf{e}_2, ..., \mathbf{e}_{N+2P-2}$ and noise space eigenvectors are $\mathbf{e}_{M+1}, \mathbf{e}_{M+2}, ..., \mathbf{e}_{N+2P-2}$. As the mutual coupling matrix of full array $\overline{\mathbf{C}}$ is a band-symmetric Toeplitz matrix, the steering vector can be rewritten as [41],

$$\overline{\mathbf{C}}\tilde{\mathbf{a}}(\theta)=\mathbf{T}\left[\tilde{\mathbf{a}}(\theta)\right]\mathbf{c} \tag{3.11}$$

where $(N+2P-2)\times(N+2P-2)$ $\overline{\mathbf{C}}$ is the mutual coupling matrix of extended ULA shown in (3.12).

$$\overline{\mathbf{C}}=\begin{bmatrix} 1 & c_1 & \cdots & c_{P-1} & \cdots & 0 \\ c_1 & 1 & c_1 & \cdots & \ddots & 0 \\ \vdots & c_1 & 1 & \ddots & \cdots & c_{P-1} \\ c_{P-1} & \cdots & \ddots & \ddots & c_1 & \vdots \\ 0 & \ddots & \cdots & c_1 & 1 & c_1 \\ 0 & \cdots & c_{P-1} & \cdots & c_1 & 1 \end{bmatrix} \tag{3.12}$$

$P\times 1$ vector $\mathbf{c}$ is composed of the nonzero entries of first column of $\mathbf{C}$ and is given by (3.13).

$$\mathrm{c}_i=\mathrm{C}_{i1}, i=1,\cdots,P. \tag{3.13}$$

The $(N+2P-2)\times P$ matrix $\mathbf{T}[\tilde{\mathbf{a}}(\theta)]$ can be expressed as the sum of the following two $(N+2P-2)\times P$ matrices $\mathbf{T}_1[\tilde{\mathbf{a}}(\theta)]$ and $\mathbf{T}_2[\tilde{\mathbf{a}}(\theta)]$ as

$$\mathbf{T}[\tilde{\mathbf{a}}(\theta)] = \mathbf{T}_1[\tilde{\mathbf{a}}(\theta)] + \mathbf{T}_2[\tilde{\mathbf{a}}(\theta)] \tag{3.14}$$

$$\mathbf{T}_1[\tilde{\mathbf{a}}(\theta)]_{i,j} = \begin{cases} [\tilde{\mathbf{a}}(\theta)]_{i+j-1} & i+j \le N+2P-1 \\ 0 & otherwise. \end{cases} \tag{3.15}$$

$$\mathbf{T}_2[\tilde{\mathbf{a}}(\theta)]_{i,j} = \begin{cases} [\tilde{\mathbf{a}}(\theta)]_{i-j+1} & i \ge j \ge 2 \\ 0 & otherwise. \end{cases} \tag{3.16}$$

$(N+2P-2)\times P$ matrix $\mathbf{T}[\tilde{\mathbf{a}}(\theta)]$ is orthogonal to the noise subspace of full array output covariance matrix, i.e,

$$e_i^H \mathbf{T}\left[\tilde{\mathbf{a}}(\theta_j)\right]\mathbf{c}=0, \quad i=M+1,\cdots,N+2P-2,\ j=1,\cdots,M. \tag{3.17}$$

Substituting the DOA angle estimates found in (3.10) into (3.17), we define a $\mathbf{Q}$ matrix as follows

$$\mathbf{Q} = \begin{bmatrix} \overline{\mathbf{E}}_{\mathbf{n}}^H \mathbf{T}\left[\tilde{\mathbf{a}}(\theta_1)\right] \\ \vdots \\ \overline{\mathbf{E}}_{\mathbf{n}}^H \mathbf{T}\left[\tilde{\mathbf{a}}(\theta_M)\right] \end{bmatrix} = [\mathbf{q_1}\ \mathbf{q_2}\ \cdots, \mathbf{q_P}] \tag{3.18}$$

Then we have,

$$\mathbf{Qc} = 0. \tag{3.19}$$

Given $\mathbf{c}(1) = 1$, (3.19) can be rewritten as

$$\mathbf{Q}(:, 2:P)\mathbf{c}(2:P) = -\mathbf{q}_1 \tag{3.20}$$

where $\mathbf{c}(:, 2:P) = [c_1 c_2 \cdots c_{P-1}]^T$, $\mathbf{Q}(:, 2:P) = [\mathbf{q}_2 \cdots \mathbf{q}_P]$. We can finally apply the least squares method to find the mutual coupling coefficients in (3.21).

$$\mathbf{c}(2:P) = -\mathbf{Q}(:, 2:P)^{\dagger}\mathbf{q}_1, \quad \mathbf{c}(1) = 1. \tag{3.21}$$

In equation (3.21), $(.)^{\dagger}$ denotes pseudo-inversion. After determining coupling coefficient vector $\mathbf{c}$, we can refine DOA estimation by using estimated mutual coupling matrix $\hat{\overline{\mathbf{C}}}$ and the noise subspace matrix $\hat{\overline{\mathbf{E}}}_{\mathbf{n}}$ of full array to improve the precision of estimation.

$$P_{MU}(\theta) = \frac{1}{\left\| \overline{\mathbf{E}}_{\mathbf{n}}^H \overline{\mathbf{C}} \tilde{\mathbf{a}}(\theta) \right\|^2} \tag{3.22}$$

3.1.3 The Summary of the Algorithm

The implementation of the applied algorithm [1] for an $N + 2P - 2$ element ULA array can be summarized as follows:

1. Compute data covariance matrix of full array with auxiliary sensors and the covariance matrix of middle N-element sub-array.

$$\hat{\overline{\mathbf{R}}}_{\mathbf{x}} = \frac{1}{K}\sum_{i=1}^{K}\overline{\mathbf{x}}(i)\overline{\mathbf{x}}^{H}(i) \tag{3.23}$$

where $\overline{\mathbf{x}}(i) = [x_1(i), x_2(i), \cdots, x_{N+2P-2(i)}]^T$. The covariance matrix of middle sub-array can be found as

$$\hat{\tilde{\mathbf{R}}}_{\mathbf{x}} = \hat{\overline{\mathbf{R}}}_{\mathbf{x}}(\text{P:N+P-1,P:N+P-1}) \tag{3.24}$$

2. Get the noise subspace eigenvectors $\hat{\overline{\mathbf{E}}}_{\mathbf{n}}$ and $\hat{\tilde{\mathbf{E}}}_{\mathbf{n}}$ of full array and middle sub-array respectively.

3. Estimate the DOA angles with MUSIC algorithm using the smaller noise subspace matrix $\hat{\tilde{\mathbf{E}}}_{\mathbf{n}}$.

$$P_{\text{MU}}(\theta) = \frac{1}{\left\|\hat{\tilde{\mathbf{E}}}_{\mathbf{n}}^{\mathbf{H}}\mathbf{a}(\theta)\right\|^2}; \tag{3.25}$$

4. Estimate the mutual coupling matrix $\hat{\overline{\mathbf{C}}}$ by solving equation (3.21) with estimated DOA angles found in step-3.

5. Using estimated mutual coupling matrix $\hat{\overline{\mathbf{C}}}$ and full array output noise subspace matrix $\hat{\overline{\mathbf{E}}}_{\mathbf{n}}$, improve the DOA angle estimates with (3.26).

$$P_{MU}(\theta) = \frac{1}{\left\|\hat{\overline{\mathbf{E}}}_{\mathbf{n}}^{H}\hat{\overline{\mathbf{C}}}\tilde{\mathbf{a}}(\theta)\right\|^2} \tag{3.26}$$

3.2 Simulation Results

In this part of the study, the simulation results are shown to illustrate the performance of applied algorithm [1]. We use 10 element ULA as the base array for the simulations. The distance between adjacent elements in the ULA is half a wavelength, i.e.,

$\lambda/2$. The number of mutual coupling coefficients is three. Therefore, two auxiliary sensors are added on each side of the array to form a new ULA with the same array configuration of base array. The sources are generated as equal power and they are uncorrelated with each other. Source signals are Gaussian process and noise is both spatially and temporally white with variance σ^2. Then, the input SNR of *i*th signal can be shown as $10\log_{10}(\sigma_i^2/\sigma^2)$. In simulations, source angles are considered between -90 and 90 degrees and the spectrum search step size is 0.1°. The mutual coupling vector is assumed to be $\mathbf{c} = [1, 0.43301 - 0.25i, 0.14142 - 0.14142i]^T$. The number of snapshots is selected as 100. In the first simulation, the estimation resolution and accuracy of the method is presented. We consider two independent signals, M=2 arrive at the array from $\theta_1 = 15^\circ$ and $\theta_2 = \theta_1 + \Delta\theta$. There are 100 Monte Carlo trials, L=100 for each experiment. The RMSE for DOA angle estimation is defined as $RMSE_\theta = \sqrt{\frac{1}{ML}\sum_{l=1}^{L}\sum_{i=1}^{M}\left(\hat{\theta}_{il} - \theta_i\right)^2}$, where $\hat{\theta}_{il}$ is the estimation of θ_i in the *l*th experiment. The RMSE versus the angle separation is shown in Figure 3.1. The applied method is compared with algorithm in [41] and MUSIC algorithm in different array and coupling conditions. From Figure 3.1 to Figure 3.6, the applied method is shown as line with circle. The algorithm in [41] is shown as line with triangle. The simulation results of MUSIC algorithm is shown as line with star, square and cross in different conditions. As it is seen from Figure 3.1, by using auxiliary sensors in unknown mutual coupling , the estimation accuracy of applied method is nearly equal to the algorithm [41] with known coupling. The performance of the applied method is also nearly same with MUSIC algorithm in no coupling case as angle interval increases from 8° to 15°.

Figure 3.2 shows the DOA estimation performance for different SNR levels. There are three distinct sources (M=3) arrive at the array from $\theta_1 = -30^\circ$, $\theta_2 = 15^\circ$ and $\theta_3 = 45^\circ$. The DOA angles are estimated with auxiliary sensors in unknown mutual coupling. It is seen that applying MUSIC algorithm with extended ULA, the results are nearly same with the 10 sensor array with no mutual coupling for high SNR.

Figure 3.3 shows the DOA estimation performance in the same scenario in terms of the number of snapshots. The number of snapshots increased from 50 to 1000 at SNR =0dB. As the number of snapshots is increased the performance of MUSIC algorithm with auxiliary sensors improves and approaches to the results in [41] with known

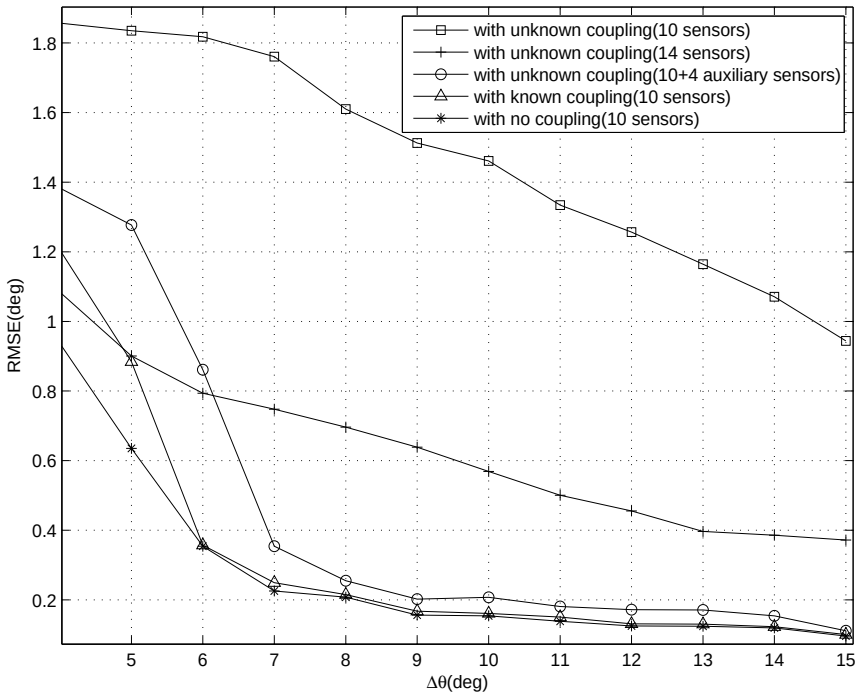

Figure 3.1: Performance of the algorithms for the angle interval when two sources are located at 15 and $15 + \Delta\theta$, snapshots = 100 and SNR = 0dB

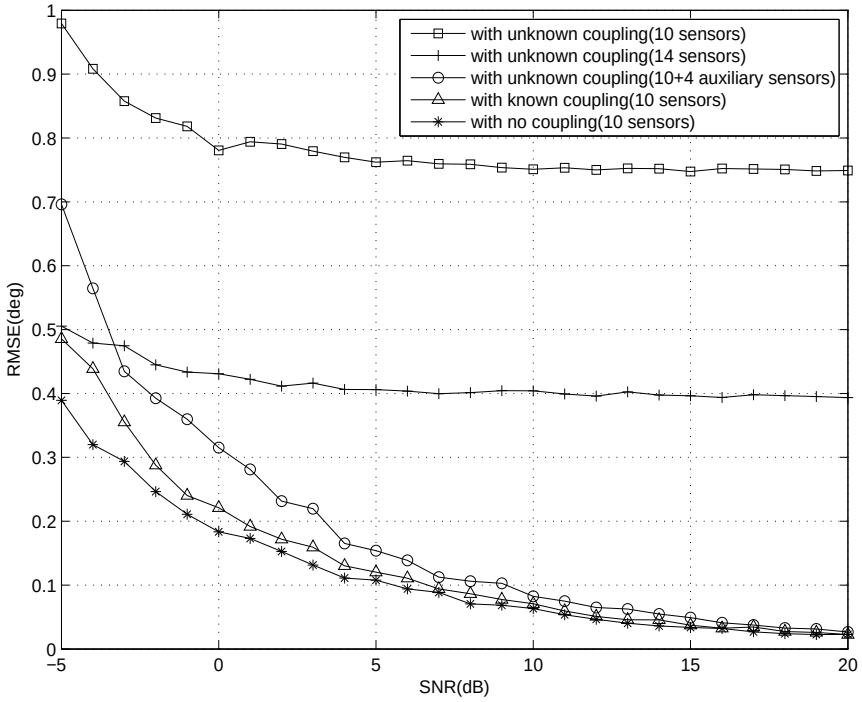

Figure 3.2: Performance for three sources located at -30, 15 and 45 degrees with respect to increasing SNR, snapshots = 100

coupling and the MUSIC algorithm without mutual coupling.

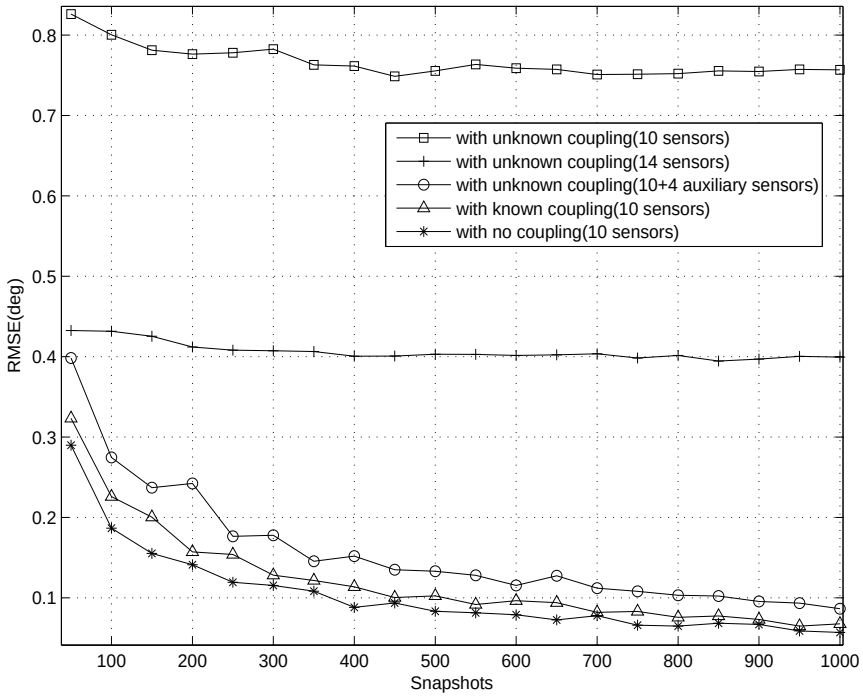

Figure 3.3: Performance for three sources located at -30, 15 and 45 degrees with respect to increasing snapshots, SNR = 0dB

In Figure 3.4, algorithms are compared when the array elements change from 8 to 32. As the array elements increase, the RMSE of applied algorithm with auxiliary sensors becomes nearly equal with the method in [41] with known coupling and MUSIC algorithm without mutual coupling.

Next, we illustrate the DOA estimation performance of applied algorithm for correlated sources with different SNR levels and number of snapshots. There are three correlated signals where $\theta_1 = -30^\circ$, $\theta_2 = 15^\circ$ and $\theta_3 = 45^\circ$. The positive semi-definite correlation matrix of the far-field source signals defined in [1] can be written as,

$$\mathbf{R_s} = \begin{bmatrix} 1 & 0.3\exp(-0.3j\pi) & 0.3\exp(-0.3j\pi) \\ 0.3\exp(0.3j\pi) & 1 & 0.3\exp(0.3j\pi) \\ 0.3\exp(0.3j\pi) & 0.3\exp(-0.3j\pi) & 1 \end{bmatrix}.$$

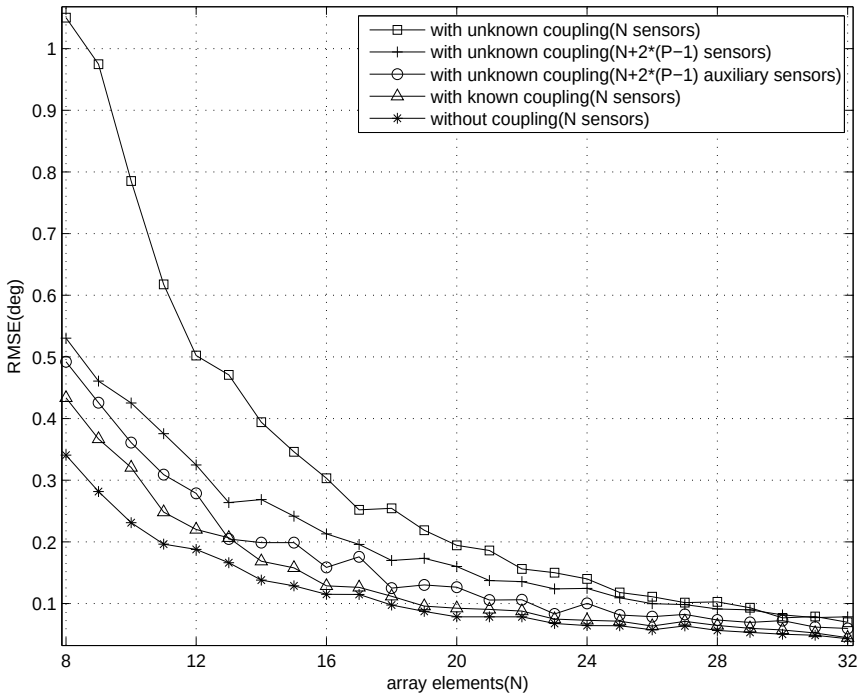

Figure 3.4: Performance for three sources located at -30, 15 and 45 degrees with respect to increasing array elements, snapshots = 100, SNR = 0dB

Figure 3.5 and Figure 3.6 show the performance results for correlated signals. It is seen that, the applied method with auxiliary sensors shows good estimation accuracy in the presence of independent or correlated sources for the given scenario.

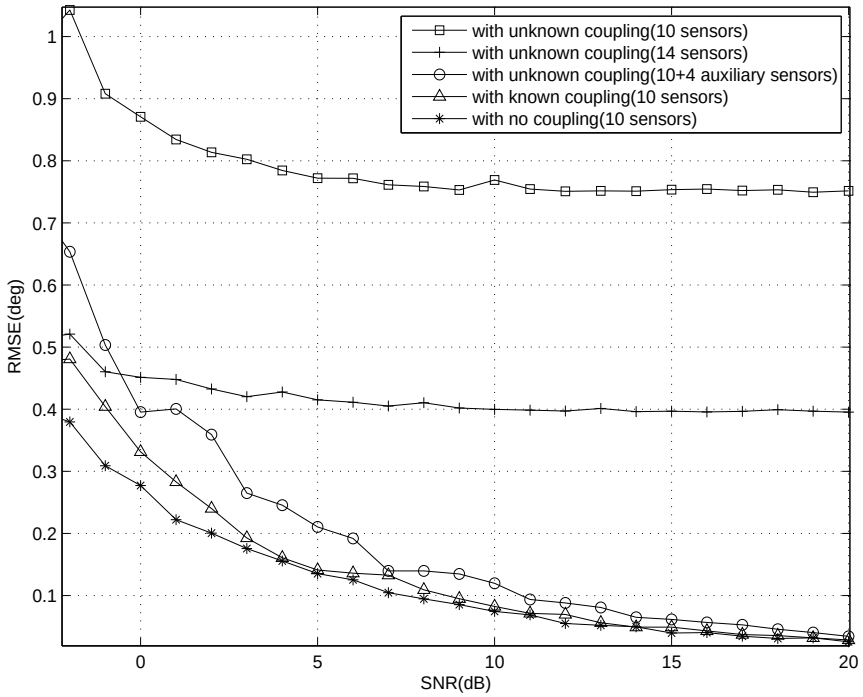

Figure 3.5: Performance for three correlated sources located at -30, 15 and 45 degrees with respect to increasing SNR, snapshots = 100

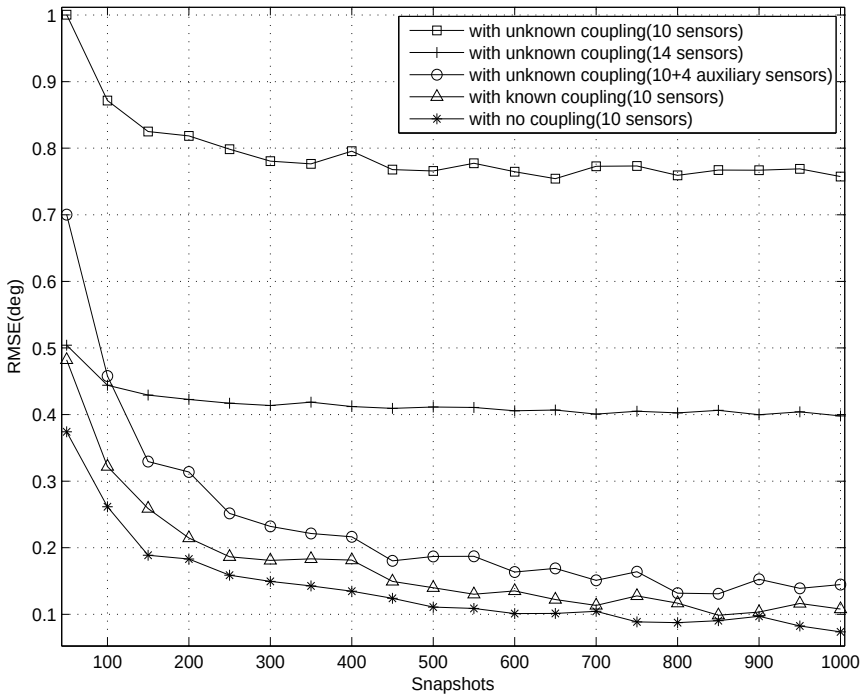

Figure 3.6: Performance for three correlated sources located at -30, 15 and 45 degrees with respect to increasing snapshots, SNR = 0dB

In Figure 3.7 and 3.8, RMSE results of mutual coupling coefficient estimation is illustrated for increasing SNR levels and snapshots respectively. DOA angle estimates are used for coupling coefficient estimation as stated previously in section 3.1.2. The RMSE for coupling estimation is defined as $\sqrt{\frac{1}{L(P-1)}\sum_{l=1}^{L}\sum_{i=1}^{P-1}\left(\hat{c}_{pl}-c_p\right)^2}$, where $\hat{c}_{pl}$ is the estimation of c_p in the lth Monte Carlo trial. It is seen that coupling coefficient estimation performance increases with increasing SNR levels and snapshot values.

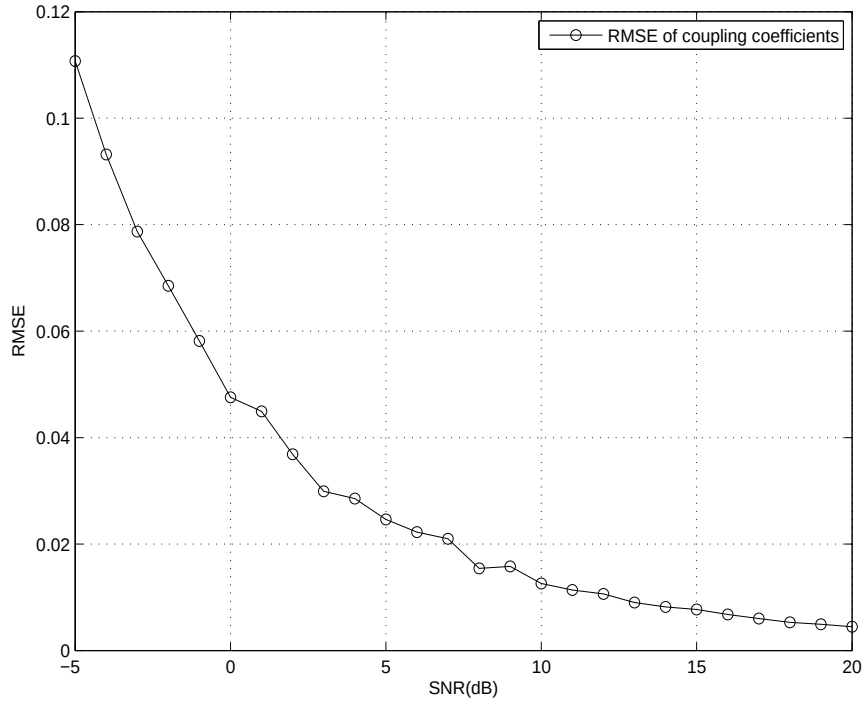

Figure 3.7: Mutual coupling coefficient estimation performance with respect to increasing SNR, snapshots = 100

In the last simulation, the DOA estimates are refined by using the estimated coupling coefficients and the larger noise subspace of 14-element ULA. The applied algorithm results are compared with MUSIC algorithm estimates which are found in the presence of unknown and no mutual coupling case with the same array configuration for different SNR levels, number of snapshots and number of array elements.

As it is seen from Figure 3.9, 3.10 and 3.11 that by using estimated coupling coefficients, the estimation accuracy increases and the resulting RMSE value approach to the RMSE value found in no coupling condition.

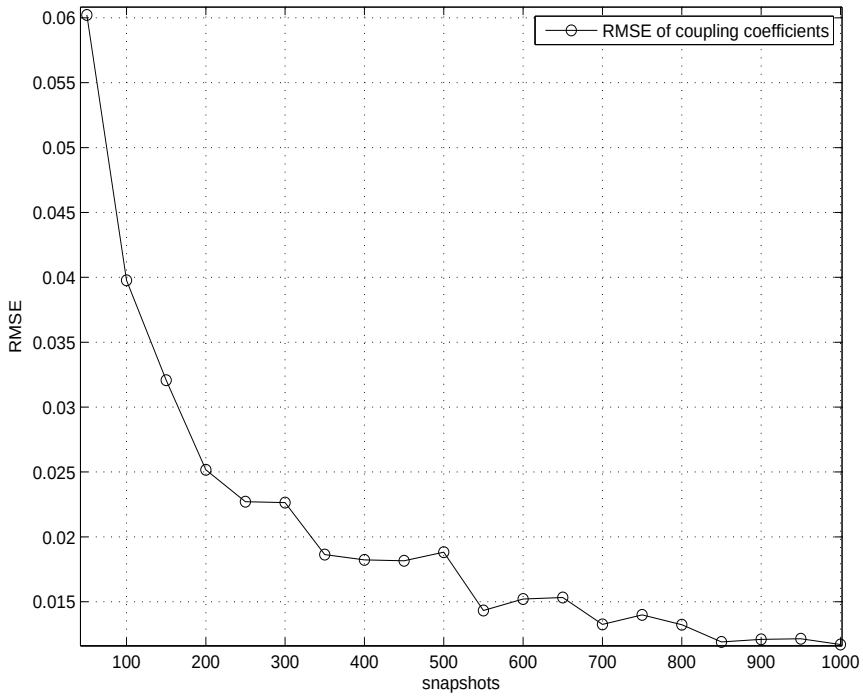

Figure 3.8: Mutual coupling coefficient estimation performance with respect to increasing snapshots, SNR = 0dB

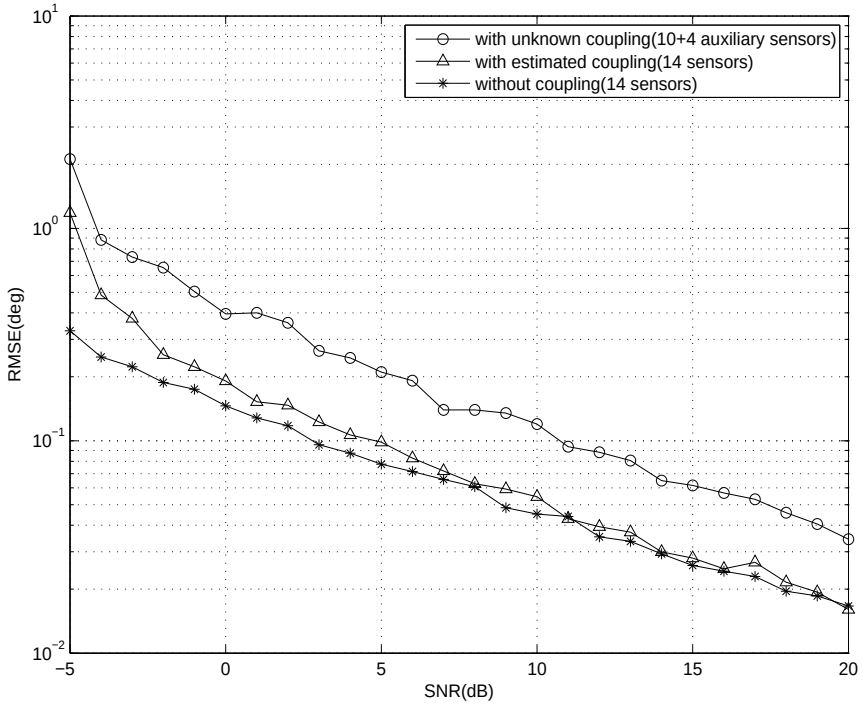

Figure 3.9: DOA estimation performance of the algorithms with respect to increasing SNR, snapshots = 100

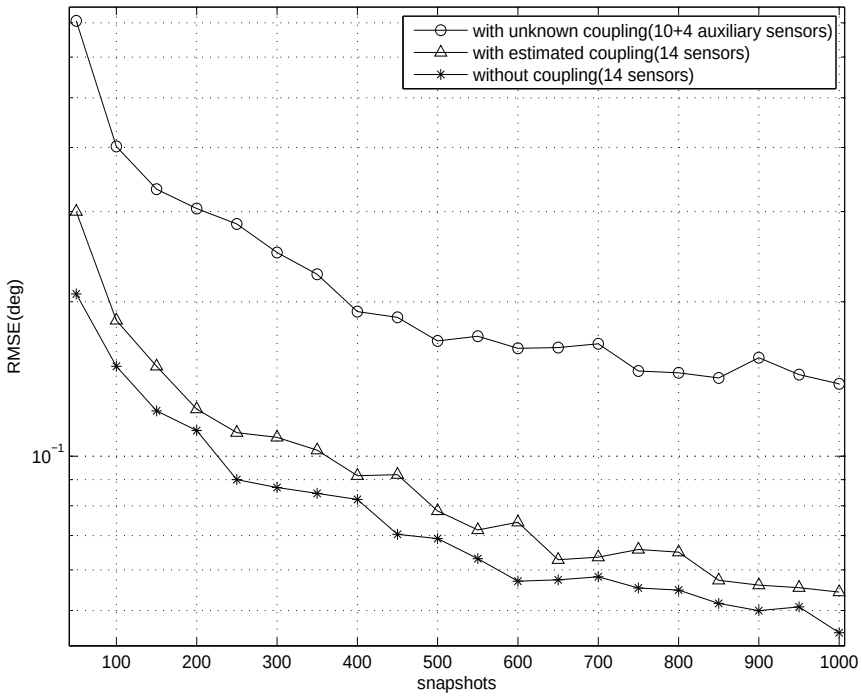

Figure 3.10: DOA estimation performance of the algorithms with respect to increasing snapshots, SNR = 0dB

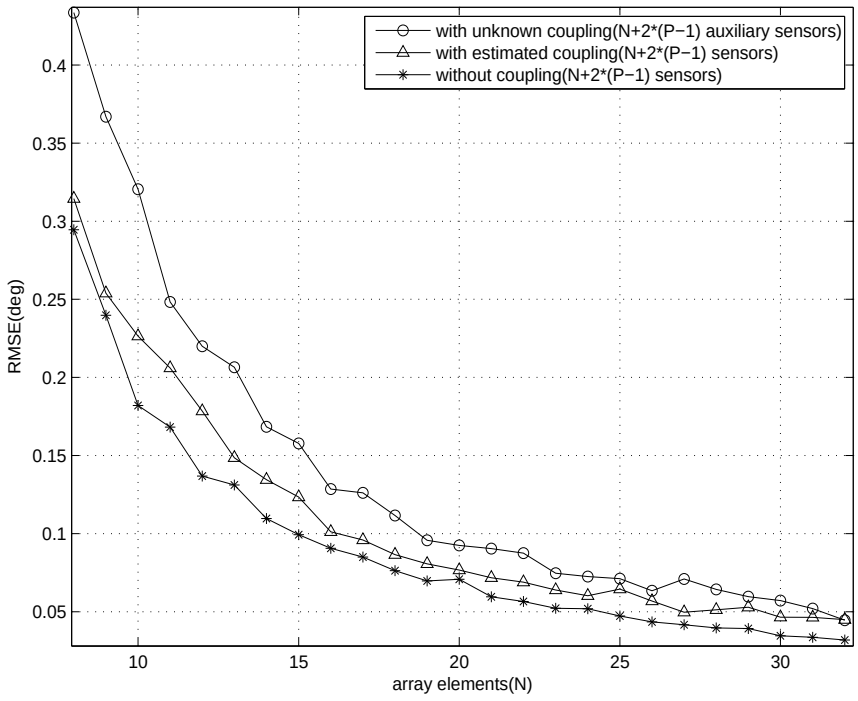

Figure 3.11: DOA estimation performance of the algorithms with respect to increasing array elements, SNR = 0dB, snapshots = 100

CHAPTER 4

TWO DIMENSIONAL DOA ESTIMATION USING UNIFORM RECTANGULAR ARRAY WITH MUTUAL COUPLING

In this chapter, joint estimation of azimuth and elevation angles with uniform rectangular array(URA) in the presence of mutual coupling is presented. Firstly, 2-D DOA angles are estimated in the presence of unknown sensor coupling. Then, mutual coupling coefficients are estimated with the DOA estimates obtained in the first step. Finally, two dimensional refined search of the DOA angles performed with the estimated mutual coupling coefficients. Several Monte Carlo experiments are realized and it is observed that the refined angle estimates are more accurate than the initial DOA estimates in unknown mutual coupling. The computational load of two dimensional spectrum search is reduced and the negative effect of mutual coupling between the sensors is eliminated with the algorithm in [34]. The organization of this chapter is as follows. In the first part, problem formulation and algorithm steps are explained. In the second part, the simulation results for 2-D spectral MUSIC and the method in [34] are presented.

4.1 Problem Statement

In this section, DOA estimation in the presence of known and unknown mutual coupling and estimation of mutual coupling coefficients will be presented. Applied algorithm steps [34] will be described.

4.1.1 DOA estimation with Known Mutual Coupling

It is assumed that uniform rectangular array is composed of $M \times N$ array elements which are positioned with half wavelength, $\lambda/2$, interval. K narrow-band source signals ,$(\theta_1, \varphi_1), ..., (\theta_K, \varphi_K)$, are uncorrelated with noise $\mathbf{n}(t)$ which is zero-mean, white and Gaussian with variance σ^2. θ and φ are the azimuth and elevation angles of source signals respectively. If the sensors are identical and far-field assumption is made, sensor output vector of $M \times N$ element array is given as:

$$\mathbf{x}(t) = \mathbf{CAs}(t) + \mathbf{n}(t) \tag{4.1}$$

where $\mathbf{C}$ is *MN* $\times$ *MN* mutual coupling matrix, $\mathbf{A}$ is the steering matrix, $\mathbf{s}(t)$ is source signal vector and $\mathbf{n}(t)$ is noise vector respectively. Columns of the steering matrix $\mathbf{A}$ are composed of steering vectors $\mathbf{a}(\theta_i, \varphi_i)$ which is defined as

$$\mathbf{a}(\theta_i, \varphi_i) = \mathbf{a}_y(\theta_i, \varphi_i) \otimes \mathbf{a}_x(\theta_i, \varphi_i), i = 1, .., K \tag{4.2}$$

where K is the number of sources and the expression $\otimes$ denotes the Kronecker tensor product. $\mathbf{a}_y(\theta_i, \varphi_i)$ and $\mathbf{a}_x(\theta_i, \varphi_i)$ are phase expression caused by the propagation delay of the array elements and $\mathbf{A} = [\mathbf{a}(\theta_1, \varphi_1), \ldots, \mathbf{a}(\theta_K, \varphi_K)]$ is the array steering matrix composed of $\mathbf{a}(\theta_i, \varphi_i)$.

$$\mathbf{a}_p(\theta_i, \varphi_i) = [1, \beta_p(\theta_i, \varphi_i), ..., {\beta_p}^{N-1}(\theta_i, \varphi_i)]^T, p = x, y \tag{4.3}$$

$$\beta_x(\theta_i, \varphi_i) = \exp\{j\frac{2\pi d_x}{\lambda}\cos\theta_i sin\varphi_i\}, p = x \tag{4.4}$$

$$\beta_y(\theta_i, \varphi_i) = \exp\{j\frac{2\pi d_y}{\lambda}\sin\theta_i sin\varphi_i\}, p = y \tag{4.5}$$

In (4.4) and (4.5), d_x and d_y are the distance between the sensors in x and y axis, λ, is the wavelength, θ_i and φ_i are the azimuth and elevation angles which the estimator

try to find respectively. Mutual coupling coefficients are expressed as $\mathbf{c}_x, \mathbf{c}_y, \mathbf{c}_{xy}$. Mutual coupling is rapidly decreasing with increasing distance between the array elements.$\mathrm{MN} \times \mathrm{MN}$ mutual coupling matrix is band symmetric Toeplitz matrix and given as in (4.6).

$$\mathbf{C} = \begin{bmatrix} \mathbf{C}_1 & \mathbf{C}_2 & 0 & \dots & 0 \\ \mathbf{C}_2 & \mathbf{C}_1 & \mathbf{C}_2 & \dots & 0 \\ \vdots & \ddots & \ddots & \ddots & \vdots \\ 0 & \dots & \mathbf{C}_2 & \mathbf{C}_1 & \mathbf{C}_2 \\ 0 & \dots & 0 & \mathbf{C}_2 & \mathbf{C}_1 \end{bmatrix} \tag{4.6}$$

$$\mathbf{C}_1 = toeplitz\{[1, c_x, 0, \dots, 0]\} \tag{4.7}$$

$$\mathbf{C}_2 = toeplitz\{[c_x, c_{xy}, 0, \dots, 0]\} \tag{4.8}$$

The covariance matrix of **y**(t) can be derived as,

$$\mathbf{R_x} = E\left\{\mathbf{x}(t)\mathbf{x}^H(t)\right\} = \mathbf{CAR_sA}^H\mathbf{C}^H + \sigma^2\mathbf{I} \tag{4.9}$$

where $(.)^H$ denotes the conjugate transpose of a matrix, $\mathbf{R}_s$ is the source correlation matrix, and **I** is the identity matrix. $\mathbf{E}_s$ and $\mathbf{E}_n$ are the eigenvectors obtained from the singular value decomposition of sample correlation matrix and they span the signal and noise subspaces respectively. The manifold matrix is defined as $\mathbf{Ca}(\theta, \varphi)$ in mutual coupling condition and it is orthogonal to the noise subspace matrix $\mathbf{E}_n$.

$$\left\|\mathbf{E_n^H Ca}(\theta_i, \varphi_i)\right\|_2^2 = 0, \text{ for } i = 1, 2, \dots, K. \tag{4.10}$$

In known mutual coupling case, 2-D MUSIC algorithm estimates the DOA angles as the maxima of the following spectrum,

$$P_{\mathrm{MUSIC}}(\theta, \varphi) = \frac{1}{\|\mathbf{E_n^H Ca}(\theta, \varphi)\|^2} \tag{4.11}$$

4.1.2 DOA estimation with Unknown Mutual Coupling

DOA estimation performance of 2-D MUSIC algorithm degrades if the mutual coupling matrix, **C**, is unknown. To resolve mutual coupling effect, the sensors located on the boarders of URA are set as auxiliary sensors. $(\mathrm{M}-2) \times (\mathrm{N}-2)$ size of the

central portion of the array output is used for DOA angle estimation. The signals received in new condition is modeled as in (4.12),

$$\tilde{\mathbf{x}}(t) = \mathbf{P}\mathbf{x}(t) = \mathbf{PCA}\mathbf{s}(t) + \mathbf{P}\mathbf{n}(t) \tag{4.12}$$

where $\mathbf{P}$ is a $[(\mathrm{M}-2)\times(\mathrm{N}-2)]\times \mathrm{MN}$ matrix and $\mathbf{J}$ is a $(\mathrm{N}-2)\times \mathrm{N}$ size matrix defined in (4.13) and (4.14).

$$\mathbf{P} = \begin{bmatrix} \mathbf{O} & \mathbf{J} & \dots & \mathbf{O} & \mathbf{O} \\ \vdots & \vdots & \ddots & \vdots & \vdots \\ \mathbf{O} & \mathbf{O} & \dots & \mathbf{J} & \mathbf{O} \end{bmatrix} \tag{4.13}$$

where $\mathbf{O}$ is a zero matrix of size $(\mathrm{N}-2)\times \mathrm{N}$.

$$\mathbf{J} = \begin{bmatrix} 0 & 1 & \dots & 0 & 0 \\ \vdots & \vdots & \ddots & \vdots & \vdots \\ 0 & 0 & \dots & 1 & 0 \end{bmatrix} \tag{4.14}$$

If we define,

$$\mathbf{P}\mathbf{n}(t) = \tilde{\mathbf{n}}(t), \quad \mathbf{PC} = \tilde{\mathbf{C}} \tag{4.15}$$

The signals received from the middle subarray of URA can be written as

$$\tilde{\mathbf{x}}(t) = \tilde{\mathbf{C}}\mathbf{A}\mathbf{s}(t) + \tilde{\mathbf{n}}(t) \tag{4.16}$$

Then, correlation matrix of the received signals can be shown as in (4.17).

$$\tilde{\mathbf{R}}_{\mathbf{x}} = E\left\{\tilde{\mathbf{x}}(t)\tilde{\mathbf{x}}^H(t)\right\} = \tilde{\mathbf{C}}\mathbf{A}\mathbf{R}_{\mathbf{s}}\mathbf{A}^H\tilde{\mathbf{C}}^H + \sigma^2\tilde{\mathbf{I}} \tag{4.17}$$

Using singular value decomposition, we can obtain $\tilde{\mathbf{E}}_{\mathbf{s}}$ and $\tilde{\mathbf{E}}_{\mathbf{n}}$ matrices whose columns span the signal and noise subspaces of middle subarray correlation matrix respectively. The steering matrix of the middle subarray of URA, $\tilde{\mathbf{a}}(\theta,\varphi)$, can be defined as follows,

$$\tilde{\mathbf{a}}(\theta,\varphi) = \tilde{\mathbf{a}}_y(\theta,\varphi) \otimes \tilde{\mathbf{a}}_x(\theta,\varphi) \tag{4.18}$$

$$\tilde{\mathbf{a}}_x(\theta,\varphi) = \left[1, \beta_x(\theta,\varphi), \dots, \beta_x^{N-3}(\theta,\varphi)\right]^T \tag{4.19}$$

$$\tilde{\mathbf{a}}_y(\theta,\varphi) = \left[1, \beta_y(\theta,\varphi), \dots, \beta_y^{M-3}(\theta,\varphi)\right]^T \tag{4.20}$$

The middle URA manifold vector in unknown sensor coupling is presented as $\tilde{\mathbf{C}}\mathbf{a}(\theta,\varphi)$. The manifold vector can be rewritten in terms of the ideal manifold vector of central portion of URA as $c(\theta,\varphi)\tilde{\mathbf{a}}(\theta,\varphi)$ which will be illustrated from (4.21) to (4.23) [34]. The steering matrix $\tilde{\mathbf{C}}\mathbf{a}$ can be reformulated as,

$$\begin{aligned}\tilde{\mathbf{C}}\mathbf{a} &= \begin{bmatrix} \tilde{\mathbf{C}}_2 & \tilde{\mathbf{C}}_1 & \tilde{\mathbf{C}}_2 & 0 & \dots & 0 \\ 0 & \tilde{\mathbf{C}}_2 & \tilde{\mathbf{C}}_1 & \tilde{\mathbf{C}}_2 & \dots & 0 \\ \vdots & \vdots & \ddots & \ddots & \ddots & \vdots \\ 0 & \dots & 0 & \tilde{\mathbf{C}}_2 & \tilde{\mathbf{C}}_1 & \tilde{\mathbf{C}}_2 \end{bmatrix} \begin{bmatrix} \mathbf{a}_x \\ \mathbf{a}_x\beta_y \\ \vdots \\ \mathbf{a}_x\beta_y^{M-1} \end{bmatrix} \\ &= \tilde{\mathbf{a}}_y \otimes \left(\tilde{\mathbf{C}}_2\mathbf{a}_x + \tilde{\mathbf{C}}_1\mathbf{a}_x\beta_y + \tilde{\mathbf{C}}_2\mathbf{a}_x\beta_y^2\right)\end{aligned} \tag{4.21}$$

where $\tilde{\mathbf{C}}_1$ and $\tilde{\mathbf{C}}_2$ are the $(M-2)\times N$ matrices which construct the mutual coupling matrix of middle URA. $\mathbf{a}_x$ and $\tilde{\mathbf{a}}_y$ are the steering vectors defined in (4.3) and (4.20), respectively. The same approach in (4.21) can also be applied for $\tilde{\mathbf{C}}_1$ and $\tilde{\mathbf{C}}_2$ matrices as,

$$\begin{aligned}\tilde{\mathbf{C}}_1\mathbf{a}_x &= \left(c_x + \beta_x + c_x\beta_x^2\right)\tilde{\mathbf{a}}_x \\ \tilde{\mathbf{C}}_2\mathbf{a}_x &= \left(c_{xy} + c_y\beta_x + c_{xy}\beta_x^2\right)\tilde{\mathbf{a}}_x.\end{aligned} \tag{4.22}$$

Then, utilizing (4.22) in (4.21) we get,

$$\begin{aligned}\tilde{\mathbf{C}}\mathbf{a} &= \left(\beta_x\beta_y + \beta_y\left(1+\beta_x^2\right)c_x + \beta_x\left(1+\beta_y^2\right)c_y\right. \\ &\quad \left. + \left(1+\beta_x^2\right)\left(1+\beta_y^2\right)c_{xy}\right)\tilde{\mathbf{a}}_y \otimes \tilde{\mathbf{a}}_x \\ &= c(\theta,\varphi)\tilde{\mathbf{a}}(\theta,\varphi).\end{aligned} \tag{4.23}$$

where $c(\theta,\varphi)$ denotes mutual coupling which is scalar and different from zero. Then, the DOAs can be estimated directly by using the orthogonality between $\tilde{\mathbf{a}}(\theta_i,\varphi_i)$ and $\tilde{\mathbf{E}}_{\mathbf{n}}^H$ as in (4.24) [34].

$$\left\|\tilde{\mathbf{E}}_{\mathbf{n}}^H\tilde{\mathbf{C}}\mathbf{a}(\theta_i,\varphi_i)\right\| = 0 \Longrightarrow \left\|\tilde{\mathbf{E}}_{\mathbf{n}}^H\tilde{\mathbf{a}}(\theta_i,\varphi_i)\right\| = 0, \text{ for } i = 1,\dots,K \tag{4.24}$$

where K is the number of uncorrelated signals. Finally, we estimate DOA angles in the presence of unknown mutual coupling with the K largest peaks of the function defined in (4.25).

$$P_{MU}(\theta,\varphi) = \frac{1}{\left\|\tilde{\mathbf{E}}_{\mathbf{n}}^H\tilde{\mathbf{a}}(\theta,\varphi)\right\|^2} \tag{4.25}$$

4.1.3 Mutual Coupling Coefficient Estimation

Mutual coupling coefficients are estimated using estimated DOA angles obtained in section 4.1.2 and the output of full array including auxiliary sensors. Utilizing the band symmetric Toeplitz property of $\mathbf{C}_1$ and $\mathbf{C}_2$ matrices which form the mutual coupling matrix, the following equation can be written [27, 30].

$$\mathbf{C}_i\mathbf{a}_x = \mathbf{T}_x\mathbf{c}_i \quad i = 1, 2 \tag{4.26}$$

where $\mathbf{c_1} = [1, c_x]^T$, $\mathbf{c_2} = [c_y, c_{xy}]^T$ and $\mathbf{T}_x = (\mathbf{T}_{x1} + \mathbf{T}_{x2})$ is a matrix of size $\mathrm{N} \times 2$. We also define $\mathbf{T}_y = (\mathbf{T}_{y1} + \mathbf{T}_{y2})$, which is a matrix of size $\mathrm{M} \times 2$. $\mathbf{T}_x$ and $\mathbf{T}_y$ matrices are defined as,

$$\mathbf{T}_{x1_{ij}} = \begin{cases} \mathbf{a}_{x_{i+j-1}} & i + j \leq N + 1 \\ 0 & otherwise. \end{cases} \tag{4.27}$$

$$\mathbf{T}_{x2_{ij}} = \begin{cases} \mathbf{a}_{x_{i-j+1}} & i \geq j \geq 2 \\ 0 & otherwise. \end{cases} \tag{4.28}$$

$$\mathbf{T}_{y1_{ij}} = \begin{cases} \mathbf{a}_{y_{i+j-1}} & i + j \leq M + 1 \\ 0 & otherwise. \end{cases} \tag{4.29}$$

$$\mathbf{T}_{y2_{ij}} = \begin{cases} \mathbf{a}_{y_{i-j+1}} & i \geq j \geq 2 \\ 0 & otherwise. \end{cases} \tag{4.30}$$

Then, rewriting (4.26) with $\mathbf{T}_x$ and $\mathbf{T}_y$ matrices, we have the following equation to solve the mutual coupling coefficients.

$$\mathbf{Ca} = (\mathbf{T}_y \otimes \mathbf{T}_x) \begin{bmatrix} \mathbf{c}_1 \\ \mathbf{c}_2 \end{bmatrix} = \mathbf{Tc} \tag{4.31}$$

$\mathbf{T}$ is orthogonal to the matrix, $\mathbf{E_n}$, which spans the noise subspace of full array output covariance matrix.

$$\left\|\mathbf{E}_n^H\mathbf{T}(\theta_i, \varphi_i)\mathbf{c}\right\|_2^2 = 0, i = 1, 2, ...K \tag{4.32}$$

where K is the number of sources. Estimated DOA angles in section 4.1.2 are written in (4.32), and we define a $\mathbf{Q}$ matrix in equation (4.33).

$$\mathbf{Q} = \begin{bmatrix} \mathbf{E}_{\mathbf{n}}^{H}\mathbf{T}(\tilde{\theta}_1, \tilde{\varphi}_1) \\ \vdots \\ \mathbf{E}_{\mathbf{n}}^{H}\mathbf{T}(\tilde{\theta}_K, \tilde{\varphi}_K) \end{bmatrix} = [\mathbf{q_1}\, \mathbf{q_2}\, \mathbf{q_3}\, \mathbf{q_4}] \tag{4.33}$$

Define a $\mathbf{Q}_2 = [\,\mathbf{q}_2\, \mathbf{q}_3\, \mathbf{q}_4]$ matrix and apply least squares method to the equations in (4.32) and (4.33), mutual coupling coefficients can be estimated as in (4.34).

$$[\mathbf{c}_x, \mathbf{c}_y, \mathbf{c}_{xy}]^T = \mathbf{Q}_2{}^{\dagger}\mathbf{q}_1 \tag{4.34}$$

where $(.)^{\dagger}$ denotes pseudo-inversion of a matrix.

4.2 Simulation Results

In this section, performance of the applied algorithm [34] for URA composed of 10 rows and 10 columns with half wavelength, $\lambda/2$,interval is shown with different simulations. The source signals are generated equal power and they are uncorrelated with each other. Source signals are Gaussian processes and the additive noise is assumed to be temporally and spatially stationary, zero-mean white Gaussian and statistically independent of the signals term. To resolve the uncorrelated signals, the scanning is performed over angle area $[0°, 90°] \times [0°, 90°]$ for azimuth and elevation angles. Rough search precision and refined search precision are $1°$ and $0.1°$ respectively. Mutual coupling coefficients are assumed to be $c_x = c_y = 0.3527 + 0.4854i$, $c_{xy} = 0.0927 - 0.2853i$. The simulation model consists of four signal arriving at angles $(74°.132, 35°.095), (40°.125, 20°.142), (54°.112, 66°.131),$
$(28°.119, 41°.086)$. The estimation accuracy is measured by RMSE of 100 independent Monte Carlo trials for different SNR levels and snapshots.

In Figure 4.1, 4.2, 4.3 and 4.4 are the simulation results of SNR and number of snapshots dependencies of four sources. The performance of applied method and standard MUSIC algorithm is simulated in the presence of unknown mutual coupling.

In Figure 4.1 and 4.2, SNR level increased from -10dB to 10dB for azimuth and elevation estimation and in Figure 4.3 and 4.4, the number of snapshots increased form 50 to 1000 to compare the RMSE of the applied method with the MUSIC algorithm. As seen in these figures, the applied method has an important performance increase over the standard MUSIC algorithm. The RMSE of applied algorithm decreases close to zero as SNR level or snapshots increases while the RMSE of the standard MUSIC algorithm remains at a constant error value. If the two-dimensional spectrum search is done with a resolution $0.1°$, then $901 \times 901 = 811801$ spectral point must be calculated by using MUSIC algorithm. Using twice search method in [34] $91 \times 91 + 4 \times (21 \times 21) = 10045$ spectrum points are calculated.

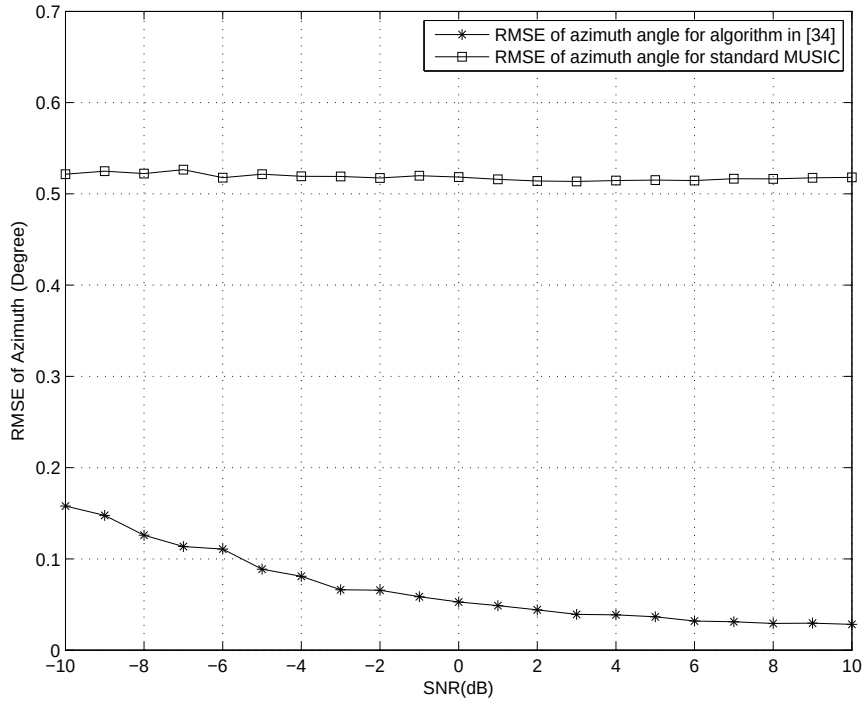

Figure 4.1: Performance of the algorithms for azimuth angle estimation with respect to increasing SNR, snapshots = 500

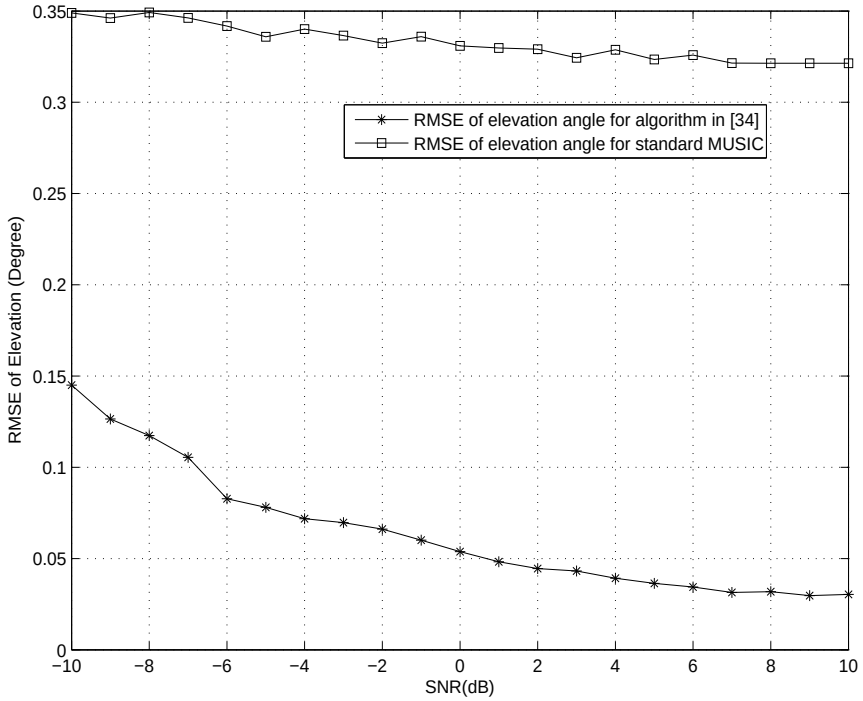

Figure 4.2: Performance of the algorithms for elevation angle estimation with respect to increasing SNR, snapshots = 500

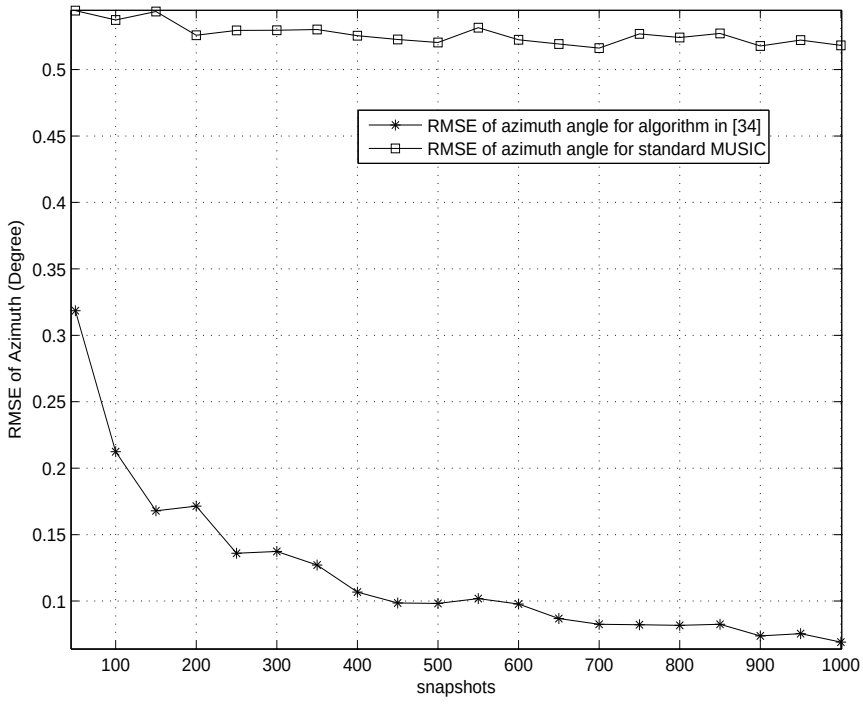

Figure 4.3: Performance of the algorithms for azimuth angle estimation with respect to increasing snapshots, SNR = -10dB

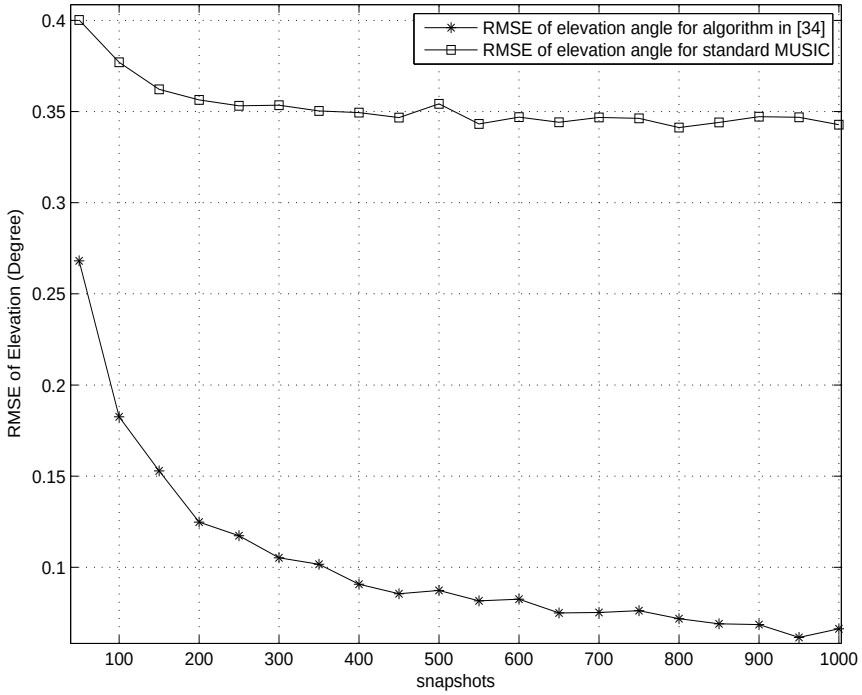

Figure 4.4: Performance of the algorithms for elevation angle estimation with respect to increasing snapshots, SNR = -10dB

In Figure 4.5 and 4.6, mutual coupling coefficient estimation performance of the applied algorithm is simulated for different SNR levels and snapshots. The estimated DOA angles in Figure 4.1, 4.2, 4.3 and 4.4 are used for estimation of coupling coefficients. In Figure 4.5 SNR level is increased form -10dB to 10dB. In Figure 4.6 number of observations increased from 50 to 1000.

In Figure 4.5 and 4.6, it is illustrated that RMSE of coupling coefficients approaches to zero and estimated coefficient values are approximate to the actual values as the SNR level and snapshots increase. We also observe that estimated azimuth and elevation angles in previous step increased the coupling coefficient estimation performance.

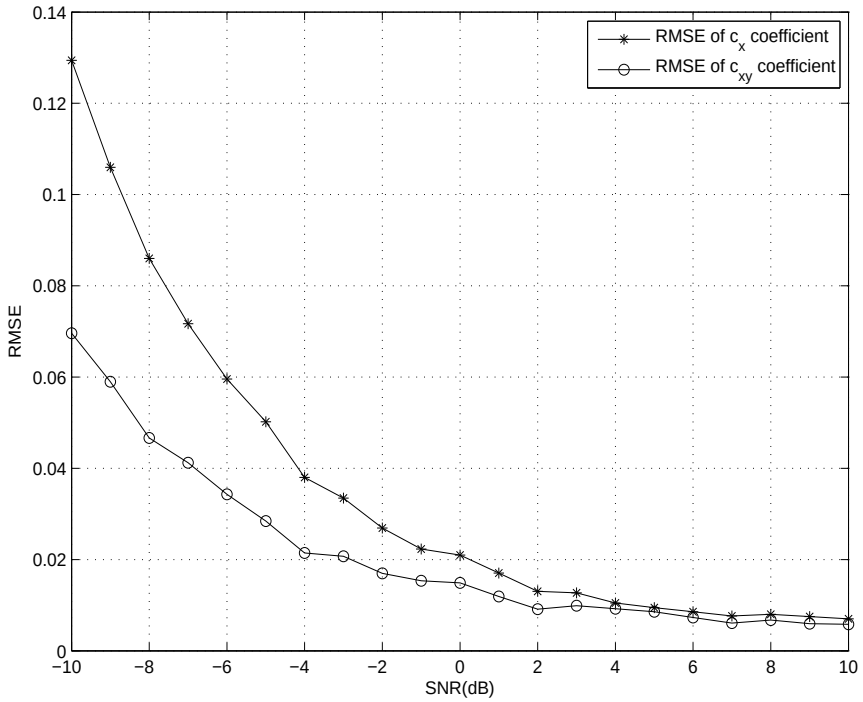

Figure 4.5: Performance of the algorithms for mutual coupling coefficients estimation with respect to increasing SNR, snapshots = 500

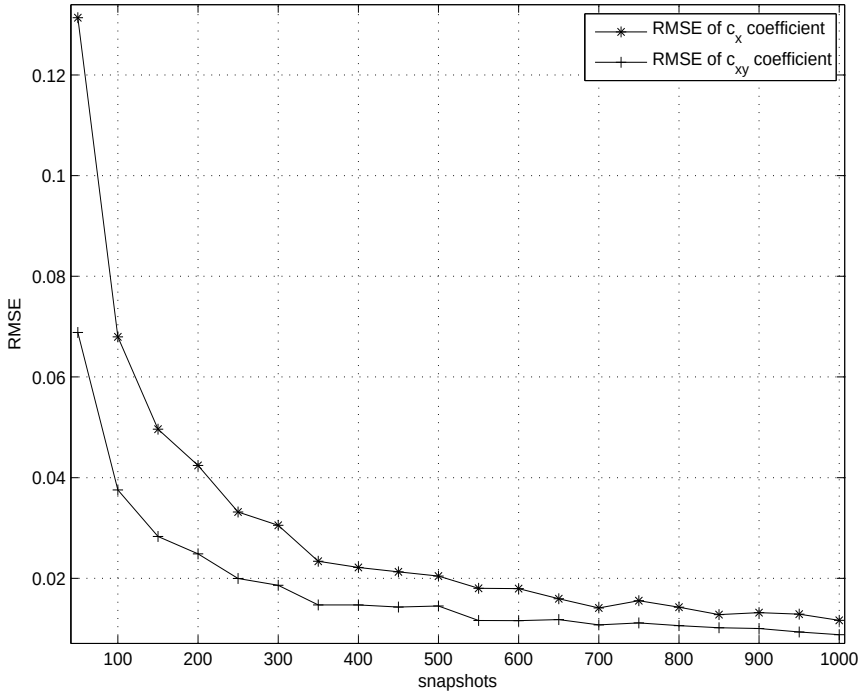

Figure 4.6: Performance of the algorithms for mutual coupling coefficients estimation with respect to increasing snapshots, SNR = 0dB

In Figure 4.7, 4.8, 4.9 and 4.10 are simulation results of DOA estimation using estimated coupling coefficients and full array output of URA including auxiliary sensors. The results are compared to the applied algorithm's DOA estimation performance in the presence of unknown mutual coupling.

In Figure 4.7 and 4.8 SNR level increased from -10dB to 10dB and in Figure 4.9 and 4.10 number of snapshots increased form 50 to 1000 to estimate azimuth and elevation angles of source signals. We observe from figures that, DOA estimation accuracy of the applied algorithm which uses estimated coupling coefficients and the full array output vector is better than the DOA estimation results obtained in the presence of unknown mutual coupling. Thus, negative effect of mutual coupling is eliminated in DOA estimation.

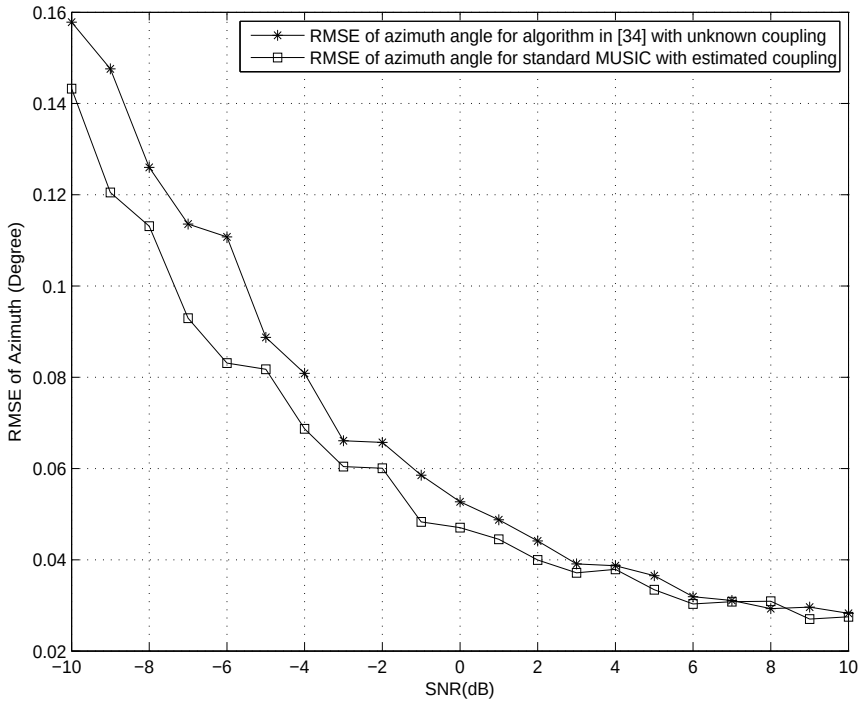

Figure 4.7: Performance of the algorithms for azimuth angle estimation with respect to increasing SNR, snapshots = 500

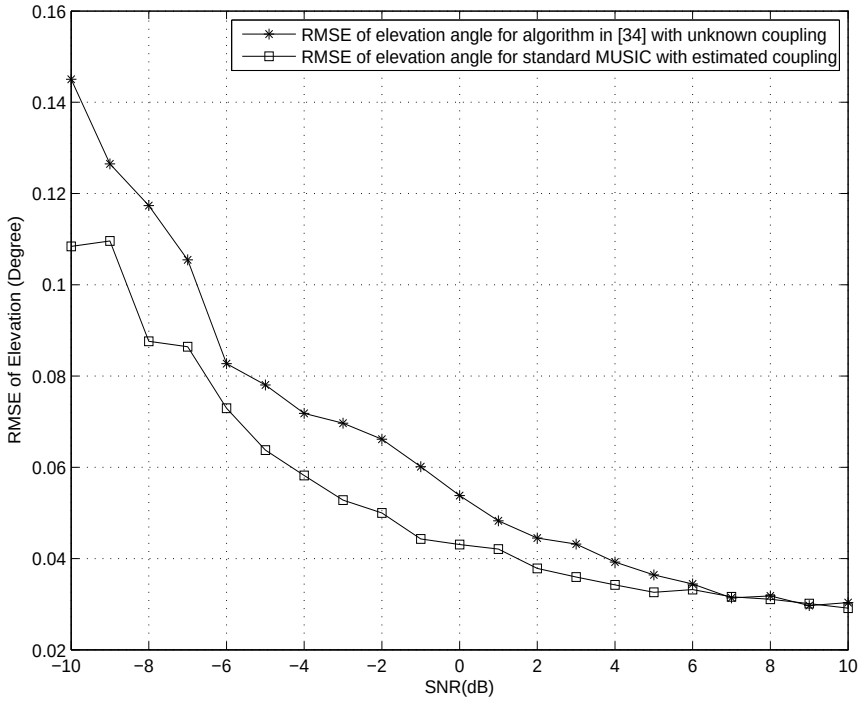

Figure 4.8: Performance of the algorithms for elevation angle estimation with respect to increasing SNR, snapshots = 500

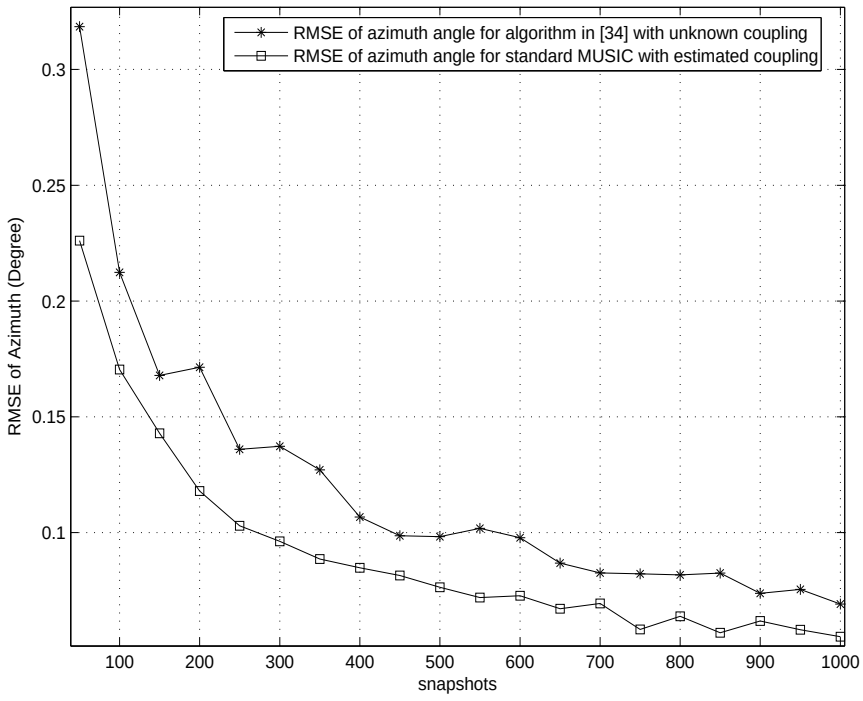

Figure 4.9: Performance of the algorithms for azimuth angle estimation with respect to increasing snapshots, SNR = -10dB

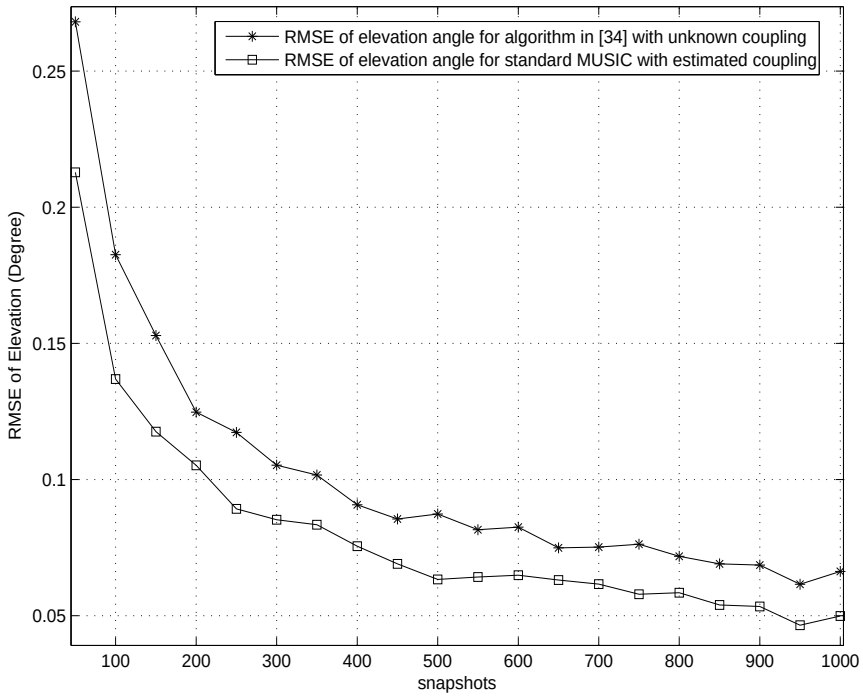

Figure 4.10: Performance of the algorithms for elevation angle estimation with respect to increasing snapshots, SNR = -10dB

CHAPTER 5

DOA ESTIMATION WITH NONUNIFORM LINEAR ARRAY IN THE PRESENCE OF MUTUAL COUPLING AND GAIN-PHASE MISMATCH

In this chapter, direction of arrival estimation with nonuniform linear array(NLA) in the presence of mutual coupling and gain-phase mismatches is considered. Self-calibration method in [29] is implemented to estimate DOAs, gain-phase mismatches and mutual coupling coefficients iteratively without using any calibration sources. The performance results of the algorithms in [29] and [30] are compared with various simulations.The estimation accuracy of the DOA angles is highly dependent to mutual coupling and gain/phase mismatch coefficients estimation. The self-calibration method in [29] is an eigenstructure based method which estimates mutual coupling and gain/phase mismatch error coefficients by using the eigenvector corresponding to the smallest eigenvalue of a matrix. The estimated coefficients are used to minimize the criterion functions to refine the DOA estimates iteratively. Meanwile, the iterative method proposed in [30] minimizes the cost functions of mutual coupling and gain/phase mismatch with a Capon-based search function. The array perturbation coefficients are estimated iteratively to minimize the estimation error below a defined threshold level. The organization of this chapter is as follows. In the first part, nonuniform linear array signal model will be described. The detailed steps of joint estimation of DOAs, gain/phase error and mutual coupling coefficients are explained in the second part. In the third part, simulation results of algorithms with different array models is presented.

5.1 Signal Model

Consider K narrow-band uncorrelated signals $s_1(t), s_2(t), ..., s_K(t)$ impinging on an M element ULA from directions $\theta_1, \theta_2, ..., \theta_K$ respectively, where inter element spacing is equal to half wavelength, $(\lambda/2)$. It is assumed that signals are stationary, zero-mean random process and uncorrelated with the noise. Sensor noises are zero-mean, white and Gaussian with variance σ^2. The array output is written as [30],

$$\mathbf{x}(t) = \mathbf{C\Gamma As}(t) + \mathbf{n}(t) \tag{5.1}$$

where $\mathbf{x}(t) = [x_1(t), x_2(t), \cdots, x_M(t)]^T$, $\mathbf{A} = [\mathbf{a}(\theta_1), \mathbf{a}(\theta_2), ..., \mathbf{a}(\theta_K)]$, $\mathbf{s}(t) = [s_1(t), s_2(t), \cdots, s_K(t)]^T$ and $\mathbf{n}(t) = [n_1(t), n_2(t), \cdots n_M(t)]^T$ denote received signal vector, ideal steering matrix, source signal vector and noise vector, respectively. The columns of steering matrix $\mathbf{A}$ is constructed by the steering vectors $\mathbf{a}(\theta)$ defined as $\mathbf{a}(\theta_k) = [1, \beta_k^1, \beta_k^2, \cdots, \beta_k^{M-1}]^T$ where $\beta_k = \exp(-j\pi \sin(\theta_k)), (k = 1, 2, \cdots, K)$. $\mathbf{C}$ denotes *M* × *M* mutual coupling matrix constructed by $1 \times M$ mutual coupling coefficient vector, $\mathbf{c} = [c_0, \cdots, c_t]^T$ and $\mathbf{\Gamma} = diag\{\mu_1 \exp^{-j\Psi_1}, \mu_2 \exp^{-j\Psi_2}, \cdots, \mu_M \exp^{-j\Psi_M}\}$ is the *M* × *M* gain/phase error matrix where μ_m and Ψ_m denotes the gain and phase of m-th sensor. NLA discussed in this algorithm is not an arbitrary nonuniform linear array. NLA is an array with N sensors which are located at some N places of M-element ULA defined in (5.1). Inter-element spacing between (*n*-1)-th and *n*-th sensor is $\frac{\lambda}{2}d_n$ where d_n is an integer. So, the *n*-th array element in NLA is located on the m_n-th position in the ULA, as

$$m_n = 1 + \sum_{k=}^{n} d_k. \tag{5.2}$$

where $1 + d_1 + d_2 + \cdots + d_N = M$. Hence, the array output of the NLA is defined as

$$\tilde{\mathrm{x}}(t) = \mathbf{F'CF\Gamma As}(t) + \mathbf{F'}\mathrm{n}(t) \tag{5.3}$$

where

$$[\mathbf{F'}]_{ij} = \begin{cases} 1 & i = n, j = m_n \\ 0 & otherwise \end{cases} \quad \text{is a } N \times M \text{ matrix}, \tag{5.4}$$

$$[\mathbf{F}]_{ij} = \begin{cases} 1 & i = j = m_n \\ 0 & otherwise \end{cases} \quad \text{is a } M \times M \text{ matrix}. \tag{5.5}$$

5.2 Joint Estimation of DOAs and Array Perturbations

We can interpret the array covariance matrix as

$$\mathbf{R} = \mathrm{E}[\tilde{\mathrm{x}}(t)\tilde{\mathrm{x}}^H(t)] \quad = \mathbf{F}'\mathbf{C}\mathbf{F}\Gamma\mathbf{A}\mathbf{R}_s\mathbf{A}^H\Gamma^H\mathbf{F}^H\mathbf{C}^H\mathbf{F}'^H + \sigma^2\mathbf{I}_N \tag{5.6}$$

where $\mathbf{R_s}$ is source correlation matrix and and $\mathbf{I_N}$ is the identity matrix. Performing eigendecomposition of $\mathbf{R}$, we can obtain $\mathbf{E_s}$ and $\mathbf{E_n}$ matrices which span signal and noise subspace of array output covariance matrix respectively. Columns of $\mathbf{F}'\mathbf{C}\mathbf{F}\mathbf{\Gamma}\mathbf{A}$ span the signal subspace, its column $\mathbf{F}'\mathbf{C}\mathbf{F}\mathbf{\Gamma}\mathbf{a}(\theta_i), (i = 1, \cdots, K)$ will be orthogonal to noise subspace. We can obtain the following equation to estimate DOA angles.

$$\|\mathbf{E}_N^H\mathbf{F}'\mathbf{C}\mathbf{F}\mathbf{\Gamma}\mathbf{a}(\theta_i)\|^2 = 0, i = 1, 2, \cdots, K. \tag{5.7}$$

The minimization of equation (5.7) with respect to [30] will be described by an iterative process in the following steps.

5.2.1 A:Initialization

1-)Set the iteration number to zero: i=0.
2-)Set the initial mutual coupling matrix and gain-phase matrix as an $M \times M$ identity matrix.

$$\mathbf{C}^{(0)} = \mathbf{I}_M, \mathbf{\Gamma}^{(0)} = \mathbf{I}_M, \tag{5.8}$$

3-) Compute the sample covariance matrix from N_{snap} samples.

$$\hat{\mathbf{R}} = \frac{1}{N_{snap}} \sum_{n=1}^{N_{snap}} \tilde{\mathbf{x}}(n)\tilde{\mathbf{x}}(n)^H \tag{5.9}$$

4-)Perform eigendecomposition on sample covariance matrix, $\hat{\mathbf{R}}$, and get the noise subspace matrix $\mathbf{E}_N$.

5.2.2 B:DOA Estimation

1-)Search the K highest peaks of the following spatial spectrum to estimate DOAs.

$$P(\theta)^{(i)} = \frac{1}{\|\mathbf{E}_N^H\mathbf{F}'\mathbf{C}(i)\mathbf{F}\mathbf{\Gamma}(i)\mathbf{a}(\theta))\|^2} \tag{5.10}$$

5.2.3 C:Gain and Phase Estimation

1-)Calculate the $N \times N$ matrix $\mathbf{Z}^{(i)}$ defined as

$$\mathbf{Z}^{(i)} = \sum_{k=1}^{K} \{(\mathbf{E}_N^H \mathbf{F}' \mathbf{C}^{(i-1)} \mathbf{Q}_k^{(i)} \mathbf{F}'^H)^H \mathbf{E}_N^H \mathbf{F}' \mathbf{C}^{(i-1)} \mathbf{Q}_k^{(i)} \mathbf{F}'^H\} \tag{5.11}$$

where $\mathbf{Q}_k^{(i)} = diag\{\mathbf{a}(\theta_k^{(i-1)})\}$.

2-)Perform eigendecomposition on $\mathbf{Z}^{(i)}$ matrix to get the eigenvector $\tilde{\mathbf{g}}^{(i)}$ which corresponds to the minimum eigenvalue of $\mathbf{Z}^{(i)}$

$$\tilde{\mathbf{g}}^{(i)} = V_{\min}\{Z^{(i)}\} = \left[[\Gamma]_{m_1 m_1}^{(i)} [\Gamma]_{m_2 m_2}^{(i)}, \ldots [\Gamma]_{m_N m_N}^{(i)}\right]^T. \tag{5.12}$$

Then, gain/phase matrix $\mathbf{\Gamma}^{(i)}$ can be computed from $\tilde{\mathbf{g}}^{(i)}$ as

$$\Gamma^{(i)} = \mathbf{F}'^H \mathrm{diag}\{\tilde{\mathbf{g}}^{(\mathrm{i})}\} \mathbf{F}'. \tag{5.13}$$

5.2.4 D:Mutual Coupling Estimation

1-)Calculate the $M \times M$ matrix $\mathbf{W}^{(i)}$ defined as

$$\mathbf{W}^{(i)} = \sum_{k=1}^{K} \{(\mathbf{E}_N^H \mathbf{F}' \mathbf{T}_k^{(i)})^H \mathbf{E}_N^H \mathbf{F}' \mathbf{T}_k^{(i)}\} \tag{5.14}$$

where $M \times (t+1)$ matrix $\mathbf{T} \equiv \mathbf{T}_1 + \mathbf{T}_2$ as

$$[\mathrm{T1}]_{p,q} = \begin{cases} [\beta]_{p+q-1} & p+q \leq M+1 \\ 0 & otherwise \end{cases} \tag{5.15}$$

$$[\mathrm{T2}]_{p,q} = \begin{cases} [\beta]_{p+q-1} & p \geq q \geq 2 \\ 0 & otherwise \end{cases} \tag{5.16}$$

and β is a $M \times 1$ vector defined as

$$\beta_K^{(i)} = \mathbf{F} \mathbf{\Gamma}^{(i)} \mathbf{a}(\theta_k{}^{(i-1)}) \tag{5.17}$$

2-)Perform eigendecomposition on $\mathbf{W}^{(i)}$ matrix to get the eigenvector $\mathbf{c}^{(i)}$ which corresponds to the minimum eigenvalue of $\mathbf{W}^{(i)}$ and as well as the $1 \times M$ mutual coupling coefficient vector.

$$\mathbf{c}^{(i)} = V_{\min}\{W^{(i)}\} = [c_0, \cdots, c_t]^T \tag{5.18}$$

Then, mutual coupling matrix $\mathbf{C}^{(i)}$ can be computed from

$$\mathbf{C}^{(i)} = \mathrm{toeplitz}(\mathbf{c}^{(\mathrm{i})}). \tag{5.19}$$

5.2.5 E:Convergence Check

Repeat steps B to D until

$$\|\mathbf{C}^{(i)}\mathbf{F}\Gamma^{(i)}\mathbf{A}^{(i-1)} - \mathbf{C}^{(i-1)}\mathbf{F}\Gamma^{(i-1)}\mathbf{A}^{(i-2)}\|^2 < \delta \tag{5.20}$$

where δ is a threshold value.

5.3 Simulations

In this section, performance of the applied method in [29] is compared with the method in [30] with three simulation scenarios. The estimation performance of DOAs, gain/phase error and mutual coupling coefficients are simulated for ULA and NLA array geometries with different SNR levels and snapshots.

5.3.1 Simulation-1:NLA Simulation Results

In the first simulation, the method in [29] and [30] are simulated for N=7 element nonuniform linear array. $K = 2$ uncorrelated sources with the assumed DOAs from -20° and 30° impinges to the array. The additive sensor noises are, zero-mean, i.i.d and white Gaussian process with variance σ^2. Suppose the Gaussian signals are of equal power, σ_K^2. Then, the input SNR is defined as $10\log_{10}(\sigma_K^2/\sigma^2)$. The inter-element spacing of the NLA is $d_1 = 0$, $d_2 = 1$, $d_3 = 1$, $d_4 = 1$, $d_5 = 2$, $d_6 = 1$, $d_7 = 3$. Mutual coupling coefficient vector is, $\mathbf{c} = [1, 0.4 + 0.3j, -0.16 + 0.12j]^T$. The gain/phase error coefficients are given by, $[1, 1.1375+0.2376j, 0.9464+0.5511j, 1.0981 + 0.0622j, 1.0838 + 0.11j, 1.0331 + 0.4140j, 1.1399 + 0.1125j]$. The performance of the algorithms are shown with root mean square error(RMSE) of the estimates for DOA, gain/phase error coefficients and mutual coupling coefficients from 100 Monte Carlo trials for each SNR levels and snapshots as:

$$\mathbf{RMSE}_\theta = \sqrt{\frac{1}{100K}(\sum_{n=1}^{100}\sum_{n=1}^{L}\|\theta_n - \theta\|_F^2)} \tag{5.21}$$

$$\mathbf{RMSE}_\Gamma = \sqrt{\frac{1}{100}(\sum_{n=1}^{100}\|\tilde{\mathbf{g}}_n - \tilde{\mathbf{g}}\|_F^2/\|\tilde{\mathbf{g}}\|_F^2)} \tag{5.22}$$

$$\mathbf{RMSE_c} = \sqrt{\frac{1}{100}(\sum_{n=1}^{100} \|\mathbf{c}_n - \mathbf{c}\|_F^2 / \|\mathbf{c}\|_F^2)} \tag{5.23}$$

where θ_n, $\tilde{\mathbf{g}}_n$ and $\mathbf{c}$ are the estimates of DOA angle, gain-phase and mutual coupling matrix at the **n**-th Monte Carlo trial, respectively. The algorithm proposed in [30] is expressed as "Friedlander's method" and the algorithm in [29] is expressed as "self-calibration method" in the following simulation results.
In Figure 5.1 and 5.2 are the estimation results of the algorithms for two uncorrelated source signals with respect to increasing SNR and number of snapshots. The RMSE of the self-calibration method decreases to zero as the SNRs and number of snapshots increase. The RMSE values of Friedlander's method is larger than the self-calibration method for all SNR levels and number of snapshots. As it is seen from these figures, the self-calibration method shows good estimation accuracy comparing to Friedlander's method.

The RMSE performance of gain/phase error coefficients estimation versus different SNR levels and number of snapshots are presented in Figure 5.3 and 5.4, respectively. It is observed that, the self-calibration method achives lower RMSE bound comparing to Friedlander's method for all SNRs and snapshots of data.

In Figure 5.5 and 5.6, the performance of the algorithms for mutual coupling coefficients estimation with respect to increasing SNR and number of snapshots is illustrated. We see that, the RMSE of self-calibration method decreases to an acceptable level as SNR and number of snapshots increase. However, the RMSE of Friedlander's method stays at a constant error level at high SNRs and number of snapshots.

In Simulation-1, it is concluded that, the self-calibration method is optimal for estimating DOA angles, gain-phase and mutual coupling coefficients with NLA configuration as compared Friedlander's method. The RMSE of self-calibration method decrease close to zero as SNR level and number of snapshots increase. However, the RMSE of Friedlander's algorithm can't decrease below a constant error value as SNR level and number of snapshots increase. The reason of the simulation results from Figure 5.1 to 5.6 is that the DOA estimation performance depends on the estimation accuracy of gain/phase error and mutual coupling coefficients. To apply Friedlander's

method with 7-element NLA geometry, three rows of a steering matrix are set to zero for 10-element ULA. Also, Friedlander's method needs to calculate the inverse of the $\mathbf{Z}^{(\mathbf{i})}$ and $\mathbf{W}^{(\mathbf{i})}$ matrices to estimate gain/phase and coupling coefficients in Equation (5.11) and (5.14), respectively. So, the singularity in these matrices causes degradation of estimation accuracy and increase RMSE of simulation results. Meanwhile, the self-calibration method uses the eigendecomposition method to estimate the array perturbations instead of calculating the inverse matrix. Thus, the estimation accuracy of self calibration method is better than Friedlander's method with nonuniform linear array.

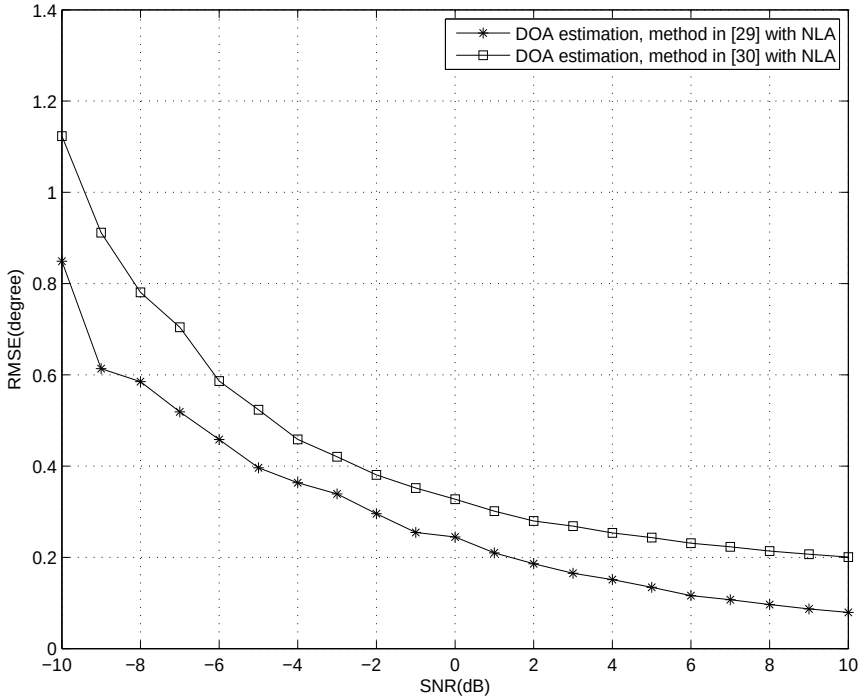

Figure 5.1: Simulation-1: DOA estimation performance of the algorithms for NLA with respect to increasing SNR, snapshots = 500

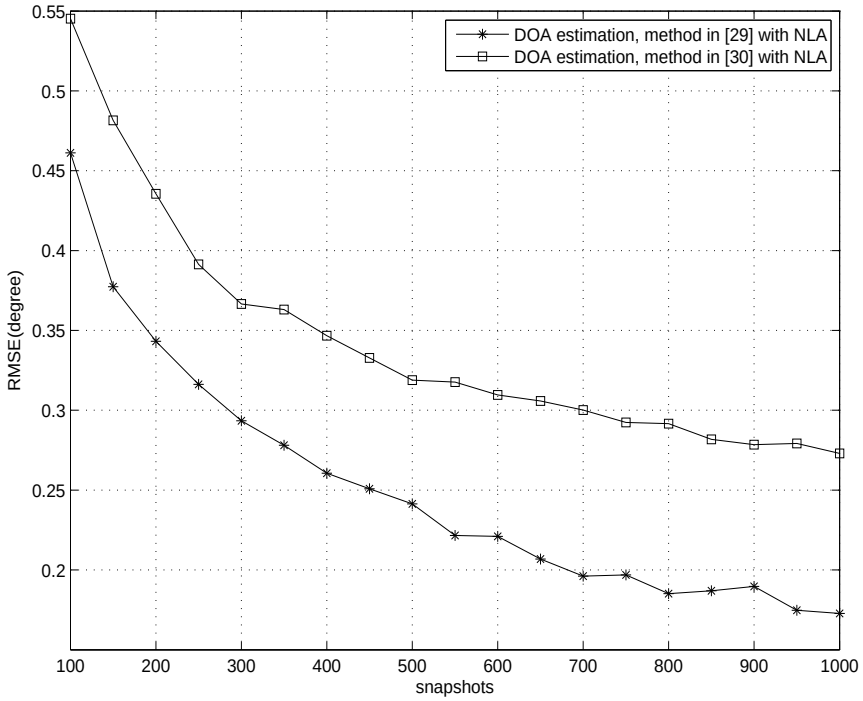

Figure 5.2: Simulation-1: DOA estimation performance of the algorithms for NLA with respect to increasing snapshots, SNR = 0dB

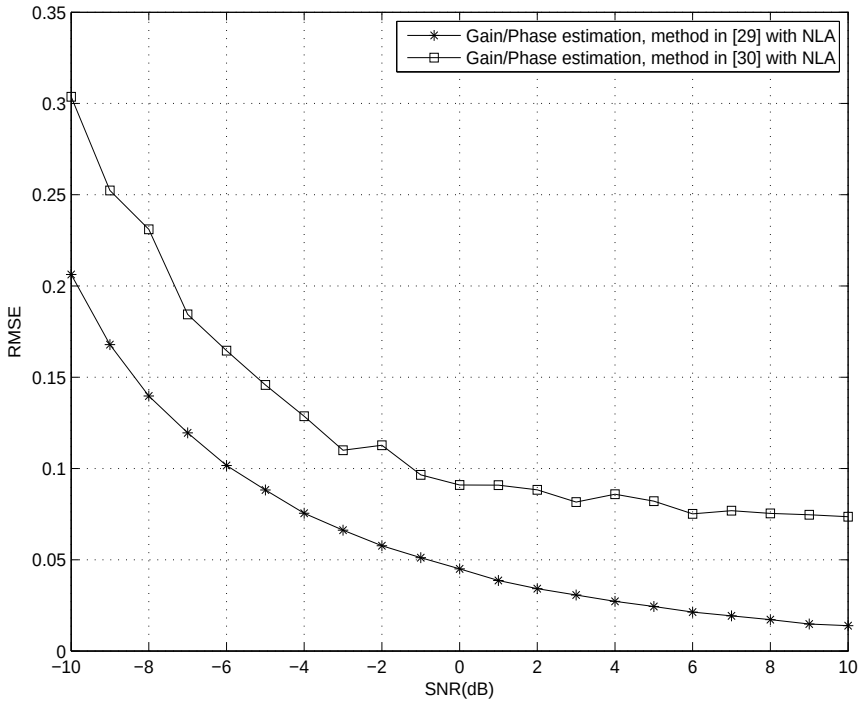

Figure 5.3: Simulation-1: Gain/Phase estimation performance of the algorithms for NLA with respect to increasing SNR, snapshots = 500

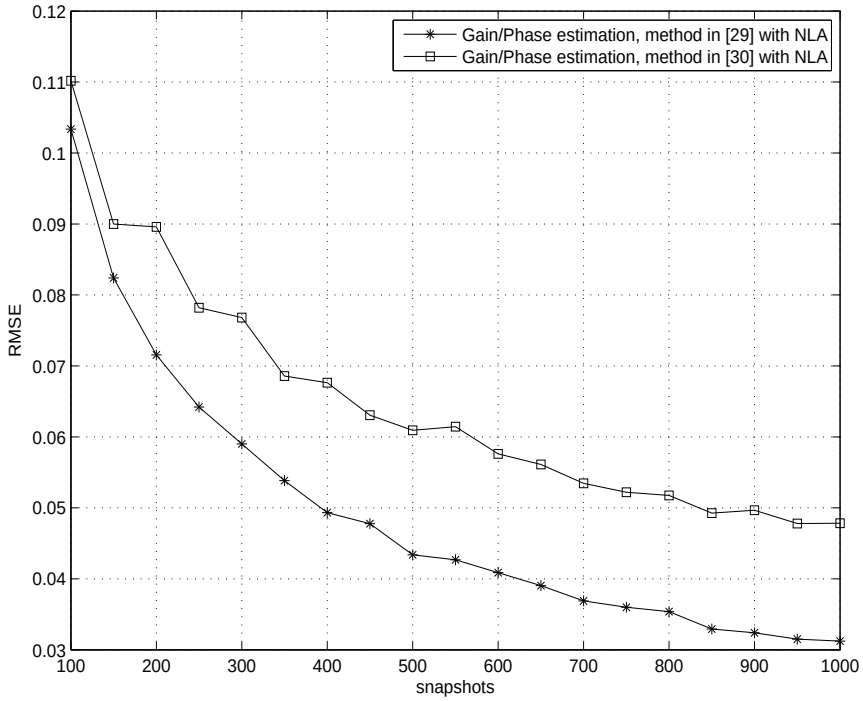

Figure 5.4: Simulation-1: Gain/Phase estimation performance of the algorithms for NLA with respect to increasing snapshots, SNR = 0dB

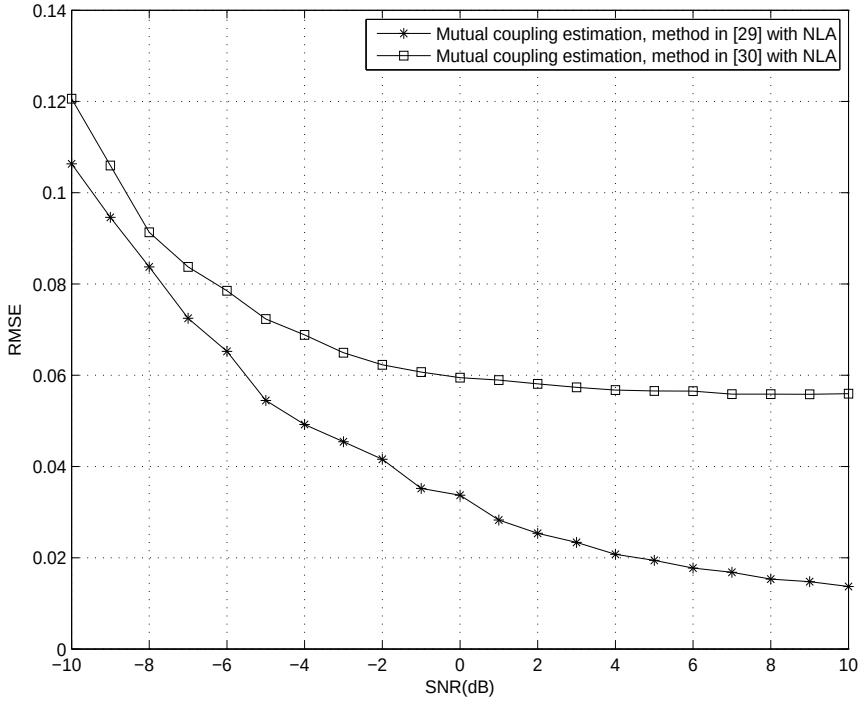

Figure 5.5: Simulation-1: Mutual Coupling estimation performance of the algorithms for NLA with respect to increasing SNR, snapshots = 500

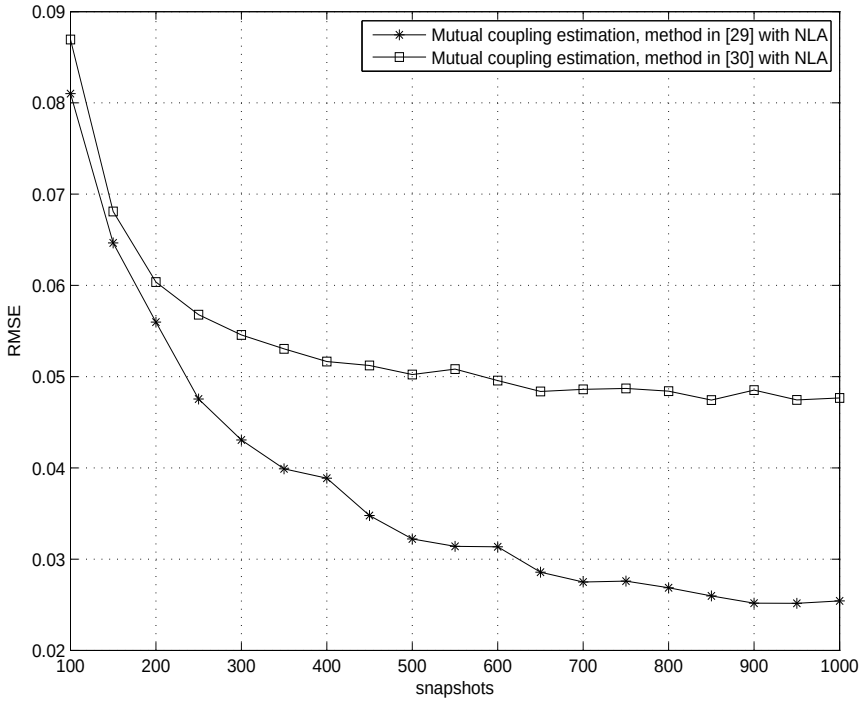

Figure 5.6: Simulation-1: Mutual Coupling estimation performance of the algorithms for NLA with respect to increasing snapshots, SNR = 0dB

5.3.2 Simulation-2:NLA and ULA Simulation Results

In the second simulation, the self-calibration method and Fridlander's method are compared with the same parameters in Simulation-1, except Friedlander's method is applied with 7-element ULA and the self-calibration method is applied with 7-element NLA configurations. The aim of the second simulation part is to see the performance of the algorithms with the array models where they are proposed to show the optimal performance to estimate DOA angles, mutual coupling and gain/phase error coefficients.

The RMSE performance of DOA estimation versus SNR and number of snapshots are presented in Figure 5.7 and 5.8. As seen in these figures, the RMSE of Friedlander's method shows slightly better performance than the self-calibration method because of no singularity problem for estimating coupling and gain/phase error coefficients. Meanwhile, DOA estimation performance of self-calibration method approaches to Friedlander's method as SNRs and number of snapshots increase.

In Figure 5.9 and 5.10, we have the estimation performance of the algorithms for gain/phase error coefficients with respect to increasing SNR and snapshots. As it is seen from these figures, Friedlander's method again shows better performance than self-calibration method owing to the better estimation accuracy of the DOA angle estimates found in the first step.

Figure 5.11 and 5.12 show the results of the algorithms for mutual coupling coefficient estimation in terms of SNRs and number of snapshots, respectively. It is observed that, the self-calibration method can't achieve the RMSE bound of Friedlander's method because the estimated DOAs and gain/phase error coefficients by Friedlander's method are more accurate than the estimates found in the self-calibration method which are used for mutual coupling coefficient estimation.

As a result, Friedlander's method has better performance than the self-calibration method because of no missing row existence in steering matrix of ULA array and no singularity problem exists to calculate the inverse of $\mathbf{Z}^{(\mathbf{i})}$ and $\mathbf{W}^{(\mathbf{i})}$ matrices in perturbation coefficients estimation.

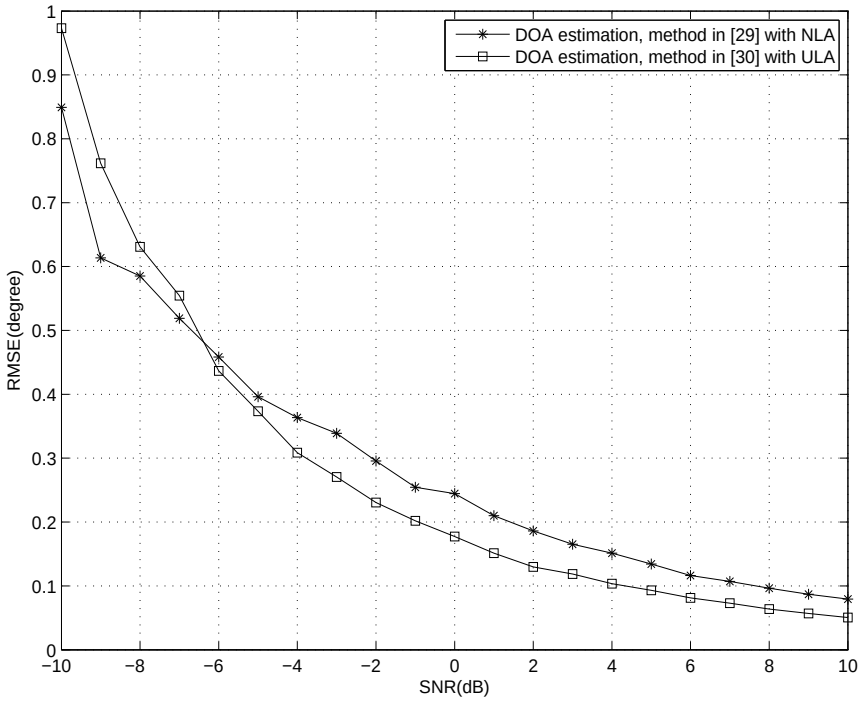

Figure 5.7: Simulation-2: DOA estimation performance of the algorithms for NLA and ULA with respect to increasing SNR, snapshots = 500

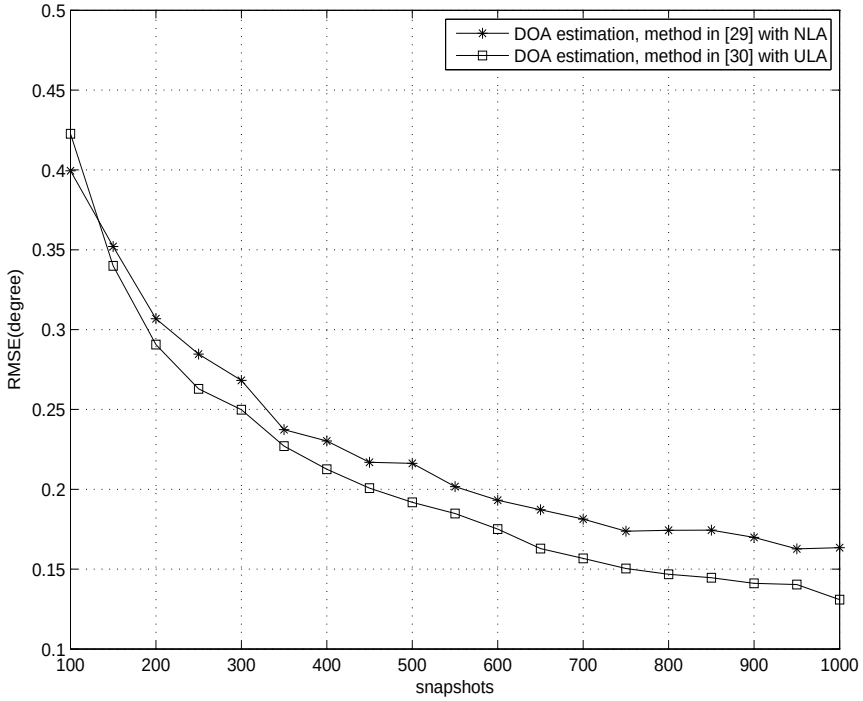

Figure 5.8: Simulation-2: DOA estimation performance of the algorithms for NLA and ULA with respect to increasing snapshots, SNR = 0dB

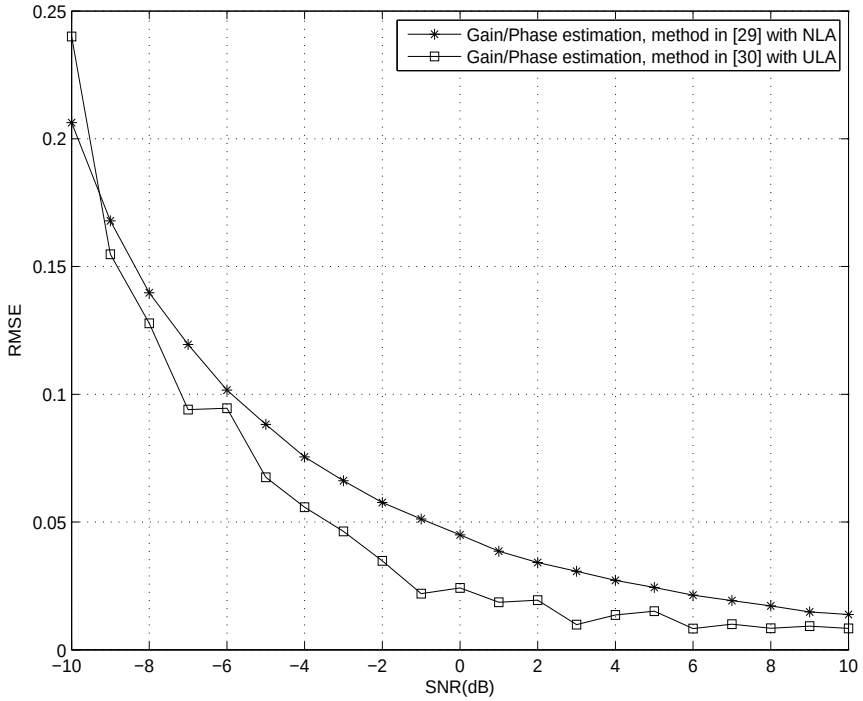

Figure 5.9: Simulation-2: Gain/Phase estimation performance of the algorithms for NLA and ULA with respect to increasing SNR, snapshots = 500

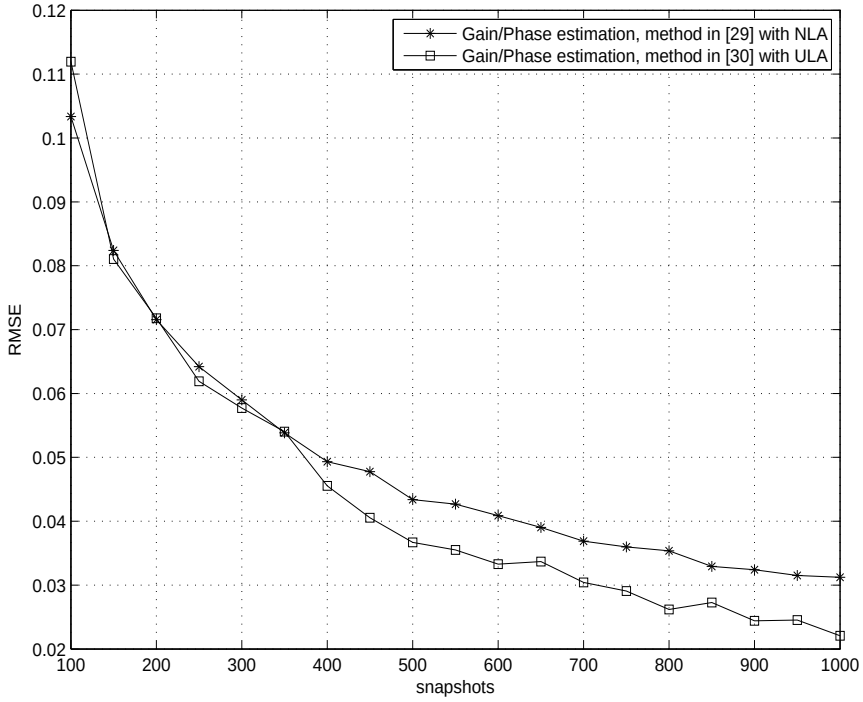

Figure 5.10: Simulation-2: Gain/Phase estimation performance of the algorithms for NLA and ULA with respect to increasing snapshots, SNR = 0dB

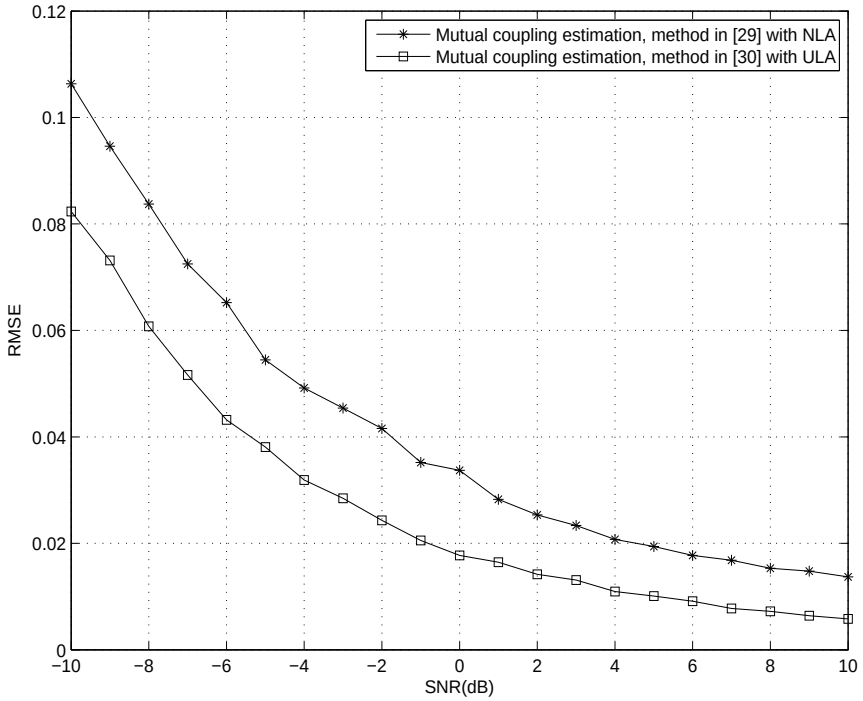

Figure 5.11: Simulation-2: Mutual Coupling estimation performance of the algorithms for NLA and ULA with respect to increasing SNR, snapshots=500

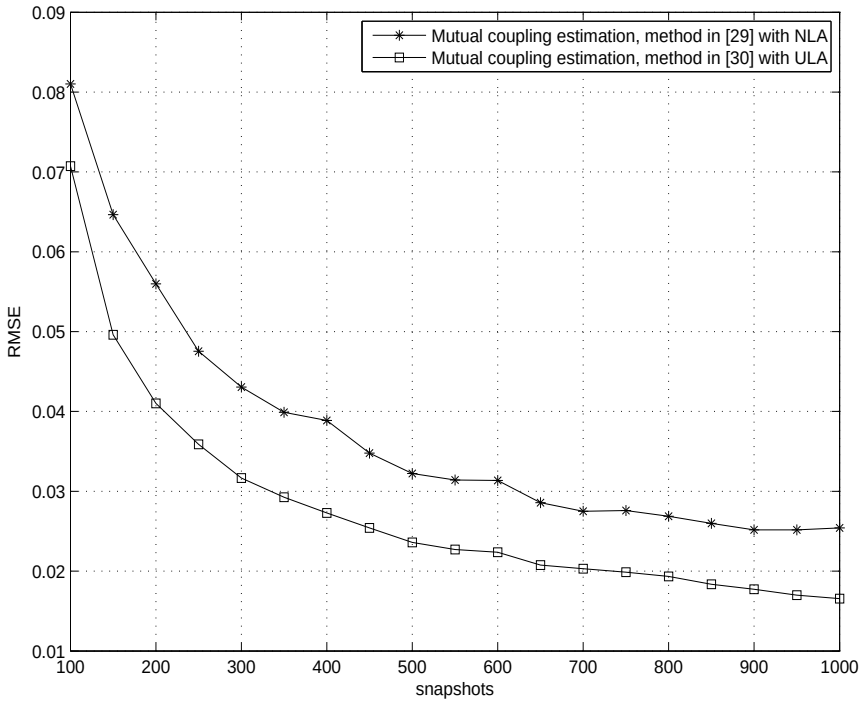

Figure 5.12: Simulation-2: Mutual Coupling estimation performance of the algorithms for NLA and ULA with respect to increasing snapshots, SNR = 0dB

5.3.3 Simulation-3:ULA Simulation Results

In the last simulation, the self-calibration method and Fridlander's method are applied with 7-element ULA. The remaining simulation parameters are same with the previous simulations.

In Figure 5.13 and 5.14, the performance results of the algorithms are illustrated for DOA estimation with respect to increasing SNR and number of snapshots. As seen in these figures, the RMSE of Friedlander's method decrease to zero as SNR and number of snapshots increase. However, the RMSE of self-calibration method stays at a constant level at high SNRs and number of snapshots. It can be observed that, Friedlander's method estimates coupling and gain/phase coefficients accurately comparing to self-calibration method for ULA which are used in the estimation of DOAs.

In Figure 5.15 and 5.16 are the simulation results of SNR and number of snapshots dependencies of the algorithms for gain/phase error coefficients estimation. In Figure 5.15, it is illustrated that Friedlander's method shows better RMSE performance for all SNR values comparing to the self-calibration method. In Figure 5.16, it is seen that the RMSE of Friedlander's method decrease to zero for increasing number of snapshots whereas the RMSE values of the self-calibration method stay at a constant level at high SNR values. It can be seen that, the estimated DOA angles in the first step has an important affect for gain/phase error coefficients estimation.

Figure 5.17 and Figure 5.18 present the results of the algorithms for mutual coupling coefficient estimation. As seen in these figures, Friedlander's method achieves lower RMSE bound for all SNRs and number of snapshots comparing to the self-calibration method. As the estimated DOAs and gain/phase error coefficients are used in the mutual coupling coefficients estimation, the accuracy of these estimates has a large impact for mutual coupling coefficients estimation.

We can conclude that, the self-calibration algorithm which estimates DOAs, gain/phase error and mutual coupling coefficients with the eigenvector that corresponds to the minimum eigenvalue of $\mathbf{Z}^{(\mathbf{i})}$ and $\mathbf{W}^{(\mathbf{i})}$ matrices can't provide good estimation accuracy with uniform linear array. Friedlander's method, which minimizes the cost

function of array perturbations with Capon-based search function provides good estimation performance with ULA configuration.

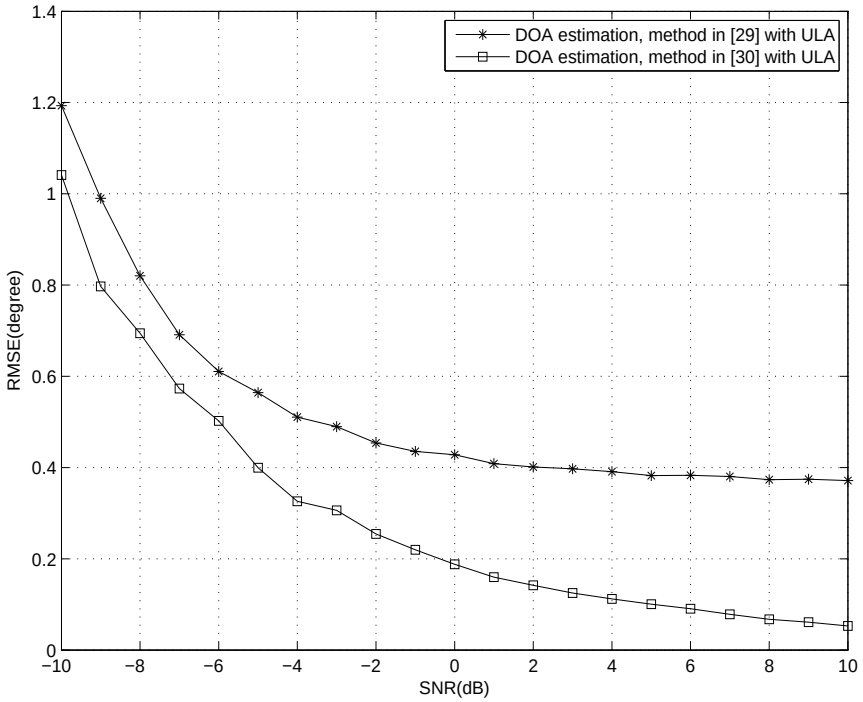

Figure 5.13: Simulation-3: DOA estimation performance of the algorithms for ULA with respect to increasing SNR, snapshots = 500

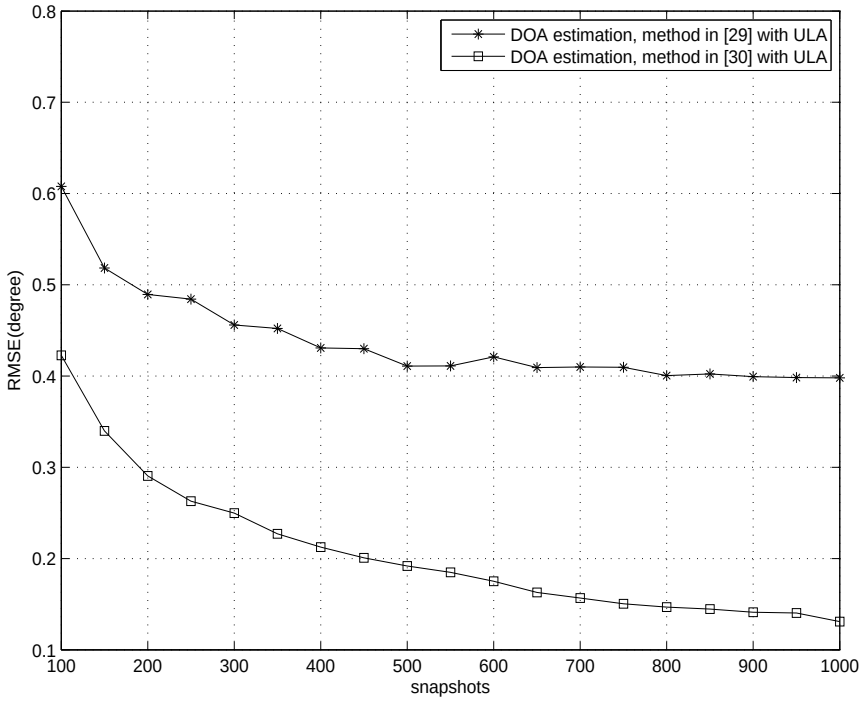

Figure 5.14: Simulation-3: DOA estimation performance of the algorithms for ULA with respect to increasing snapshots, SNR = 0dB

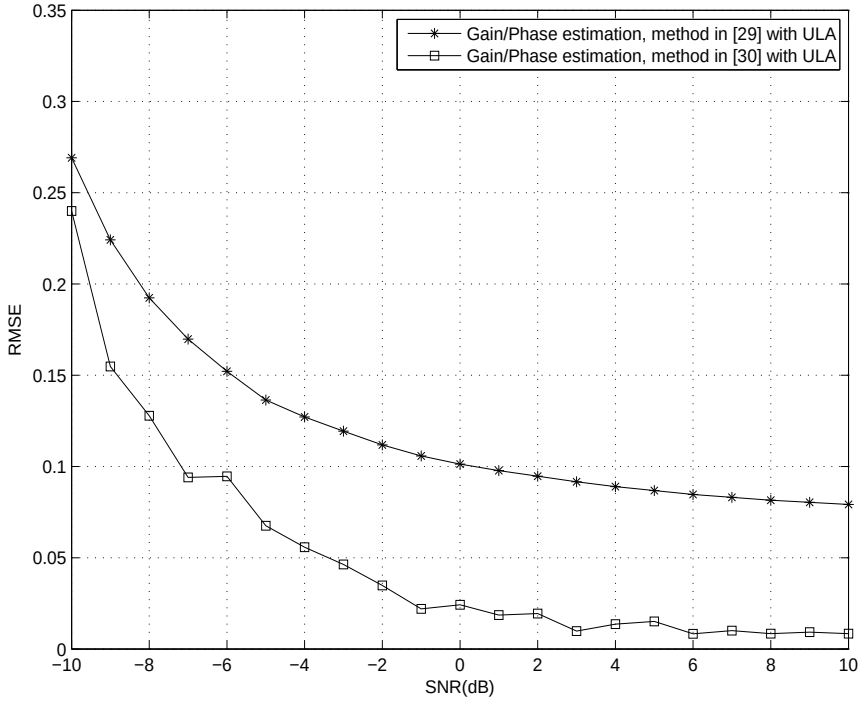

Figure 5.15: Simulation-3: Gain/Phase estimation performance of the algorithms for ULA with respect to increasing SNR, snapshots = 500

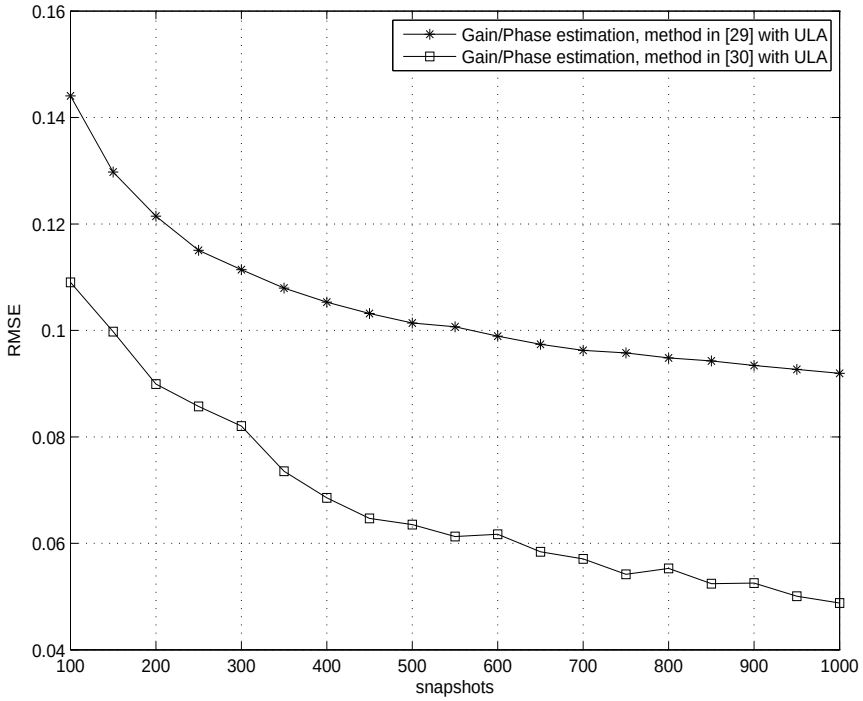

Figure 5.16: Simulation-3: Gain/Phase estimation performance of the algorithms for ULA with respect to increasing snapshots, SNR = 0dB

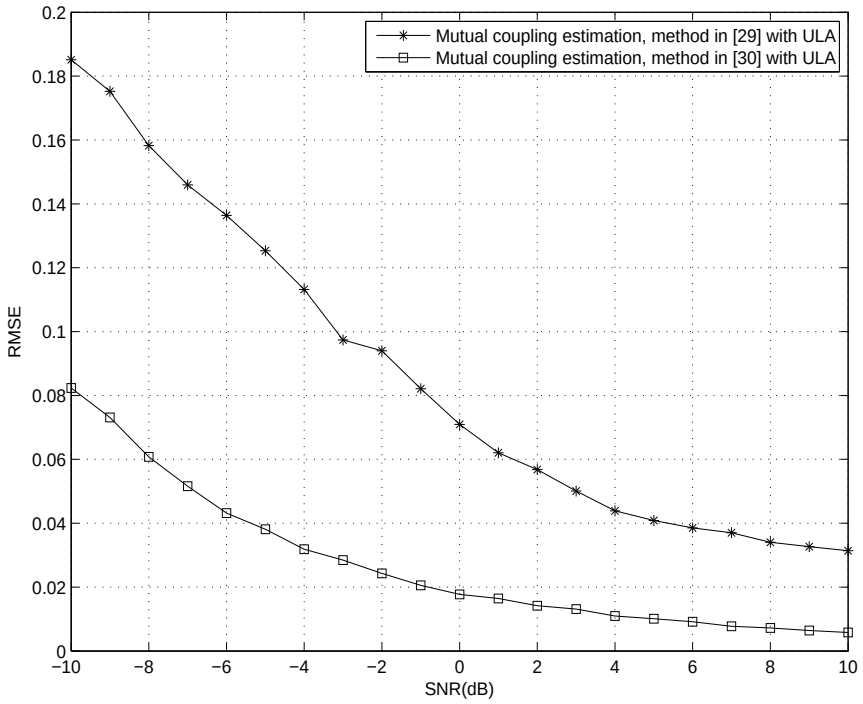

Figure 5.17: Simulation-3: Mutual Coupling estimation performance of the algorithms for ULA with respect to increasing SNR, snapshots = 500

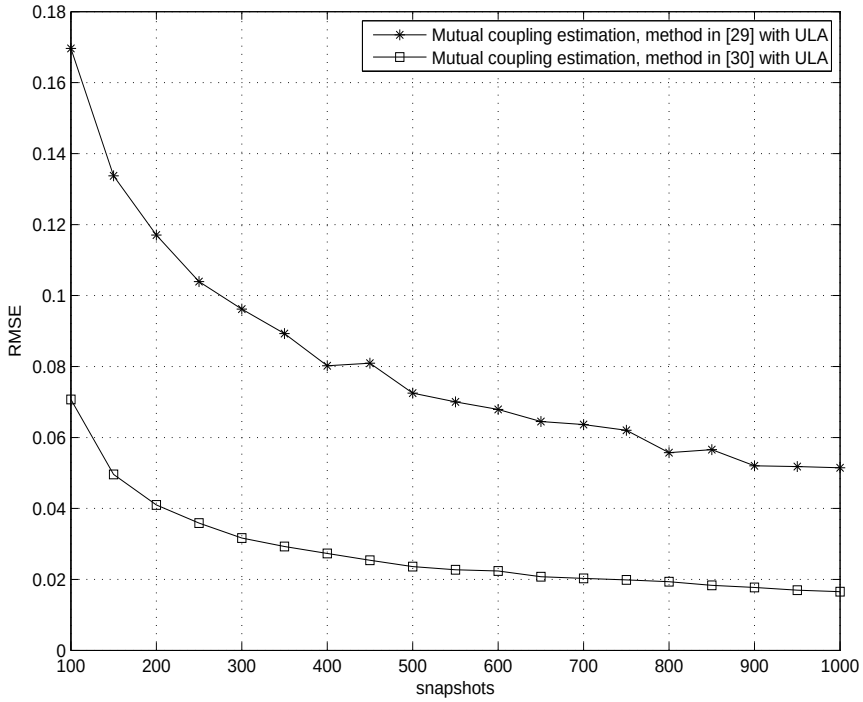

Figure 5.18: Simulation-3: Mutual Coupling estimation performance of the algorithms for ULA with respect to increasing snapshots, SNR = 0dB

CHAPTER 6

PERFORMANCE COMPARISON OF PRIOR KNOWLEDGE BASED DOA ESTIMATION ALGORITHMS

In this chapter, direction of arrival estimation using a-priori knowledge about the location and correlation state of the signal sources is presented. Taking into account this prior knowledge in the estimation of the unknown sources, performance comparison of these algorithms is implemented with different conditions. It is observed from the simulations that, prior knowledge about some of the source positions and their correlation state is useful to estimate coherent or highly correlated sources which are closely separated. In this chapter, performance comparison of prior knowledge based methods such as Constrained MUSIC [2], PLEDGE [3]-[33], POWDER [4] and the subspace based Forward Backward Spatial Smoothing MUSIC(FBSS-MUSIC) in [5] and Root-MUSIC in [42] are presented with various simulations. The estimation accuracy of the methods for different correlation level of signal sources are also presented in the simulations.

DOA estimation problem is turned into a polynomial rooting problem in the ULA geometry for POWDER and PLEDGE methods. PLEDGE method is an extension of MODE [32] method which is an ML based method proposed for ULA. POWDER method is also applicable for any array geometries. However, the computational complexity in minimization step of POWDER method increases for other array geometries. POWDER method has less computational load for ULA implementation [4]. Constrained MUSIC method estimates DOA angles with examining the roots of the spectrum polynomial for ULA. Constrained MUSIC method also has an extension for 2-D DOA estimation. This method is applicable for UCA array to estimate the

azimuth and elevation angles. The DOAs are estimated with spectral search based approach for UCA. Root MUSIC is a fast subspace method which estimates DOAs with polynomial rooting for ULA. FBSS-MUSIC method is a search based method which can be only applied for ULA due to the Vandermode structure of array manifold. The organization of this chapter is as follows. The signal model and algorithm steps of prior knowledge based methods are given in the second and third part, respectively. In the fourth part, simulation results of the algorithms are illustrated.

6.1 Signal Model

Assume that *d* narrow-band signals impinging on an m element ULA from directions $\bar{\theta} = \begin{bmatrix}\theta^{\mathrm{T}} & \vartheta^{\mathrm{T}}\end{bmatrix}^{\mathrm{T}}$ where θ and ϑ indicate DOA angles of unknown and known sources, respectively. Inter element spacing between the array elements is equal to half wavelength as $(\lambda/2)$. The signals and noise are modeled as zero-mean, i.i.d. circularly symmetric complex Gaussian random processes. The array output is written as [43],

$$\mathbf{y}(t) = \mathbf{A}(\bar{\theta})\mathbf{x}(t) + \mathbf{n}(t), \quad t = 0, \ldots, N-1. \tag{6.1}$$

where $\mathbf{x}(t) \in \mathbb{C}^{d\times 1}$ denotes signal vector, $\mathbf{A}(\bar{\theta}) \in \mathbb{C}^{m\times d}$ denotes array steering matrix and $\mathbf{n}(t) \in \mathbb{C}^{m\times 1}$ denotes noise vector, respectively. Here, *m* indicates the number of array elements and *d* is the number of signal sources. The unknown and known terms are stated as subindexes *u* and *k*, i.e, d_u means the number of unknown signals. The spatial covariance matrices of signal and noise vectors represented as $cov(\mathbf{x}(t)) = \mathbf{P}$ and $cov(\mathbf{n}(t)) = \sigma^2\mathbf{I}$. Then, the covariance matrix of array output can be written as,

$$\mathbf{R} = \mathbf{A}\mathbf{P}\mathbf{A}^H + \sigma^2\mathbf{I} \tag{6.2}$$

where $(.)^H$ denotes conjugate-transpose operator. The steering matrix and covariance matrix of signal vector are represented as,

$$\mathbf{A}(\bar{\theta}) = [\mathbf{A}(\theta) \quad \mathbf{A}(\vartheta)] \triangleq [\mathbf{A}_u \quad \mathbf{A}_k] \tag{6.3}$$

$$\mathbf{P} = \begin{bmatrix}\mathbf{P}_u & \mathbf{P}_{uk} \\ \mathbf{P}_{uk}^H & \mathbf{P}_k\end{bmatrix} \tag{6.4}$$

In (6.3), $\mathbf{A}_u$ and $\mathbf{A}_k$ denote the steering matrix of unknown sources and known sources, respectively. In (6.4), $\mathbf{P}_u$, $\mathbf{P}_k$ and $\mathbf{P}_{uk}$ matrices denote correlation matrix of unknown signals, known signals and cross correlation matrix of unknown and known signals, respectively. The assumptions about prior information about known signals and correlation between the unknown and known signals will be explained in the algorithm steps of prior-knowledge based methods.

6.2 POWDER Method

Prior Orthogonally Weighted Direction Estimator (POWDER) algorithm [4] exploits the prior knowledge about some of the DOAs associated to signal sources are known and correlation state between some of the signal sources. Using the prior information in the estimator is beneficial as it will be shown in the simulation results. POWDER algorithm assumes that known and unknown signals are uncorrelated ($\mathbf{P}_{uk} = 0$). There is no assumption made about the correlation between the subset of unknown and known signals. $\mathbf{P}_u$ and $\mathbf{P}_k$ matrices can be uncorrelated or coherent. The algorithm steps of POWDER estimator in [4] will be explained in the following.
Firstly, the noise-free array output covariance matrix is obtained.

$$\mathbf{R} - \sigma^2\mathbf{I} = \mathbf{A}\mathbf{P}\mathbf{A}^H = [\mathbf{A}_u \quad \mathbf{A}_k] \begin{bmatrix} \mathbf{P}_u & \mathbf{P}_{uk} \\ \mathbf{P}_{uk}^H & \mathbf{P}_k \end{bmatrix} \begin{bmatrix} \mathbf{A}_u^H \\ \mathbf{A}_k^H \end{bmatrix} \tag{6.5}$$

Then, the known signal subspace of the steering matrix is removed by multiplying the orthogonal projector matrix $\mathbf{\Pi}_{\mathbf{A}_k}^{\perp}$ from the left of equation (6.2) ($\mathbf{A}_k^H\mathbf{\Pi}_{\mathbf{A}_k}^{\perp} = 0$) [3]-[33] as

$$\begin{aligned} (\mathbf{R} - \sigma^2\mathbf{I})\mathbf{\Pi}_{\mathbf{A}_k}^{\perp} &= \mathbf{A}_u\mathbf{P}_u\mathbf{A}_u^H\mathbf{\Pi}_{\mathbf{A}_k}^{\perp} + \mathbf{A}_k\mathbf{P}_{uk}^H\mathbf{A}_u^H\mathbf{\Pi}_{\mathbf{A}_k}^{\perp} \\ &= \mathbf{A}_u\mathbf{P}_u\mathbf{A}_u^H\Pi_{\mathbf{A}_k}^{\perp} = \mathbf{U}_s\mathbf{\Sigma}_s\mathbf{V}_s^H \end{aligned} \tag{6.6}$$

In equation (6.6), the second equality is obtained because of $\mathbf{P}_{uk} = 0$. In third equality, $\mathbf{U}_s$,$\mathbf{\Sigma}_s$ and $\mathbf{V}_s$ terms are the singular values of the unknown signal sources generated by singular value decomposition. In practice, we compute the sample covariance matrix to estimate $\mathbf{R}$ from the array output,

$$\hat{\mathbf{R}} = \frac{1}{N}\sum_{t=1}^{N}\mathbf{y}(t)\mathbf{y}^H(t) \tag{6.7}$$

Performing eigendecomposition of $\hat{\mathbf{R}}$, we can obtain $\hat{\mathbf{E}}_s$ and $\hat{\mathbf{E}}_n$ matrices which span signal and noise subspace of array output covariance matrix respectively.

$$\hat{\mathbf{R}} = \hat{\mathbf{E}}_s \hat{\mathbf{\Lambda}}_s \hat{\mathbf{E}}_s^H + \hat{\mathbf{E}}_n \hat{\mathbf{\Lambda}}_n \hat{\mathbf{E}}_n^H \tag{6.8}$$

The noise power can be estimated as

$$\hat{\sigma}^2 = \frac{1}{m - d'} \mathrm{Tr}(\hat{\mathbf{\Lambda}}_n) \tag{6.9}$$

d' is the rank of the signal subspace. ($d' = rank(\mathbf{P}_{uk}) + rank(\mathbf{P}_k)$). Using sample covariance matrix in (6.7) and the noise power estimate in (6.9), (6.6) can be rewritten as

$$\left(\hat{\mathbf{R}} - \hat{\sigma}^2 \mathbf{I}\right) \mathbf{\Pi}^{\perp}_{\mathbf{A}_k} = \hat{\mathbf{U}}_s \hat{\mathbf{\Sigma}}_s \hat{\mathbf{V}}_s^H + \hat{\mathbf{U}}_n \hat{\mathbf{\Sigma}}_n \hat{\mathbf{V}}_n^H \tag{6.10}$$

In (6.10), the singular vectors corresponding to unknown source signals are shown with $\hat{\mathbf{U}}_s$ and $\hat{\mathbf{\Sigma}}_s$ and the ones corresponding to noise subspace are shown with $\hat{\mathbf{U}}_n$ and $\hat{\mathbf{\Sigma}}_n$. Using the orthogonality between $\hat{\mathbf{V}}_s$ and $\hat{\mathbf{V}}_n^H$, (6.10) is written as

$$\hat{\mathbf{U}}_s = \left(\hat{\mathbf{R}} - \hat{\sigma}^2 \mathbf{I}\right) \mathbf{\Pi}^{\perp}_{\mathbf{A}_k} \hat{\mathbf{V}}_s \hat{\mathbf{\Sigma}}_s^{-1} \tag{6.11}$$

To estimate the unknown signals from $\hat{\mathbf{U}}_s$, we define $\mathbf{B} \in \mathbb{C}^{m \times m - d_u}$ matrix which spans the null space of steering matrix corresponding to the unknown signals $\mathbf{A}_u^H$ (i.e $\mathbf{B}^H \mathbf{A}_u = 0$). Using (6.11) and the equality $\mathbf{B}^H \mathbf{U}_s = 0$, we can write the criterion function as,

$$\mathbf{B}^H \hat{\mathbf{U}}_s = \mathbf{B}^H \left(\hat{\mathbf{R}} - \hat{\sigma}^2 \mathbf{I}\right) \mathbf{\Pi}^{\perp}_{\mathbf{A}_k} \hat{\mathbf{V}}_s \hat{\mathbf{\Sigma}}_s^{-1} \tag{6.12}$$

where **B** matrix defined as

$$\mathbf{B}(\theta) = \begin{bmatrix} b_0 & b_1 & \cdots & b_{d_u} & & \mathbf{0} \\ & \ddots & \ddots & & \ddots & \\ \mathbf{0} & & b_0 & b_1 & \cdots & b_{d_u} \end{bmatrix}^T \tag{6.13}$$

and b_i are the coefficients of the polynomial

$$b_0 \prod_{i=1}^{d_u} (z - e^{-j\pi \sin(\theta_i)}) \triangleq b_0 z^{d_u} + b_1 z^{d_u - 1} + \ldots + b_{d_u} \tag{6.14}$$

The true DOA angles parameterize $\mathbf{B}$ matrix through (6.14), so minimization of (6.12) with respect to **B** matrix gives unknown DOA angle estimates. So the DOA estimation problem is reduced to polynomial rooting for ULA. A search based method

should be used for arbitrary arrays in general.

Now, we will express the detailed steps of criterion function minimization. To construct the criterion function, residual vector is defined as $\boldsymbol{\epsilon} = \mathrm{vec}(\hat{\mathbf{U}}_s^H \mathbf{B})$. Then, the criterion function becomes,

$$\hat{\theta} = \arg\min_{\theta} \boldsymbol{\epsilon}^H \mathbf{W} \boldsymbol{\epsilon} \tag{6.15}$$

where $\mathbf{W} > 0$ is a positive definite weighting matrix. The weighting matrix is chosen to minimize the asymptotic variance of the unknown doa angle estimates. The elements of $\mathbf{B}$ matrix are collected as vector $\mathbf{b} = [b_0\, b_1 \cdots b_{du}]^T$. Using the coefficient vector $\mathbf{b}$, the residual vector can be written as

$$\boldsymbol{\epsilon} = \mathrm{vec}\left(\hat{\mathbf{U}}_s^H \mathbf{B}\right) = \left(\mathbf{I}_{m-d} \otimes \hat{\mathbf{U}}_s^H\right) \mathrm{vec}(\mathbf{B}) \triangleq \mathbf{K}\mathbf{b} \tag{6.16}$$

where $\mathbf{K} = (\mathbf{I}_{m-d} \otimes \hat{\mathbf{U}}_s^H)\Psi$. The selection matrix Ψ is obtained from $\mathrm{vec}(\mathbf{B}) = \Psi \mathbf{b}$. The identity $\mathrm{vec}(\mathbf{ABC}) = (\mathbf{C}^T \otimes \mathbf{A})\mathrm{vec}(\mathbf{B})$ is used in (6.16) where the $\mathbf{A}$, $\mathbf{B}$ and $\mathbf{C}$ matrices are compatible in dimension. Using (6.16), the criterion function in (6.15) can be written as

$$V(\theta) = \boldsymbol{\epsilon}^H \mathbf{W} \boldsymbol{\epsilon} = \mathbf{b}^H \mathbf{K}^H \mathbf{W} \mathbf{K} \mathbf{b} \tag{6.17}$$

The minimization of the criterion function in (6.17) is done according to weighting matrix $\mathbf{W}$. The weighting matrix is defined as

$$\mathbf{W} = \mathrm{E}[\boldsymbol{\epsilon}\boldsymbol{\epsilon}^H]^{-1} \tag{6.18}$$

which produces the minimum variance estimates of unknown DOAs in (6.17) [44]. In order to find a solution to the weighting matrix in (6.18), using (6.10) the residual vector in (6.16) is rewritten as

$$\begin{aligned} \boldsymbol{\epsilon} &= \mathrm{vec}\left(\hat{\mathbf{U}}_s^H \mathbf{B}\right) \\ &= \left(\mathbf{B}^{\mathrm{T}} \otimes \boldsymbol{\Sigma}_s^{-1} \mathbf{V}_s^H \boldsymbol{\Pi}_{\mathbf{A}_k}^{\perp}\right) \mathrm{vec}\left(\hat{\mathbf{R}} - \hat{\sigma}^2 \mathbf{I}\right) \triangleq \mathbf{M}\hat{\mathbf{f}} \end{aligned} \tag{6.19}$$

where $\mathbf{M} = (\mathbf{B}^{\mathrm{T}} \otimes \boldsymbol{\Sigma}_s^{-1} \mathbf{V}_s^H \boldsymbol{\Pi}_{\mathbf{A}_k}^{\perp})$ and $\hat{\mathbf{f}} = \mathrm{vec}(\hat{\mathbf{R}} - \hat{\sigma}^2 \mathbf{I})$, respectively. The noise power estimate can be written as in [45], $\hat{\sigma}^2 = \frac{1}{m-d'} \mathrm{vec}^H(\mathbf{I}_m - \mathbf{E}_s \mathbf{E}_s^H) \mathrm{vec}(\hat{\mathbf{R}})$, then using the noise power estimate in (6.19), $\hat{\mathbf{f}}$ can be written as

$$\hat{\mathbf{f}} = \mathrm{vec}(\hat{\mathbf{R}}) - \frac{1}{m-d'} \mathrm{vec}(\mathbf{I}_m) \mathrm{vec}^H(\mathbf{I}_m - \mathbf{E}_s \mathbf{E}_s^H) \mathrm{vec}(\hat{\mathbf{R}}) \tag{6.20}$$

H matrix can be defined as

$$\mathbf{H} = \mathbf{M}\left(\mathbf{I}_{m^2} - \frac{1}{m-d'}\mathrm{vec}(\mathbf{I}_m)\mathrm{vec}^H(\mathbf{I}_m - \mathbf{E}_s\mathbf{E}_s^H)\right) \tag{6.21}$$

The residual vector can be written in terms of **H** matrix as, $\epsilon = \mathbf{H}vec(\hat{\mathbf{R}})$. Using the result in [44], the covariance matrix of $\hat{\mathbf{R}}$ is $cov(vec(\hat{\mathbf{R}})) = N^{-1}(\mathbf{R}^T \otimes \mathbf{R})$ Hence, we find

$$\mathrm{E}[\boldsymbol{\epsilon}\boldsymbol{\epsilon}^H] = \frac{1}{N}\mathbf{H}(\mathbf{R}^{\mathrm{T}} \otimes \mathbf{R})\mathbf{H}^H \tag{6.22}$$

which is a full rank matrix respectively. Using (6.22) in (6.18), we can find the weighting matrix to minimize the cost function in (6.17).
The summary of POWDER method is given as follows [4]:

- 1: Input estimated covariance matrix $(\hat{\mathbf{R}})$, number of source signals (d), number of non-coherent unknown DOA $(d_u{}')$, number of non-coherent known DOA $(d_k{}')$, DOA parameters of known sources ϑ, tolerance factor for estimated unknown DOA angles (tol) or maximum iteration number for minimization(iter).
- 2: Find from the Input, the number of array elements(*m*), the selection matrix $(\mathbf{\Psi})$, projection matrix orthogonal to the known signal subspace $(\mathbf{\Pi}^{\perp}_{\mathbf{A}_k})$, noise subspace eigenvalues of estimated covariance matrix $(\hat{\mathbf{\Lambda}}_n)$, signal subspace eigenvector of estimated covariance matrix $(\hat{\mathbf{E}}_s)$.
- 3: Estimate the noise power as, $(\hat{\sigma}^2 = \frac{1}{m-d'}\mathrm{Tr}(\hat{\mathbf{\Lambda}}_n))$.
- 4: Find the singular vectors $\hat{\mathbf{U}}_s$,$\hat{\mathbf{\Sigma}}_s$ and $\hat{\mathbf{V}}_s^H$ corresponding to $(d_u{}')$ principal singular values from the SVD of $(\hat{\mathbf{R}} - \hat{\sigma}^2\mathbf{I})\mathbf{\Pi}^{\perp}_{\mathbf{A}_k}$.
- 5: Initialize **B** matrix from $\mathbf{b} = [1\,0\,\cdots\,0]$, **K** matrix from $\mathbf{K} = (\mathbf{I}_{m-d} \otimes \hat{\mathbf{U}}_s^H)\Psi$, and iteration number to zero (iter = 0).
- 6: **repeat**
  - 7: Find the weighting matrix, $\hat{\mathbf{W}}^{iter}$.
  - 8: Find the estimated unknown DOA angles $\hat{\theta}^{iter+1}$ by minimizing (6.17).
  - 9: Find $\mathbf{B}^{iter+1}$ matrix from $\hat{\theta}^{iter+1}$ and update $\hat{\mathbf{M}}^{iter+1}$ from the equation $\mathbf{M} = (\mathbf{B}^{\mathrm{T}} \otimes \mathbf{\Sigma}_s^{-1}\mathbf{V}_s^H\mathbf{\Pi}^{\perp}_{\mathbf{A}_k})$.

- 10: Increase the iteration number.

- 11: **until** ($|\hat{\theta}^{iter}$ - $\hat{\theta}^{iter\text{-}1}| < tol$) OR ($iter > iter_{max}$).

- 12: Output: $\hat{\theta}^{iter}$ as the final estimated unknown DOA angle.

6.3 PLEDGE Method

Prior Knowledge(PLEDGE) [3]-[33] is an extension of Method of Direction Estimation (MODE)[32] algorithm. MODE is a Maximum Likelihood estimator which minimizes a criterion function according to subspace projection. MODE estimates all of the angles of arrival and does not use the a-priori information about the known DOAs. There is no assumption made for signal correlation matrix $\mathbf{P}$ for MODE. Eigendecomposition of sample correlation matrix $\hat{\mathbf{R}}$ as in (6.8) is performed to find the eigenvectors and eigenvalues $\hat{\mathbf{E}}_s$, $\hat{\mathbf{\Lambda}}_s$ and $\hat{\mathbf{E}}_n$, $\hat{\mathbf{\Lambda}}_n$ corresponding to signal and noise subspace, respectively. The derivation of MODE and PLEDGE algorithms will be given from [33] in this section. Define a polynomial which is based on the true DOA angles as,

$$b_0 z^d + b_1 z^{d-1} + \ldots + b_d = b_0 \prod_{i=1}^{d} (z - e^{-j\pi \sin(\theta_i)}). \tag{6.23}$$

Roots of the polynomial are on the unit circle and conjugate symmetric, where $b_i = {b_{d-i}}^H$. Using the polynomial coefficients in (6.23), $\mathbf{B}^H \in \mathbb{C}^{(m-d)\times m}$ matrix is defined as

$$\mathbf{B}^H = \begin{bmatrix} b_d & b_1 & \cdots & b_{d_0} & & \mathbf{0} \\ & \ddots & \ddots & & \ddots & \\ \mathbf{0} & & b_d & \cdots & b_1 & b_0 \end{bmatrix}^T \tag{6.24}$$

and b_i are the coefficients of the polynomial in (6.23). The criterion function for MODE algorithm is defined as [32],

$$V_{MODE}(\mathbf{b}) = Tr[\mathbf{B}(\hat{\mathbf{B}}^H\hat{\mathbf{B}})^{-1}\mathbf{B}^H\hat{\mathbf{E}}_s\hat{\mathbf{\Lambda}}\hat{\mathbf{E}}_s^H] \tag{6.25}$$

where $\hat{\mathbf{\Lambda}} = {\hat{\mathbf{\Lambda}}_\mathbf{s}}^{-1}(\hat{\mathbf{\Lambda}}_\mathbf{s} - \hat{\sigma}^2\mathbf{I})^2$ is the noise free signal subspace eigenvalue matrix, and ($\hat{\sigma}^2 = \frac{1}{m-d'}\mathrm{Tr}(\hat{\mathbf{\Lambda}}_n)$) is the noise power estimate. $\hat{\mathbf{B}}$ is defined from the estimate of $\mathbf{b} = [b_0, b_1, \cdots, b_d]^T$. $(\hat{\mathbf{B}}^H\hat{\mathbf{B}}) = \mathbf{I}$ is initialized and the cost function of MODE in

(6.25) is minimized with estimated $\tilde{\mathbf{b}}$ coefficients in iterative process. The criterion function in (6.25) can be written as

$$V_{MODE}(\mathbf{b}) = \|Hb\|^2 \tag{6.26}$$

where $\mathbf{H}$ matrix is estimated with the coefficient vector $\tilde{\mathbf{b}}$. The true DOA angles parameterize $\hat{\mathbf{B}}$ matrix through equation (6.23), so minimization of (6.26) with respect to $\hat{\mathbf{B}}$ matrix gives unknown DOA angle estimates. The angles of the roots found from polynomial (6.23) provide the DOA angle estimates.

We will give a brief summary about the estimation of $\mathbf{H}$ matrix from [32] which is used for minimizing the cost function of MODE and PLEDGE algorithms. Consider *n* narrow-band signals on *m*-element ULA. The rank of signal correlation matrix is shown as d'. The noise power estimate is calculated from the noise subspace eigenvalues as in (6.27).

$$\hat{\sigma}^2 = \frac{1}{(m-n)}\mathrm{Tr}(\hat{\mathbf{\Lambda}}_n) \tag{6.27}$$

The cost function for MODE method is defined as,

$$\hat{\theta} = \arg\min_{\mathbf{b}\in\mathbf{D}} f_W(\mathbf{b}) \tag{6.28}$$

where the initial value of $\mathbf{W}$ is an identity matrix and $\mathbf{W} = (\hat{\mathbf{B}}^H\hat{\mathbf{B}})$. $\hat{\mathbf{B}}$ is constructed by the estimated $\tilde{\mathbf{b}}$ coefficients. In (6.28), $\mathbf{D}$ is the non-zero roots of polynomial defined in (6.23). A matrix with size $(m \times d')$ is defined as,

$$[\tilde{\mathbf{s}}_1, \cdots, \tilde{\mathbf{s}}_n] = \begin{bmatrix} \tilde{\mathbf{s}}_{1,1} & \cdots & \tilde{\mathbf{s}}_{1,n} \\ \cdots & \cdots & \cdots \\ \tilde{\mathbf{s}}_{m,1} & \cdots & \tilde{\mathbf{s}}_{m,n} \end{bmatrix} = \hat{\mathbf{S}}\left(\hat{\mathbf{\Lambda}} - \hat{\sigma}\mathbf{I}\right)^{1/2} \tag{6.29}$$

where $\hat{\mathbf{S}}$ is the $(m \times d')$ signal subspace matrix, and $\left(\hat{\mathbf{\Lambda}} - \hat{\sigma}\mathbf{I}\right)^{1/2}$ is the $(d' \times d')$ square root of noise free signal subspace eigenvalues. Then, it is observed from (6.29) that, an equality in (6.30) can be defined as,

$$\mathbf{B}^H\tilde{\mathbf{s}}_k = \begin{bmatrix} \tilde{\mathbf{s}}_{n+1,k} & \cdots & \tilde{\mathbf{s}}_{1,k} \\ \cdots & \cdots & \cdots \\ \tilde{\mathbf{s}}_{m,k} & \cdots & \tilde{\mathbf{s}}_{m-n,k} \end{bmatrix} \mathbf{b} \triangleq \tilde{\mathbf{S}}_k\mathbf{b} \tag{6.30}$$

where $\mathbf{B}^H$ is an $(m-n) \times m$ Slyvester matrix formed in (6.24) and $\tilde{\mathbf{s}}_k$ is a $(m \times 1)$ vector which is the n^{th} column of (6.29). $\tilde{\mathbf{S}}_k$ is a $(m-n) \times (n+1)$ non-symmetric Toeplitz

matrix which is formed by the each column of (6.30). Then, assume Cholesky multiplier of W matrix is $W^{1/2}$. Then, a matrix is defined as,

$$\mathbf{H} = \begin{bmatrix} \tilde{\mathbf{W}}^{1/2} & \tilde{\mathbf{S}}_1 \\ \cdots & \cdots \\ \tilde{\mathbf{W}}^{1/2} & \tilde{\mathbf{S}}_n \end{bmatrix} \tag{6.31}$$

where the size of $\mathbf{H}$ matrix is $n(m-n) \times (n+1)$.

Hence, the criterion function for MODE method defined in 6.28 can be rewritten in terms of $\mathbf{H}$ as,

$$f_W(\mathbf{b}) \|\mathbf{H}\mathbf{b}\|^{\mathbf{2}} \tag{6.32}$$

where $\|.\|^2$ denotes the norm of a matrix. Thus, the derivation of $\mathbf{H}$ matrix and the criterion function of MODE in terms of $\mathbf{H}$ matrix is summarized.

PLEDGE algorithm is applied to the MODE to use the a-priori knowledge in the estimator. In PLEDGE, knowing some of the DOA angles means knowing some of the roots of the polynomial defined in (6.23). The polynomial can be splitted into two parts as

$$b_0 = \prod_{i=1}^{d} (z - e^{-j\pi \sin(\theta_i)}) = \mathbf{P}_k(z)\mathbf{P}_u(z) \tag{6.33}$$

where

$$\mathbf{P}_u(z) = \tilde{b_0} \prod_{i=1}^{d_u} (z - e^{-j\pi \sin(\bar{\theta_i})}) = \tilde{b_0} z^{d_u} + \ldots + \tilde{b}_{d_u} \tag{6.34}$$

and

$$\mathbf{P}_k(z) = \tilde{b_0} \prod_{i=d_u+1}^{d} (z - e^{-j\pi \sin(\bar{\theta_i})}) = c_0 z^{d_k} + \ldots + c_{d_k} \tag{6.35}$$

$\mathbf{P}_k(z)$ is the polynomial of the known DOA angles with d_k roots and $\mathbf{P}_u(z)$ has d_u roots related to the unknown DOA angles. The polynomial coefficients of $\mathbf{P}_k(z)$ and $\mathbf{P}_u(z)$ are defined as $\mathbf{c} = [c_0, \ldots, c_{d_k}]$ and $\tilde{\mathbf{b}} = [\tilde{b_0}, \tilde{b_1}, \ldots, \tilde{b_{d_u}}]$, respectively. The polynomial coefficients of (6.33) can be written as convolution of $\tilde{\mathbf{b}}$ and $\mathbf{c}$ in the form of matrix as

$$\mathbf{b} = \mathbf{C}\tilde{\mathbf{b}} \tag{6.36}$$

where $\mathbf{C} \in \mathbb{C}^{(d_u+1)\times(d+1)}$ is a Toeplitz matrix

$$\mathbf{C} = \begin{bmatrix} c_0 & c_1 & \cdots & c_{d_k} & & \mathbf{0} \\ & \ddots & \ddots & & \ddots & \\ \mathbf{0} & & \cdots & c_0 & c_1 & c_{d_k} \end{bmatrix}^T \tag{6.37}$$

and the elements of $\mathbf{C}$ matrix is constructed from the known DOAs coefficient vector $\mathbf{c}$. Using (6.36) in (6.26), the criterion function for the PLEDGE algorithm is defined as

$$V_{PLEDGE}(\mathbf{b}) = \|\mathbf{HC}\tilde{\mathbf{b}}\|^2 \tag{6.38}$$

The summary of the PLEDGE algorithm is given as follows [33]:

- 1: Compose Toeplitz $\mathbf{C}$ matrix with the known DOA angles.
- 2: Eigendecompose the sample covariance matrix $\hat{\mathbf{R}}$ and initialize $(\hat{\mathbf{B}}^H\hat{\mathbf{B}})^{-1} = \mathbf{I}$. Then form $\mathbf{H}$ with the equalities from (6.27) to (6.31).
- 3: Minimizing the cost function in (6.38), find the estimates of $\tilde{\mathbf{b}}$ which are conjugate symmetric and $\|\mathbf{b}\| = \mathbf{1}$. Using the estimated coefficients $\tilde{\mathbf{b}}$ in (6.36), form $(\hat{\mathbf{B}}^H\hat{\mathbf{B}})^{-1}$ matrix and update $\mathbf{H}$ matrix.
- 4: Minimize the PLEDGE cost function in (6.38) again to find polynomial coefficients $\tilde{\mathbf{b}}$, then find the unknown DOAs by rooting the polynomial in (6.34).

6.4 Constrained-MUSIC Method

Constrained MUSIC(C-MUSIC) [2] method uses a-priori information about the known DOAs in the estimator. This method applies orthogonal projection to the sample covariance matrix of the array output. The known signal subspace extracted by pre- and post-multiplying orthogonal projection matrix with the sample covariance matrix. Thus, reduced dimension data set only includes signal subspace of unknown signals. The derivation of the C-MUSIC algorithm [2] is given in this section. The sample covariance matrix $\hat{\mathbf{R}}$ is calculated from the array output. The eigenstructure of the covariance matrix is shown as

$$\hat{\mathbf{R}} = \hat{\mathbf{V}}\hat{\mathbf{\Lambda}}\hat{\mathbf{V}}^H = \begin{bmatrix}\hat{\mathbf{V}}_s & \hat{\mathbf{V}}_n\end{bmatrix}\begin{bmatrix}\hat{\mathbf{\Lambda}}_s & 0\\ 0 & \hat{\mathbf{\Lambda}}_n\end{bmatrix}\begin{bmatrix}\hat{\mathbf{V}}_s^H\\ \hat{\mathbf{V}}_n^H\end{bmatrix} \tag{6.39}$$

where $\hat{\mathbf{V}}_s, \mathbf{\Lambda}_s$ and $\hat{\mathbf{V}}_n, \mathbf{\Lambda}_n$ denotes signal and noise subspace eigenvectors and eigenvalues, respectively. Define $\mathbf{A}_c$ matrix whose columns are constructed from steering

vectors of known signals. Then, applying QR decomposition to $\mathbf{A}_c$ we have,

$$\mathbf{A}_c = \left[\mathbf{Q}_{c1}^{(m\times d_k)}\mathbf{Q}_{c2}^{(m\times(m-d_k))}\right]\begin{bmatrix}\mathbf{T}_{c1}^{(d_k\times d_k)}\\ \mathbf{0}^{(m-d_k)\times d_k)}\end{bmatrix} \tag{6.40}$$

where m is the number of array elements, $\mathbf{d}_k$ is number of known signals and $(.)^H$ denotes conjugate transpose, respectively. In (6.40), $\mathbf{Q}_{c1}$ has an orthonormal basis for the columns of $\mathbf{A}_c$ matrix. Spectral MUSIC algorithm [9] minimizes following function without using the a-priori knowledge about the known sources as,

$$f(\theta) = \arg\min_{\theta} \mathbf{a}^H(\theta)\hat{\mathbf{V}}_n\hat{\mathbf{V}}_n^H\mathbf{a}(\theta) \tag{6.41}$$

where $\hat{\mathbf{V}}_n$ is the noise subspace eigenvector of $\hat{\mathbf{R}}$. To use the constrained information in $\mathbf{Q}_{c1}$ about known DOAs, pre- and post- multiply the correlation matrix with projection matrix $\mathbf{Q}_{c2}\mathbf{Q}_{c2}^H$ which is orthogonal to the known signals found in (6.40) as,

$$\hat{\mathbf{R}}_c = \mathbf{Q}_{c2}\mathbf{Q}_{c2}^H\hat{\mathbf{R}}\mathbf{Q}_{c2}\mathbf{Q}_{c2}^H \tag{6.42}$$

where $\hat{\mathbf{R}}_c$ matrix contains only the unknown signals and noise subspace. The eigenstructure of $\hat{\mathbf{R}}_c$ matrix can give the estimates of unknown signals. In [2], another efficient method is given to estimate unknown signals.

Define $\hat{\mathbf{S}}_c$ matrix from (6.42) as

$$\hat{\mathbf{S}}_c = \mathbf{Q}_{c2}^H\hat{\mathbf{R}}\mathbf{Q}_{c2} \tag{6.43}$$

and (6.42) can be rewritten in terms of $\hat{\mathbf{S}}_c$.

$$\hat{\mathbf{R}}_c = \mathbf{Q}_{c2}\hat{\mathbf{S}}_c\mathbf{Q}_{c2}^H \tag{6.44}$$

The sample covariance matrix $\hat{\mathbf{R}}$ is $m \times m$, but the $\mathbf{S}_c$ matrix is $(m - d_k) \times (m - d_k)$. Because the known signal subspace removed by $\mathbf{Q}_{c2}$ matrix. The efficiency of estimating unknown DOA angles with $\hat{\mathbf{S}}_c$ instead of $\hat{\mathbf{R}}_c$ is given in the following.

The eigenstructure of $\hat{\mathbf{S}}_c$ matrix is given as,

$$\begin{aligned}\hat{\mathbf{S}}_c = \hat{\mathbf{U}}_c\hat{\mathbf{\Lambda}}_c\hat{\mathbf{U}}_c^H = &\begin{bmatrix}\hat{\mathbf{U}}_{cs}^{(m-d_k\times d-d_k)} & \hat{\mathbf{U}}_{cn}^{(m-d_k\times m-d)}\end{bmatrix}\\ &\times\begin{bmatrix}\hat{\mathbf{\Lambda}}_{cs}^{(d-d_k\times d-d_k)} & 0\\ 0 & \hat{\mathbf{\Lambda}}_{cn}^{(m-d\times m-d)}\end{bmatrix}\\ &\times\begin{bmatrix}\hat{\mathbf{U}}_{cs}^H\\ \hat{\mathbf{U}}_{cn}^H\end{bmatrix}\end{aligned} \tag{6.45}$$

Multiply $\hat{\mathbf{S}}_c\hat{\mathbf{U}}_c = \hat{\mathbf{U}}_c\hat{\mathbf{\Lambda}}_c$ from the left by $\mathbf{Q}_{c2}$ and using $\mathbf{Q}_{c2}^H\mathbf{Q}_{c2} = \mathbf{I}$,we obtain

$$\mathbf{Q}_{c2}\hat{\mathbf{S}}_c\mathbf{Q}_{c2}^H\mathbf{Q}_{c2}\hat{\mathbf{U}}_c = \mathbf{Q}_{c2}\hat{\mathbf{U}}_c\hat{\mathbf{\Lambda}}_c \tag{6.46}$$

As $\mathbf{Q}_{c2}\hat{\mathbf{S}}_c\mathbf{Q}_{c2}^H = \hat{\mathbf{R}}_c$ is defined in (6.43), then (6.46) becomes,

$$\hat{\mathbf{R}}_c\mathbf{Q}_{c2}\hat{\mathbf{U}}_c = \mathbf{Q}_{c2}\hat{\mathbf{U}}_c\hat{\mathbf{\Lambda}}_c. \tag{6.47}$$

It can be seen from (6.47) that, $\mathbf{Q}_{c2}\hat{\mathbf{U}}_c$ denotes the eigenvectors of $\hat{\mathbf{R}}_c$ with respect to the eigenvalues of unknown signals. The criterion function for C-MUSIC method in terms the eigenstructure of $\hat{\mathbf{S}}_c$ becomes,

$$f(\theta) = \arg\min_{\theta} \mathbf{a}^H(\theta)\mathbf{Q}_{c2}\hat{\mathbf{U}}_{cn}\hat{\mathbf{U}}_{cn}^H\mathbf{Q}_{c2}^H\mathbf{a}(\theta) \tag{6.48}$$

Thus, the eigenstructure of $\mathbf{S}_c$ matrix should be estimated instead of $\mathbf{R}_c$ to implement C-MUSIC effectively. The roots of the $f(\theta)$ which are closest to the unit circle are computed with root-MUSIC.

The estimation performance of the prior knowledge based methods and subspace based FBSS-MUSIC and Root-MUSIC methods can be summarized in Table 6.1 according to the correlation state between the unknown and known signal sources. $\mathbf{P}_u$, $\mathbf{P}_k$, $\mathbf{P}_{uk}$ denotes the signal correlation between unknown signals, known signals and cross correlation between known and unknown signals. The ✓ expression in the table implies that the algorithm has good estimation performance for the given scenario.

Table 6.1: Summary of the Prior-Knowledge Based and Subspace Based Methods

Correlation State	POWDER Method	PLEDGE Method	C-MUSIC Method	FBSS-MUSIC Method	Root MUSIC Method
Uncorrelated Signals $\mathbf{P}_{uk} = 0$ $\mathbf{P}_u, \mathbf{P}_k$ diagonal.	✓		✓		✓
Coherent Signals $\mathbf{P}_{uk} = 0$ $\mathbf{P}_u, \mathbf{P}_k$ rank deficient.	✓	✓		✓	
Coherent Signals $\mathbf{P}_{uk} \neq 0$ $\mathbf{P}_u, \mathbf{P}_k$ rank deficient.		✓		✓	
Partially Correlated Signals $\mathbf{P}_{uk} \neq 0$ $\mathbf{P}_u, \mathbf{P}_k$ diagonal.		✓	✓		
Partially Correlated Signals $\mathbf{P}_{uk} = 0$ $\mathbf{P}_u, \mathbf{P}_k$ rank deficient.	✓				

6.5 Simulations

In this section, performance of prior-knowledge based methods, C-MUSIC method [2], PLEDGE method [3]-[33], POWDER method [4] and classical subspace based methods which cannot exploit the a-priori information, FBSS-MUSIC [5] and Root-MUSIC in [42] are compared with different simulations. Number of sources, SNR level and number of snapshots, correlation degree between source signals and position of known signals are varied to see the estimation accuracy of the algorithms. The direction of arrival angles are closely separated to increase the difficulty for the estimation problem. Also, the effect of mutual coupling for a non-iterative algorithm in [46] is compared with PLEDGE method to see the estimation performance of latter in the presence of multipath and unknown sensor coupling. The performance of the algorithms are shown with root mean square error(RMSE) of the estimates for DOAs from L Monte Carlo trials for each SNR levels and snapshots as:

$$\mathrm{RMSE}_i = \sqrt{\frac{1}{L}\sum_{k=1}^{L}\left(\hat{\theta}_{ik} - \theta_i\right)^2}, \quad i = 1, \ldots, d_u \tag{6.49}$$

where $\theta_{i,k}$ is the *k*th estimate of *i*th DOA angle and L is the number of Monte Carlo trials.

In the first simulation, suppose four equal power, Gaussian source signals are assumed impinging on a 10 element ULA from directions $\vartheta = [12°20°]$ and $\theta = [10°\ 15°]$. The additive noise is assumed to be temporally and spatially stationary, zero-mean white Gaussian and statistically independent of the signals term. The unknown and known subset of signals are coherent($\mathbf{P}_k$ and $\mathbf{P}_u$ are both coherent) and the cross correlation between unknown and known signals is zero ($\mathbf{P}_{uk} = 0$). The estimation performance is given by 1000 independent Monte Carlo trials for different SNR level and snapshots.

Figure 6.1 and 6.2 show the estimation results of the methods for θ_1 with increasing SNR level and number of snapshots. POWDER method has good estimation accuracy compared to the other methods. Required SNR level for the same estimation accuracy decreased 20dB comparing to the PLEDGE and FBSS-MUSIC methods. Constrained-MUSIC method fails to separate the coherent sources and has a high

RMSE value. Constrained-MUSIC method removes the known signal subspace from the sample covariance matrix using a-priori information. However, the coherency between the unknown signals makes C-MUSIC method suboptimal in this simulation. FBSS-MUSIC method smoothes the correlation matrix and reduces the correlation between the signals. The performance of FBSS-MUSIC method approaches to PLEDGE method for increasing SNR level and number of snapshots. The estimation performance of PLEDGE and POWDER methods are better than FBSS-MUSIC method because of using a-priori knowledge about known DOAs and correlation state between the signal sources in the estimator.

In Figure 6.3 and 6.4, the algorithms are compared for their SNR and number of snapshots performances for the unknown source located at θ_2. As it is seen from these figures, POWDER method outperforms other algorithms for increasing SNR level and number of snapshots. PLEDGE method and FBSS-MUSIC method have nearly same resolution at high SNR levels and number of snapshots. C-MUSIC shows poor estimation performance because of coherence between the unknown source signals.

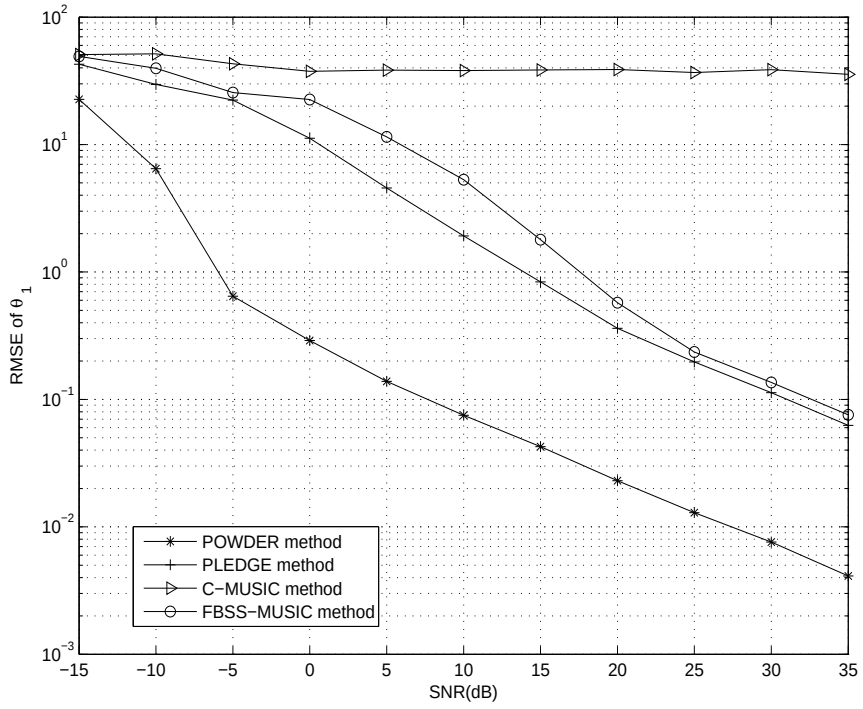

Figure 6.1: Coherent sources: Block Diagonal $\mathbf{P}$, with $\mathbf{P_k}$ and $\mathbf{P_u}$ both coherent. Known sources: $\vartheta = [12°20°]^T$, Unknown sources: $\theta = [10°15°]^T$. Showing RMSE of θ_1 versus SNR with 1000 snapshots.

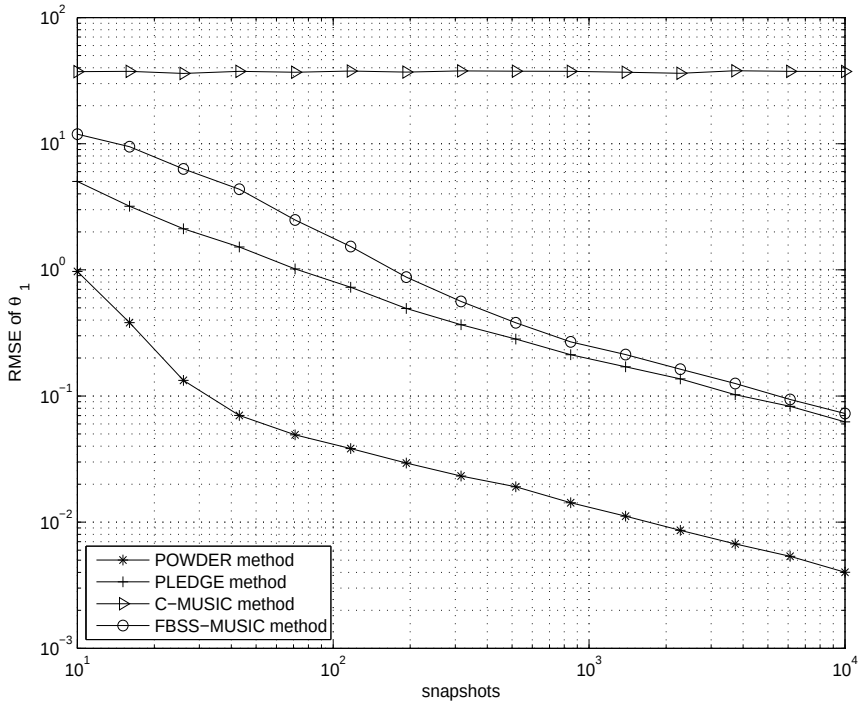

Figure 6.2: Coherent sources: Showing RMSE of θ_1 versus snapshots with SNR = 25dB; other parameters are identical to the case in Figure 6.1.

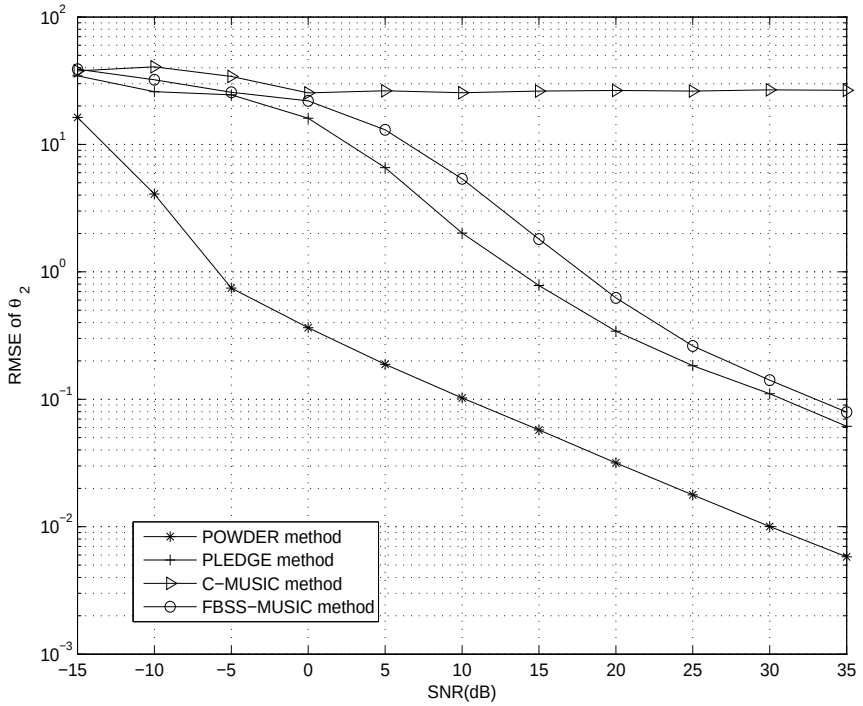

Figure 6.3: Coherent sources: Showing RMSE of θ_2 versus SNR with 1000 snapshots; other parameters are identical to the case in Figure 6.1.

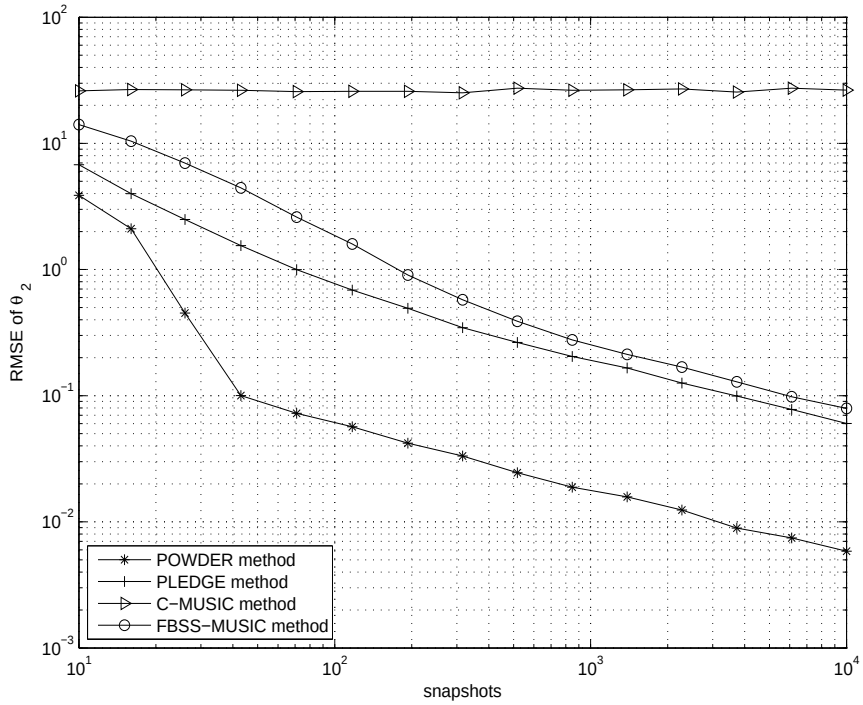

Figure 6.4: Coherent sources: Showing RMSE of θ_2 versus snapshots with SNR = 25dB; other parameters are identical to the case in Figure 6.1.

Figure 6.5, 6.6, 6.7 and 6.8 are the estimation results for uncorrelated source signals. The signal covariance matrix **P** is diagonal. The other parameters are all same with the first simulation.

It is seen from Figure 6.5 and 6.7 that, at low SNR levels POWDER method has better performance as compared to other methods. The estimation accuracy of POWDER, PLEDGE and C-MUSIC methods becomes nearly same as SNR level increases. The RMSE of Root-MUSIC method decreases as SNR level and number of snapshots increases. However, Root-MUSIC method cannot reach to the accuracy bound of other methods because of not using a-priori knowledge in the estimator.

In Figure 6.6 and 6.8, SNR = 25dB and number of snapshots varied. It is seen that, POWDER, PLEDGE and C-MUSIC methods show almost same estimation accuracy for uncorrelated source signals as the number of snapshots increases. The RMSE of Root-MUSIC method is higher than other algorithms because this method can pair the estimated signals with known signals. So, using a-priori knowledge about known DOAs enhanced the accuracy of prior knowledge based methods as compared to Root-MUSIC method for uncorrelated source signals.

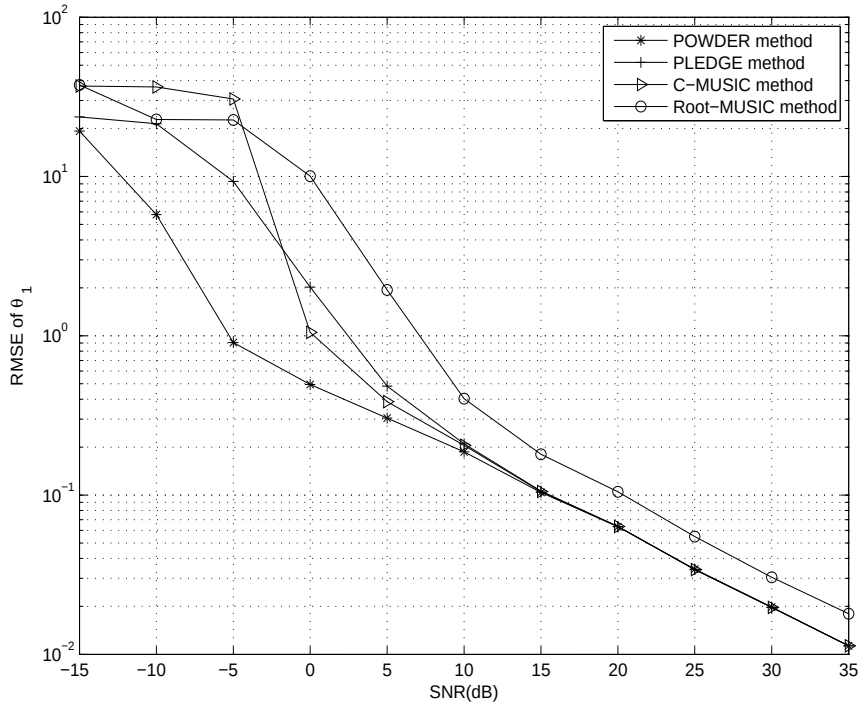

Figure 6.5: Uncorrelated sources: Diagonal $\mathbf{P}$, with $\mathbf{P_k}$ and $\mathbf{P_u}$ both uncorrelated. Known sources: $\vartheta = [12°20°]^T$, Unknown sources: $\theta = [10°15°]^T$. Showing RMSE of θ_1 versus SNR with 1000 snapshots.

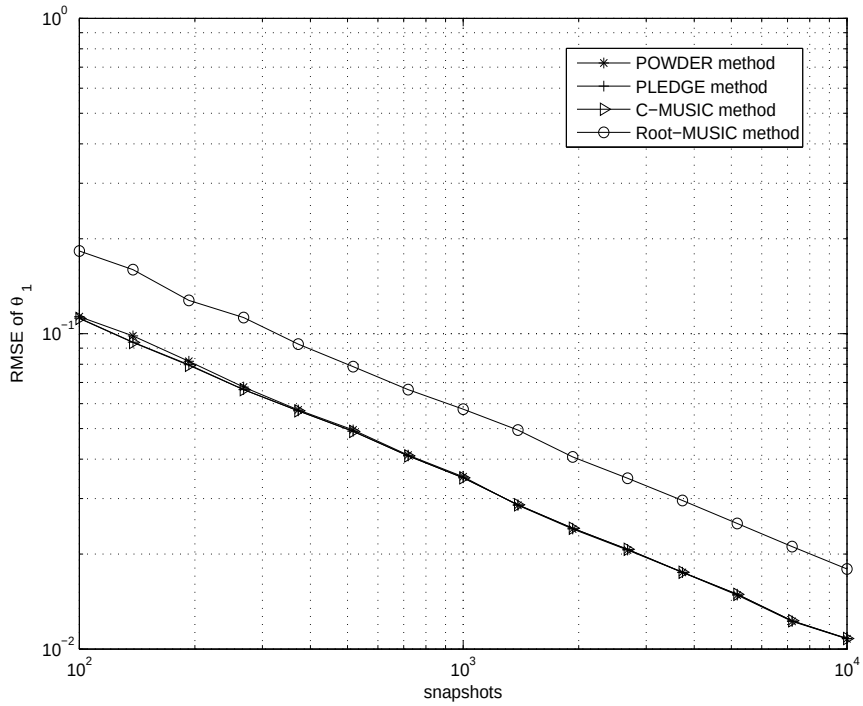

Figure 6.6: Uncorrelated sources: Showing RMSE of θ_1 versus snapshots with SNR = 25dB; other parameters are identical to the case in Figure 6.5.

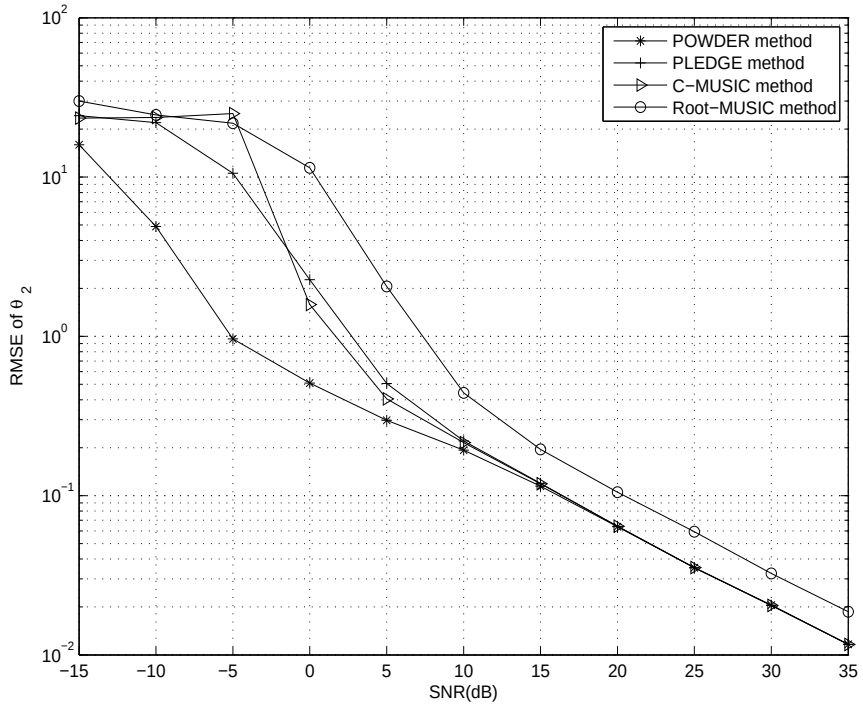

Figure 6.7: Uncorrelated sources: Showing RMSE of θ_2 versus SNR with 1000 snapshots; other parameters are identical to the case in Figure 6.5.

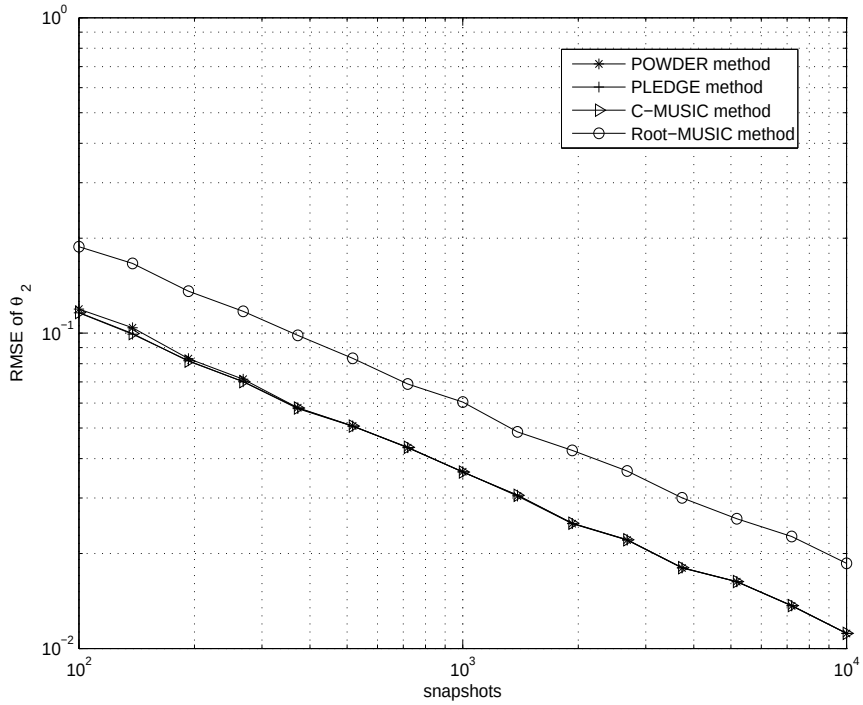

Figure 6.8: Uncorrelated sources: Showing RMSE of θ_2 versus snapshots with SNR = 25dB; other parameters are identical to the case in Figure 6.5.

In the second simulation, the source signals are partially correlated. The DOAs associated to the signal sources are $\overline{\theta}$ = $[\theta_1\, \theta_2\, \vartheta]^T$ = $[10^\circ\, 15^\circ\, 12^\circ]$, where $\vartheta = 12^\circ$ is the known DOA angle. The second unknown signal is uncorrelated with other coherent signals. The correlation coefficients between signals are given as $\rho_{12} = \rho_{23} = 0$ and $\rho_{13} = \exp(-j\pi/12)$. There exists coherence between the unknown source signal at $\theta_\mathbf{1}$ and known source signal at $\vartheta = 12^\circ$. The estimation results for unknown DOA angles are presented in terms of SNR level and number of snapshots.

In Figure 6.9, the estimation results of the algorithms presented for $\theta_\mathbf{1}$ with increasing SNR level. RMSE of POWDER method stays at a constant error value as SNR increases because of correlation between $\theta_\mathbf{1}$ and known signal. However, POWDER method shows good estimation accuracy comparing to the other methods at low SNR levels. PLEDGE method also outperforms C-MUSIC and FBSS-MUSIC at low SNRs. C-MUSIC method removes the coherent signal subspace by using a-priori knowledge about known DOA angle. So, the estimation performance of C-MUSIC method is nearly same with PLEDGE method at high SNRs. The performance of FBSS-MUSIC degrades at low SNR values as compared to the other methods because of matching closely seperated unknown signal with known signal.

In Figure 6.10, the performance of the methods are compared for $\theta_\mathbf{1}$ with increasing snapshots of data. POWDER method again has constant RMSE value due to the cross correlation between unknown and known sources. PLEDGE and C-MUSIC methods show almost same estimation performance as snapshots increases. The performance of FBSS-MUSIC method is degraded at lower snapshots of data because the estimated unknown DOAs are paired with the known DOAs. The RMSE value of FBSS-MUSIC method approaches to PLEDGE and C-MUSIC methods as the number of snapshots increases.

In Figure 6.11, the estimation results of $\theta_\mathbf{2}$ with increasing SNR level is illustrated. $\theta_\mathbf{2}$ is uncorrelated with other mutually coherent sources. It is seen that, POWDER method can achive the same accuracy with lower SNR levels as compared to other methods. The estimation performance of PLEDGE and C-MUSIC methods are almost same at high SNRs. The partial correlation between signal sources decreased the estimation performance of FBSS-MUSIC as compared to the case where the sig-

nal sources are uncorrelated.

In Figure 6.12, the estimation results of θ_2 with increasing number of snapshots is presented. POWDER method outperforms other algorithms by using the a-priori knowledge about known DOAs and the correlation state between the signal sources in the estimator. PLEDGE and C-MUSIC methods show almost same estimation performance as the number of snapshots increases. Prior knowledge based methods enhance their estimation performance by exploiting a-priori information in the estimator at low snapshots of data comparing to FBSS-MUSIC method. The performance of FBSS-MUSIC method is improved as the number of snapshots increases.

It is seen that, utilizing a-priori knowledge about cross correlation between the known and unknown signal sources has a significant role for POWDER method. PLEDGE method which removes the correlation between known and unknown signals in the estimator shows good estimation accuracy for partially correlated sources. PLEDGE method is applicable for estimating coherent, partially correlated and uncorrelated source signals. C-MUSIC removes the coherency between partially correlated signals and estimates remaining uncorrelated signals effectively. Due to the coherency between the closely separated unknown and known signals, the performance of FBSS-MUSIC is degraded at low SNR levels and snapshots as compared to the other algorithms.

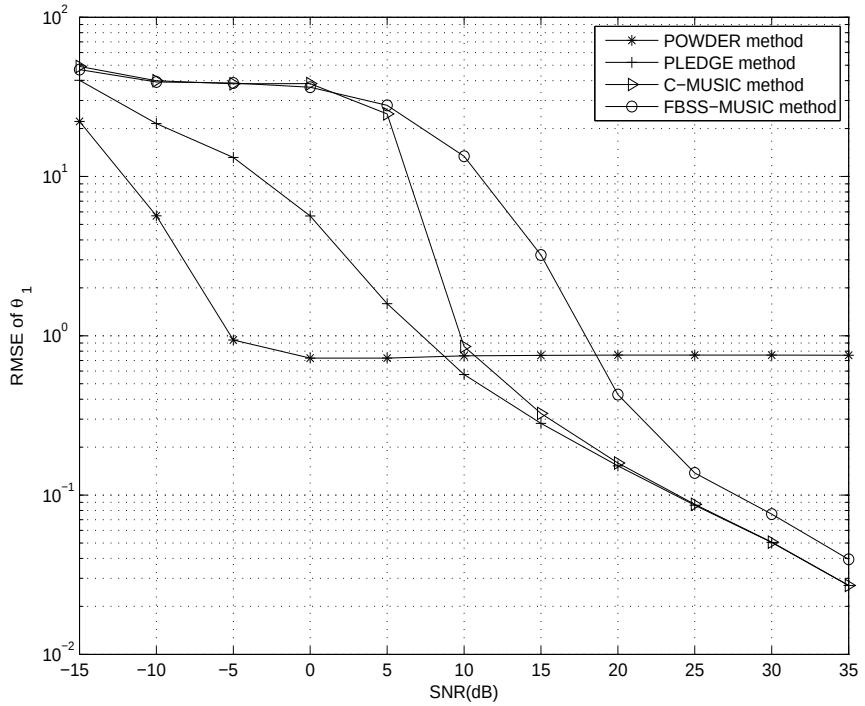

Figure 6.9: Partially-correlated sources: Equipowered source vector: $\overline{\theta}$ = $[\theta_1\, \theta_2\, \vartheta]^T$ = $[10^\circ\, 15^\circ\, 12^\circ]$. θ_2 is uncorrelated with other coherent sources, where, $\rho_{12} = \rho_{23} = 0$ $\rho_{13} = \exp(-j\pi/12)$. Showing RMSE of θ_1 versus SNR with 1000 snapshots.

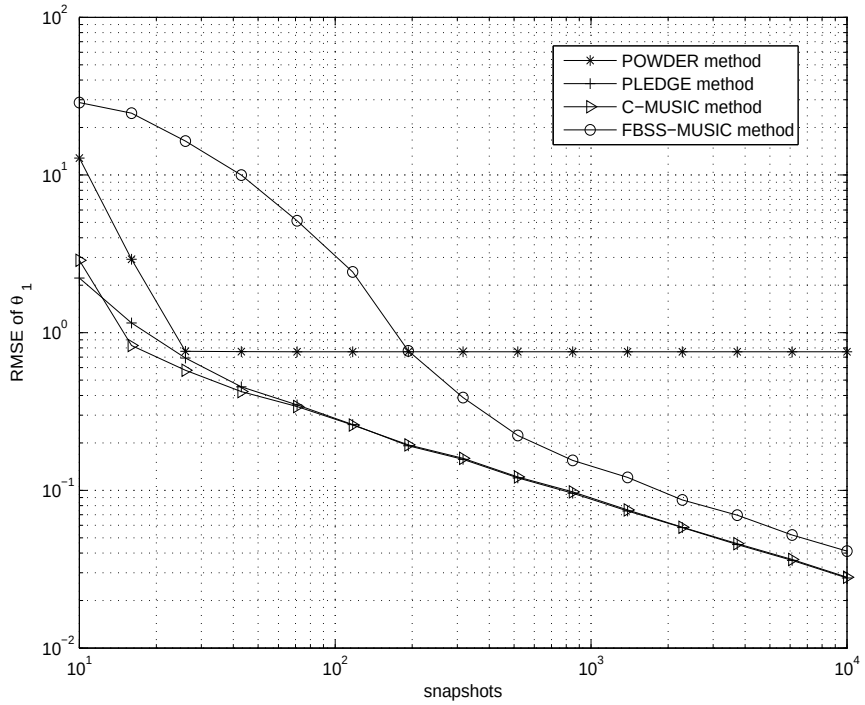

Figure 6.10: Partially-correlated sources: Showing RMSE of θ_1 versus snapshots with SNR = 25dB; other parameters are identical to the case in Figure 6.9

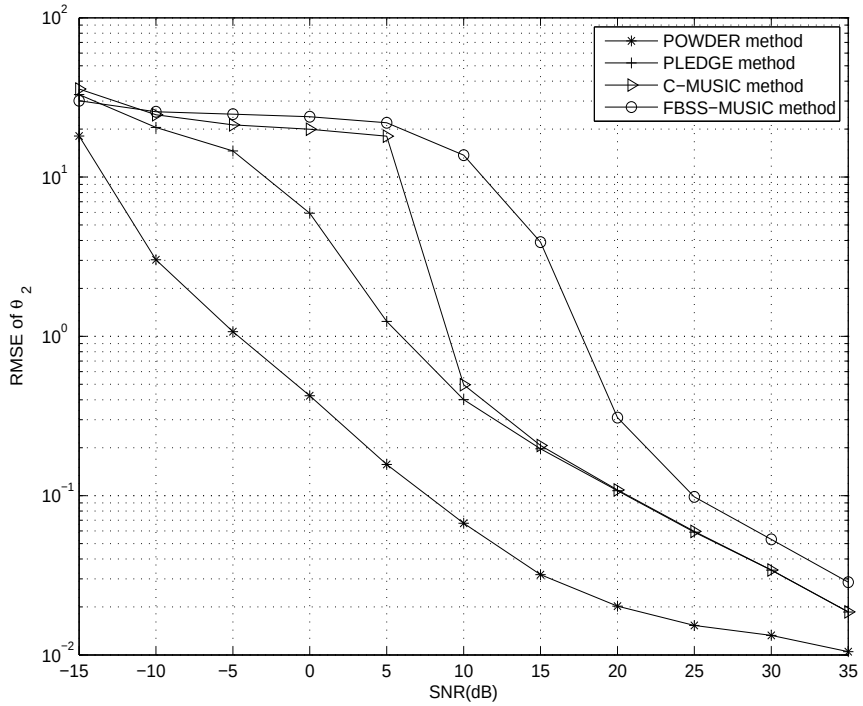

Figure 6.11: Partially-correlated sources: Showing RMSE of θ_2 versus SNR with 1000 snapshots; other parameters are identical to the case in Figure 6.9

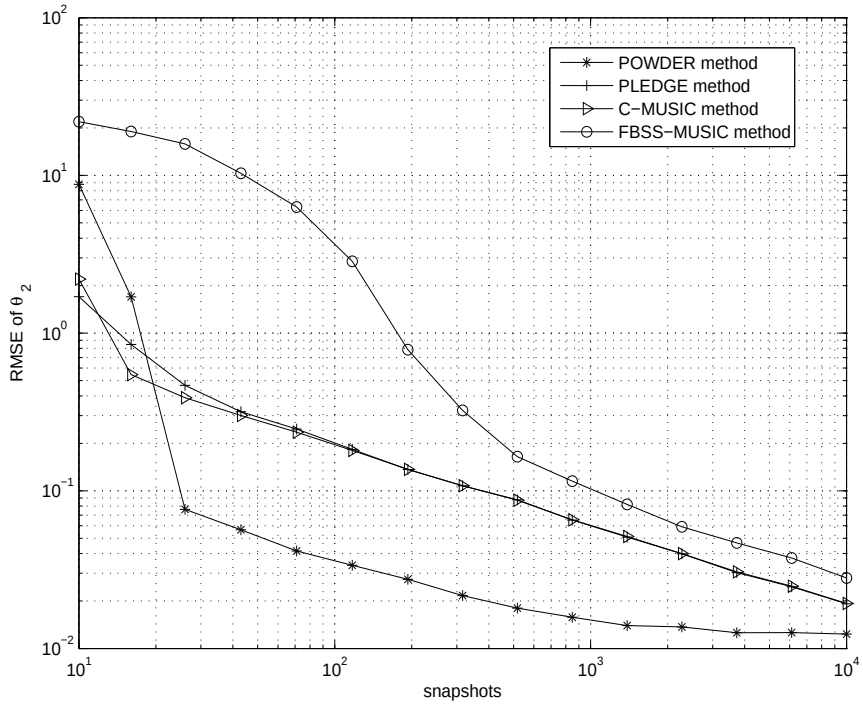

Figure 6.12: Partially-correlated sources: Showing RMSE of θ_2 versus snapshots with SNR = 25dB; other parameters are identical to the case in Figure 6.9

In Figure 6.13, 6.14, 6.15 and 6.16, all simulation parameters are same with the second simulation, except all sources coherent. The correlation coefficients between signals are given as $\rho_{12} = \rho_{13} = \exp(-j\pi/48)\ \rho_{23} = 1$.

In Figures 6.13 and 6.15, the estimation results of the algorithms are illustrated for unknown signals with increasing SNR level. The performance of POWDER method declined due to the coherence between unknown and known signals. The RMSE of POWDER method remains at a constant error value after -5dB SNR. However, POWDER method shows good estimation accuracy comparing to the other methods till 10dB SNR. C-MUSIC method is suboptimal because the orthogonal projection to the known signal subspace cannot resolve the coherency between remaining unknown signals. PLEDGE method shows good estimation performance and this method can handle both correlated and coherent signals optimally. The RMSE of FBSS-MUSIC is high at lower SNRs because of pairing the unknown signal estimate with known one. However, the estimation accuracy of FBSS-MUSIC method approximates to PLEDGE method as SNR level increases because FBSS-MUSIC smoothes the correlation matrix and reduces the coherence between the source signals.

Figure 6.14 and 6.16 show the performance of the algorithms for coherent sources with increasing number of snapshots. PLEDGE method outperforms other methods because there is no assumed structure for signal correlation matrix. PLEDGE method removes the correlation between unknown and known source signals accurately with using the a-priori information about known DOAs. FBSS-MUSIC also shows good performance compared to C-MUSIC and POWDER methods. The RMSE of FBSS-MUSIC method approaches to the PLEDGE method as the number of snapshots increases. FBSS-MUSIC method clearly identified the coherent signal sources and the smaller correlation between source signals improves the threshold behaviour of this method. The RMSE of C-MUSIC method is not decreasing with increasing snapshots because the coherence between unknown signals cannot be removed by orthogonal projection to the known signal subspace. The performance of POWDER method degraded due to the correlation between the known and unknown signals. However, POWDER method shows good estimation accuracy compared to C-MUSIC method.

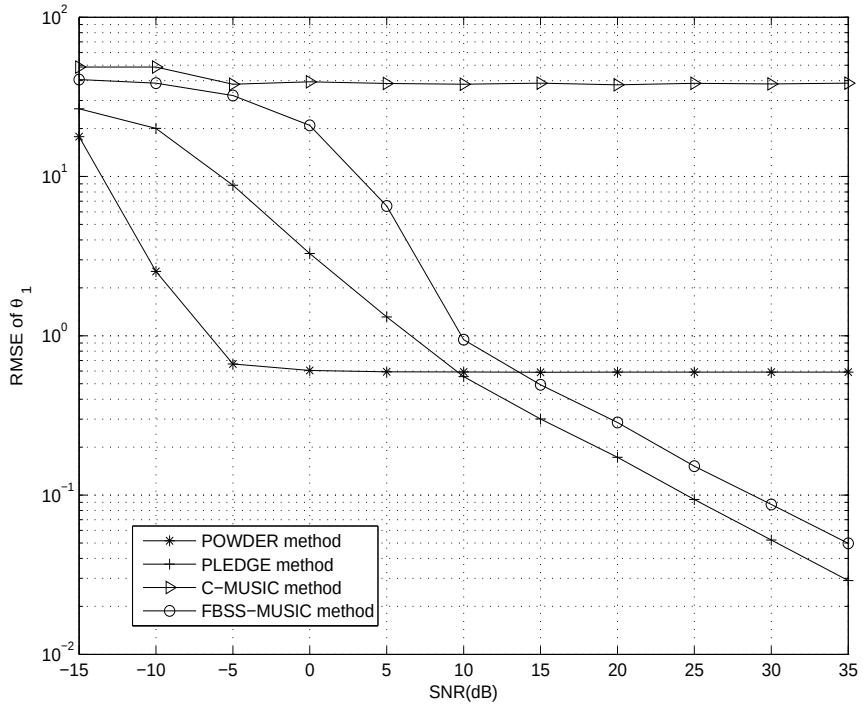

Figure 6.13: Coherent sources: Equipowered source vector: $\overline{\theta} = [\theta_1\, \theta_2\, \vartheta]^T = [10^\circ\, 15^\circ\, 12^\circ]$. All sources coherent, where, $\rho_{12} = \rho_{13} = \exp(-j\pi/48)$ $\rho_{23} = 1$. Showing RMSE of θ_1 versus SNR with 1000 snapshots.

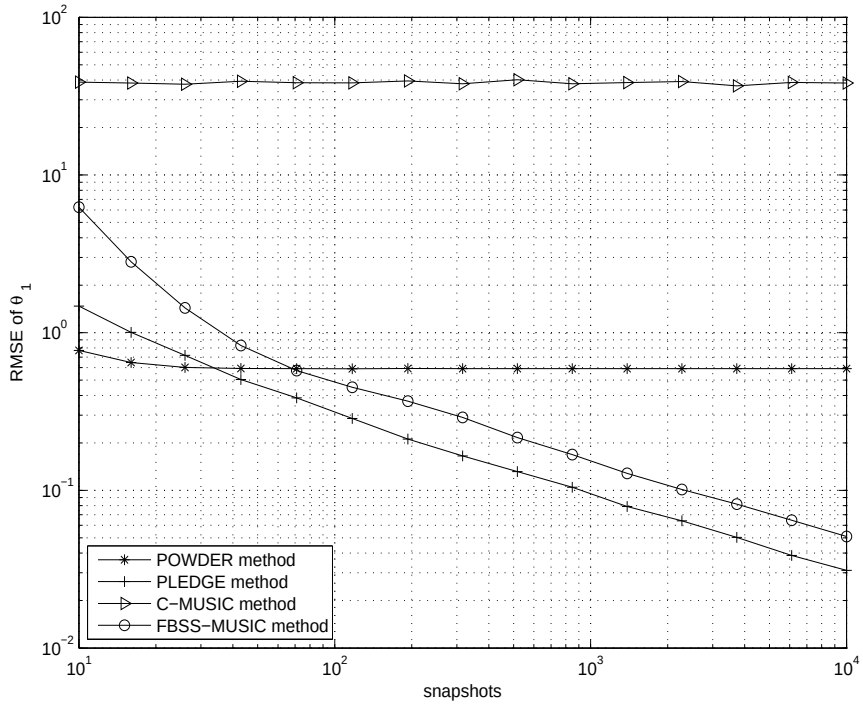

Figure 6.14: Coherent sources: Showing RMSE of θ_1 versus snapshots with SNR = 25dB; other parameters are identical to the case in Figure 6.13

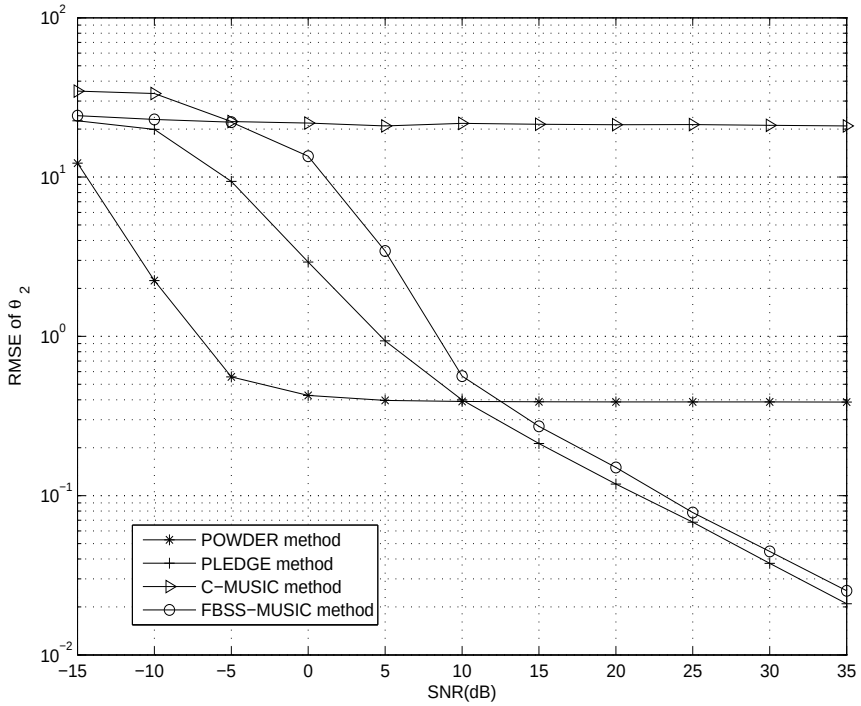

Figure 6.15: Coherent sources: Showing RMSE of θ_2 versus SNR with 1000 snapshots; other parameters are identical to the case in Figure 6.13

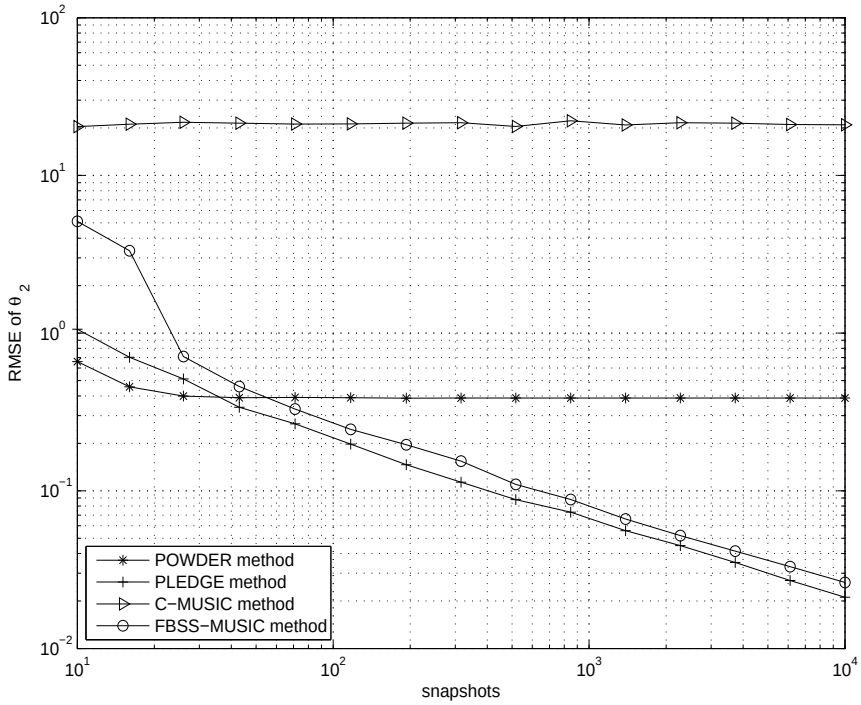

Figure 6.16: Coherent sources: Showing RMSE of θ_2 versus snapshots with SNR = 25dB; other parameters are identical to the case in Figure 6.13

In Figure 6.17, 6.18, 6.19 and 6.20, all simulation parameters are same with the second simulation, except all sources are uncorrelated.

In Figure 6.17 and 6.19, the algorithms are compared for their SNR performances. POWDER, PLEDGE and C-MUSIC methods show almost same estimation accuracy with increasing SNR. The prior knowledge based methods have better resolution than Root-MUSIC method because of using a-priori knowledge about known DOAs in the estimator. Meanwhile, for a given accuracy the required SNR for POWDER method is lower than PLEDGE and C-MUSIC methods at low SNRs.

In Figure 6.18 and 6.20, RMSE performance of the algorithms versus number of snapshots are presented for uncorrelated signals. It is seen that, prior knowledge based methods have the same estimation accuracy as the number of snapshots increases. These methods perform better than Root-MUSIC method due to exploiting the a-priori information in the estimator. We can observe that when the SNR or snapshots grows very large the prior-knowledge based methods have the same estimation performance and converge to the same RMSE.

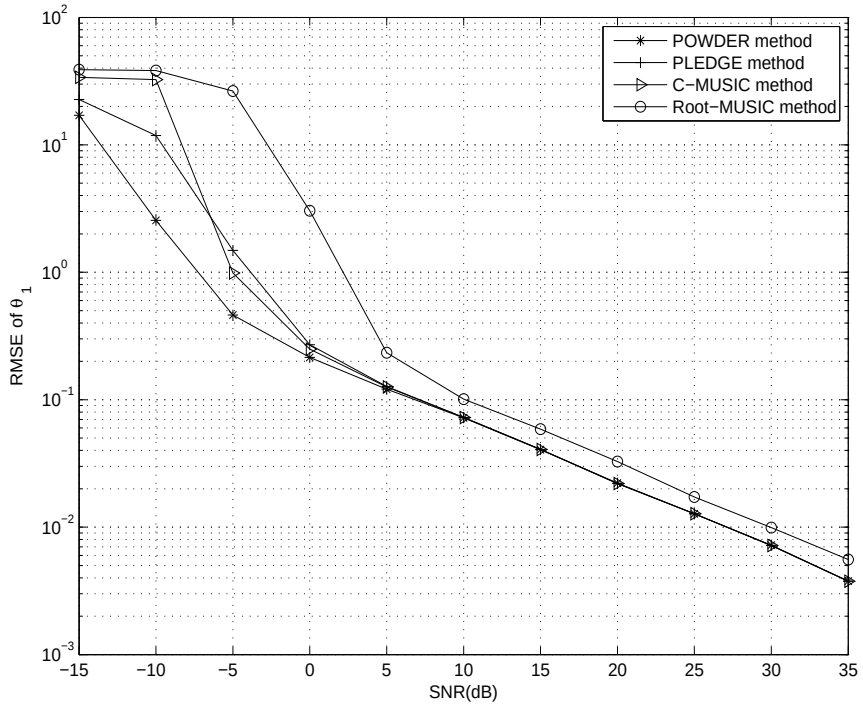

Figure 6.17: Uncorrelated sources: Equipowered source vector: $\overline{\theta} = [\theta_1\, \theta_2\, \vartheta]^T = [10^\circ\ 15^\circ\ 12^\circ]$. All sources uncorrelated, where, $\rho_{12} = \rho_{13} = \rho_{23} = 0$. Showing RMSE of θ_1 versus SNR with 1000 snapshots.

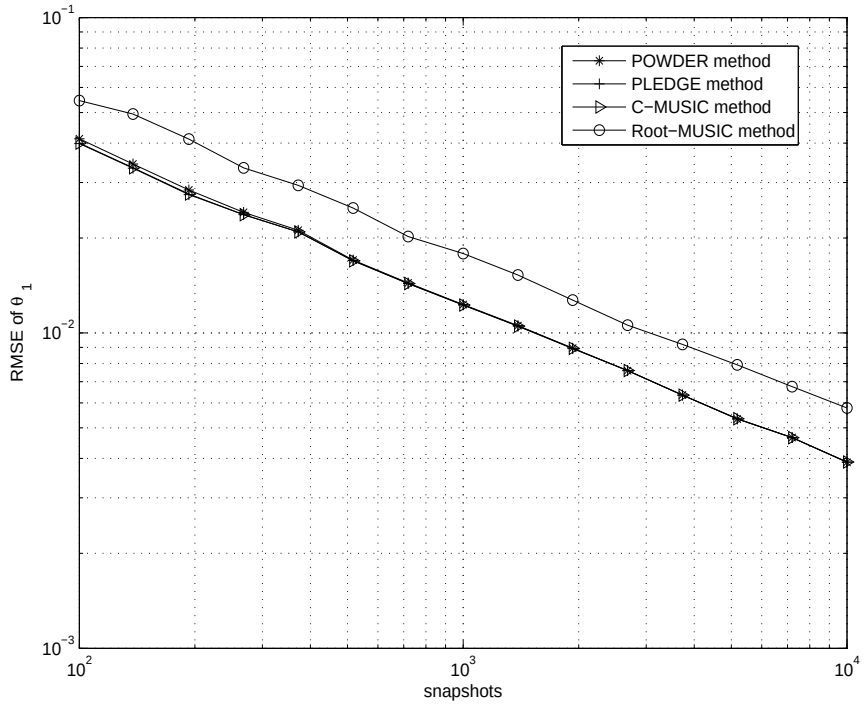

Figure 6.18: Uncorrelated sources: Showing RMSE of θ_1 versus snapshots with SNR = 25dB; other parameters are identical to the case in Figure 6.17

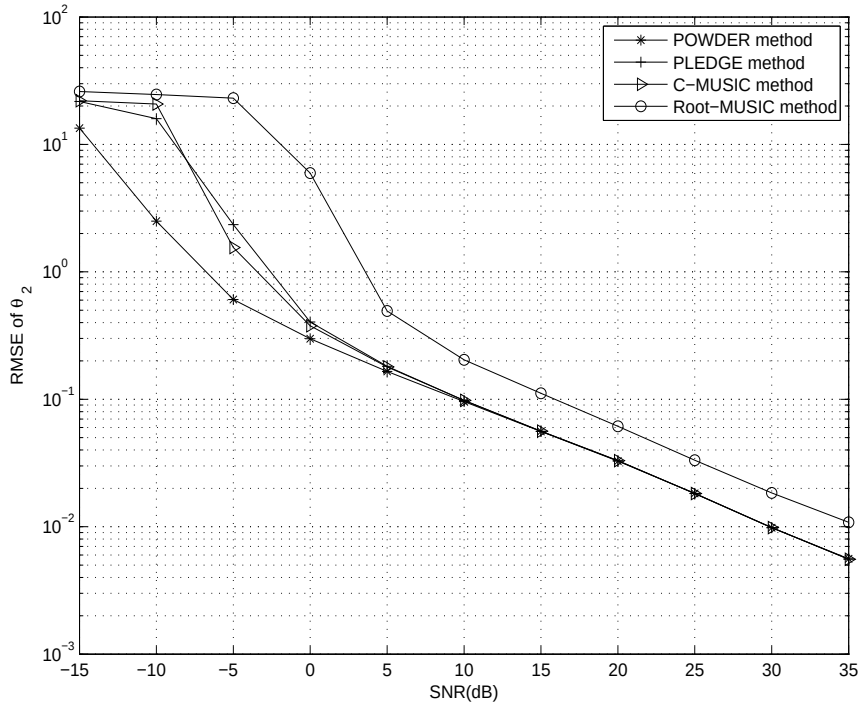

Figure 6.19: Uncorrelated sources: Showing RMSE of θ_2 versus SNR with 1000 snapshots; other parameters are identical to the case in Figure 6.17

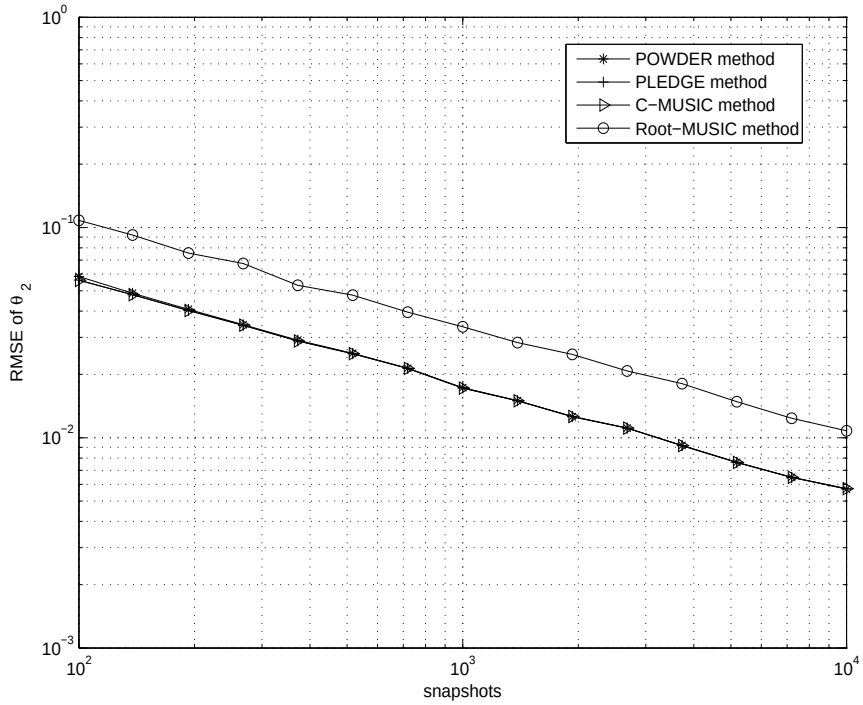

Figure 6.20: Uncorrelated sources: Showing RMSE of θ_2 versus snapshots with SNR = 25dB; other parameters are identical to the case in Figure 6.17

In the third simulation, the effect of varying the location of signal sources is analyzed. In the first scenario, there are two uncorrelated signals in the problem. One of the signal source DOA angle is known a-priori. The known source location is shifted and the estimation results of the algorithms for the unknown source DOA angle is illustrated. In the second scenario, there are three uncorrelated source signals and DOA angle of one of the signal source is known a-priori. In this case, there is prior knowledge about one known and two unknown DOA angles. One of the unknown source is varied and the estimation results of the unknown signal sources is presented.

In Figure 6.21, the known source location is varied from 10 to 13 degrees with 0.1 degree resolution. The RMSE performances of the algorithms are compared for estimation of unknown source located at $\theta = 10^{\circ}$. There are only two equal power Gaussian source signals impinging on a 10 element ULA. The source signals and additive sensor noise are uncorrelated with each other and 1000 independent Monte Carlo trials applied for the simulation with SNR = 25dB and 1000 snapshots of data.

In Figure 6.21, it is seen that POWDER method shows the best performance as compared to the other methods. Since there is no correlation between known and unknown signal sources, POWDER method can accurately estimate the closely separated sources. PLEDGE and C-MUSIC methods can't ensure the RMSE bound of POWDER method because of not using the a-priori knowledge about the correlation state between the source signals. PLEDGE and C-MUSIC methods have nearly same estimation performance as the separation between signal sources increases. The performance of Root-MUSIC is degraded because of coupling known source signal with unknown for close separations, hence the RMSE of Root-MUSIC method begins to saturate at high SNR values compared to other prior knowledge based methods. Prior knowledge about the known source location has a large impact on POWDER, PLEDGE and C-MUSIC methods for resolving closely separated signals. The RMSE of POWDER method increases as the source separation expands. Because when the source separation increases, the benefit of a-priori knowledge diminishes and classical subspace based algorithms can estimate the sources with a constant error without using a-priori knowledge.

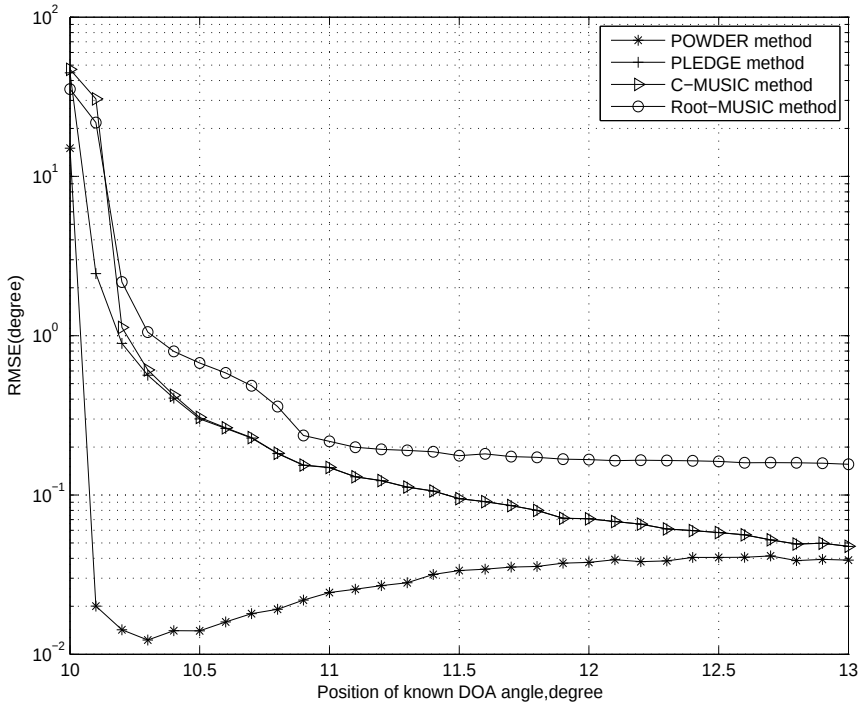

Figure 6.21: Varying the location of known signal: Equal power, uncorrelated sources. Showing RMSE of $\theta = 10^\circ$ versus varying position of known source.

In Figure 6.22, the known source is located at $\theta_3 = 10^\circ$. One of the unknown DOA angle is located at $\theta_1 = 14^\circ$ and the position of other unknown source DOA angle is varied from 14 to 17 degrees with 0.1 degree resolution. The estimation performance of the algorithms for unknown DOAs is presented. The remaining simulation parameters are same with the first scenario in the third simulation.

It is seen from Figure 6.22 that, POWDER method outperforms other methods for resolving two closely separated unknown DOA angles. As the separation between the unknown signal sources increases, the RMSE level of POWDER method decreases to an acceptable level. Meanwhile, using a-priori knowledge about the cross-correlation between unknown and known signal sources improves the performance of the POWDER method comparing to PLEDGE and C-MUSIC methods which only use the location of known source DOA angle as a-priori information in the estimator. PLEDGE method has better estimation performance than C-MUSIC and Root-MUSIC algorithms when the space between the unknown DOAs is smaller than 1 degree. However, PLEDGE and C-MUSIC methods show nearly same performance as the distance between unknown DOAs increases. Root-MUSIC method is suboptimal for the case where the separation between the unknown DOAs is smaller than 1 degree because this method cannot use a-priori knowledge in the estimator and may pair the unknown and known signals with each other. The RMSE of Root-MUSIC decreases as the space between the unknown DOAs increases. But, the other prior knowledge based methods shows better performance than Root-MUSIC method for all intervals.

In the last simulation, mutual coupling and multipath effect for PLEDGE method is illustrated. The RMSE performances of PLEDGE method and the algorithm proposed by Ye et. al in [46] are presented in the simulations. Two uncorrelated signals and two coherent signal groups with five coherent signals impinging on a 10 element ULA. Two uncorrelated sources come from $[-36^\circ, 24^\circ]$. The first coherent signal group come from $[-28^\circ, 30^\circ]$ with fading coefficients $[1, 0.8 \exp^{j114.32}]$ and the other coherent group come from $[-20^\circ, 5^\circ, 42^\circ]$ with fading coefficients $[1, 0.9 \exp^{j135.23}, 0.8 \exp^{j254.78}]$. First group of coherent signals are assumed to be known for PLEDGE method. The mutual coupling coefficients are given as $[1, 0.37 + 0.42j, 0.09 - 0.21j]$. The estimation performance is given by 1000 independent Monte Carlo trials with SNR = 5dB and 500 snapshots of data.

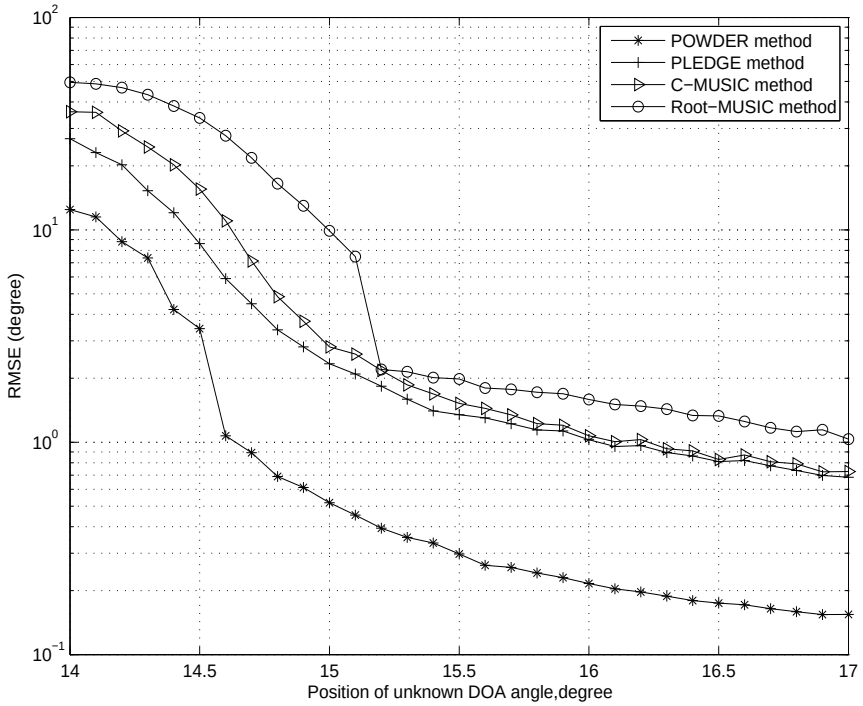

Figure 6.22: Varying the location of unknown source: Equal power, uncorrelated sources located at $\overline{\theta}$ = $[\theta_1\ \theta_2\ \vartheta]^T$ = $[14^\circ, 14 + \Delta\theta, 10^\circ]$. Showing RMSE of unknown DOAs versus varying position of one of the unknown source with $\Delta\theta = 0.1^\circ$ interval.

In Figure, 6.23 and 6.24, RMSE of the DOA estimates versus input SNR and number of snapshots are presented, respectively. It is seen that, the performance of PLEDGE method is degraded in the presence of mutual coupling. In Ye's non-iterative method, uncorrelated signals and mutual coupling coefficients are estimated with good precision, hence the coherent signals are estimated with low RMSE. Ye's method shows better estimation accuracy as compared to PLEDGE method.

In Figure 6.25 and 6.26, RMSE of the mutual coupling coefficients estimates versus input SNR and number of snapshots are presented, respectively. As seen in these figures, Ye's non-iterative method offers promising solution for mutual coupling coefficient estimation. PLEDGE method has low estimation precision for mutual coupling because the estimated unknown signals are not as accurate as the findings in the other algorithm.

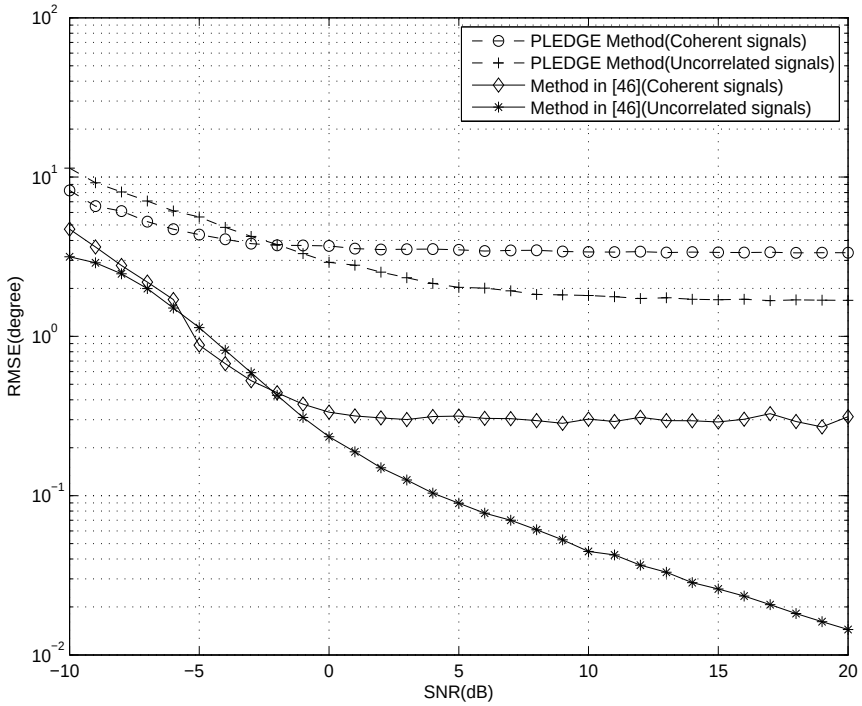

Figure 6.23: Performance of the algorithms for DOA estimation with respect to increasing SNR with snapshots = 500 for uncorrelated and coherent signals.

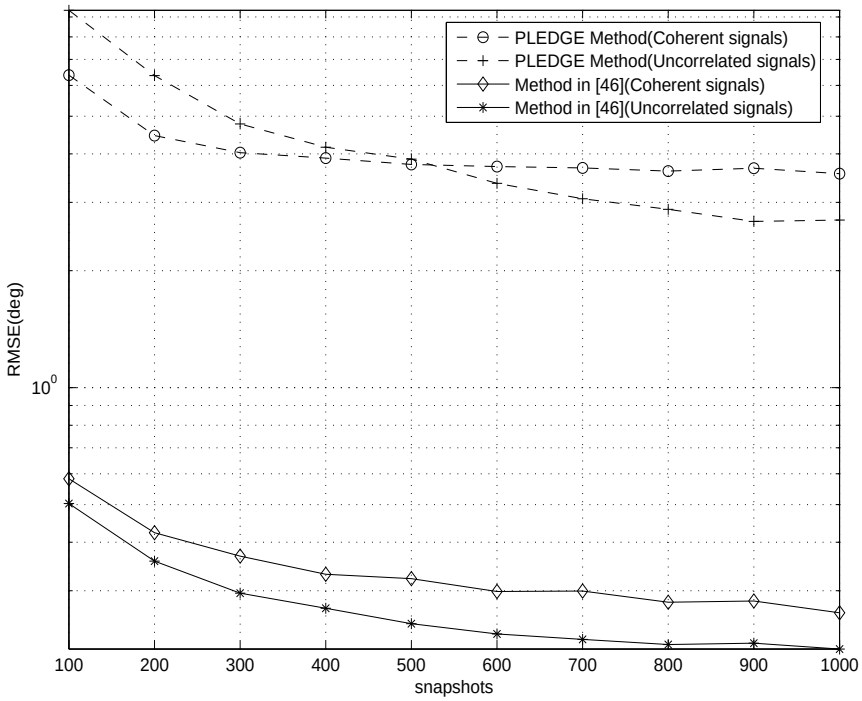

Figure 6.24: Performance of the algorithms for DOA estimation with respect to increasing snapshots with SNR = 5dB for uncorrelated and coherent signals.

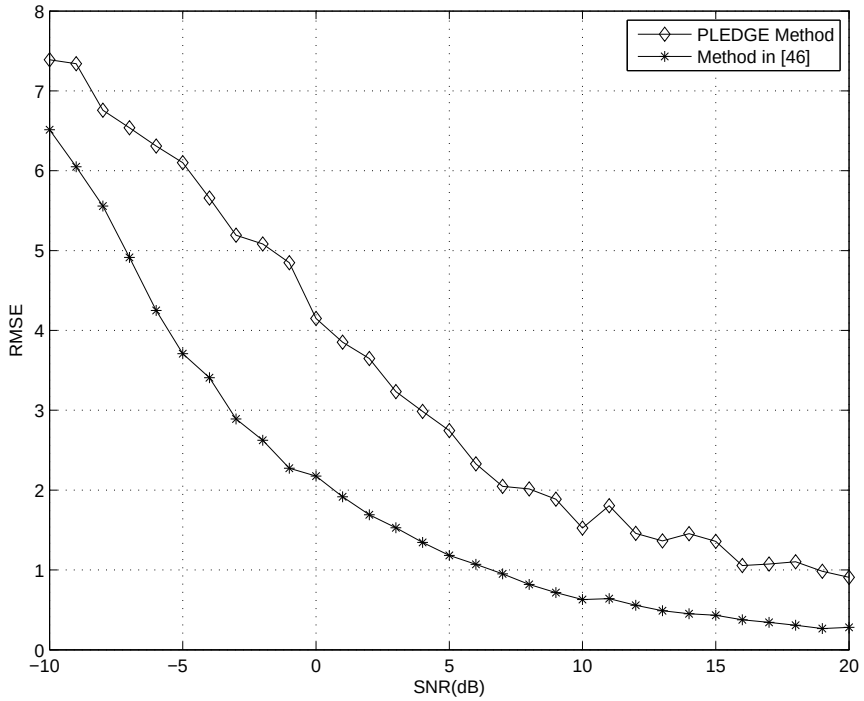

Figure 6.25: Performance of the algorithms for mutual coupling coefficients estimation with respect to increasing SNR with snapshots = 500.

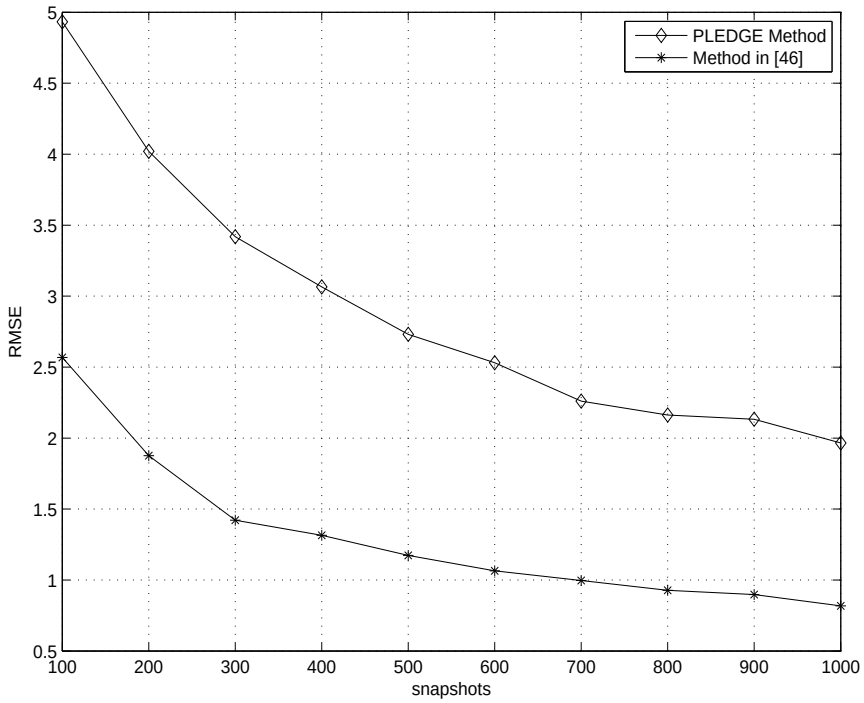

Figure 6.26: Performance of the algorithms for mutual coupling coefficients estimation with respect to increasing snapshots with SNR = 5dB.

CHAPTER 7

CONCLUSION AND FUTURE WORK

In this thesis, performance analysis of direction of arrival estimation algorithms in the presence of array imperfections and multipath for different array geometries presented. A literature survey is done in order to find the DOA estimation techniques which are suitable to implement for different array geometries. The objective is to show the effect of array imperfections and antenna array geometry selection on DOA estimation application. The benefit of exploiting prior-knowledge for DOA estimation is also illustrated with different scenarios. The algorithms are examined primarily in four parts.

In the first chapter, DOA estimation for ULA in the presence of mutual coupling is analyzed. Auxiliary sensors are used and the method in [1] is implemented for both DOA and mutual coupling coefficient estimation. It is seen that, estimated coupling coefficients provide accurate DOA angle estimates in the simulations. The performance results approach to the optimum case in [41] where mutual coupling is known. DOA estimation in higher precision is achieved as compared to standard MUSIC method with no auxiliary sensors. Correlated and independent sources are estimated successfully in unknown sensor coupling.

In the second chapter, 2-D DOA estimation for uniform rectangular array in the presence of unknown sensor coupling is considered. The algorithm in [34] is performed for 2-D DOAs and mutual coupling coefficient estimation. During simulations we observed that the DOA estimation performance of the algorithm is better than straight forward 2-D spectral MUSIC method in coupling conditions. The computational complexity of two dimensional spectrum search is decreased to a fair level by ap-

plying twice search method in the algorithm. Also, DOA refinement with estimated coupling coefficients increased the estimation accuracy.

In the third chapter, direction of arrival estimation in the presence of gain/phase mismatches and mutual coupling is performed. Friedlander's method in [30] and self-calibration method in [29] are compared for ULA and NLA.

In the first simulation, the algorithms are implemented for NLA. It is seen that, self-calibration method outperforms Friedlander's method in DOAs, gain/phase mismatch and mutual coupling coefficients estimation. Calculating the inverse of singular matrices for cost function minimization and rank deficiency in the steering matrix cause the degradation for Friedlander's method.

In the second simulation, the self-calibration method and Friedlander's method are performed for NLA and ULA, respectively. The estimation performance of the algorithms are presented with the array models where the algorithms are proposed to show the optimal performance to estimate DOAs, mutual coupling and gain/phase error coefficients. In this scenario, Friedlander's method shows slightly better performance than self-calibration method. Because there is no missing row existence in steering matrix and no singularity problem for calculating the inverse of matrices in gain/phase and coupling coefficient estimation. The self-calibration algorithm also shows good estimation accuracy comparing to Friedlander's method.

In the third simulation, both algorithms are implemented for ULA. It is observed that, Friedlander's method outperforms the self-calibration method for ULA because the cost function minimization is performed with Capon-based searching in Friedlander's method. Also, there is no singularity problem as in the first simulation for calculating the inverse of the matrices in minimization step. The self-calibration method performs eigendecomposition for the criterion function to estimate the gain/phase and coupling coefficients. However, Friedlander's method shows good accuracy compared to self-calibration method for ULA.

In the last chapter, the performance analysis of prior knowledge based DOA estimation algorithms presented. Constrained-MUSIC (C-MUSIC) [2] , Prior-knowledge based DOA estimation (PLEDGE) [3], Prior-Exploiting Orthogonally Weighted Direction Estimator(POWDER) [4], and Forward-backward spatial smoothing and MUSIC (FBSS-MUSIC) [5] algorithms are implemented and compared. It is seen that, POWDER method outperforms other algorithms if there is no correlation between the signals from unknown and known directions. The signals in the subset of known or unknown directions can be fully coherent with each other. POWDER method can estimate accurately the multipath signals by using a-priori knowledge about known signal directions and cross correlation between the signal groups.

PLEDGE method has no assumed structure about the signal correlation matrix. This method uses the prior information about signal directions to extract the known signal subspace from the cost function by polynomial rooting. PLEDGE method can handle both uncorrelated and fully coherent sources optimally. However, POWDER method shows better performance rather than PLEDGE method if the cross correlation matrix of known and unknown signals is equal to zero.

C-MUSIC method is applicable when the signals are uncorrelated or known signals are coherent with the unknown signals. C-MUSIC method uses the prior information to subtract the known signal subspace from the array output covariance matrix by orthogonal projection. C-MUSIC method has almost same estimation accuracy with PLEDGE method at high SNRs. However, C-MUSIC is suboptimal when the signals are fully coherent or unknown signals are mutually coherent.

The performance of FBSS-MUSIC is also presented in the simulations. FBSS-MUSIC can't exploit the prior information. FBSS-MUSIC shows better performance than C-MUSIC method when all signals are coherent because FBSS-MUSIC method smooths the array output covariance matrix and reduces the correlation between the signals. However, PLEDGE and POWDER method shows better results than FBSS-MUSIC in multipath because FBSS-MUSIC method can match the estimated signals from unknown directions to known ones which are closely separated. It is seen that POWDER, PLEDGE and C-MUSIC methods benefit from a-priori information to estimate the multipath signals accurately.

The impact of multipath and mutual coupling on DOA estimation is also presented in this chapter. PLEDGE algorithm is compared with Ye's non-iterative method in [46] to observe the performance of PLEDGE algorithm. There is no assumed structure for signal correlation matrix in this scenario, hence PLEDGE algorithm is applied to estimate the unknown signals in different correlation degrees. It is seen that, the estimation performance of PLEDGE algorithm is degraded in the presence of mutual coupling. Ye's non-iterative method estimates the uncorrelated signals, coherent signals and mutual coupling coefficients with good precision compared to PLEDGE method.

As a future work, prior knowledge based methods can be employed for URA in the presence of mutual coupling. The DOAs and mutual coupling coefficients estimation performance of the algorithms can be observed in 2-D case. Additionally, the a-priori knowledge based algorithms can be modified using auxiliary sensors in the estimator. Thus, we may improve the performance in the applications where mutual coupling and gain/phase mismatches exists.

REFERENCES

[1] Z. Ye , C. Liu. On the resiliency of music direction finding against antenna sensor coupling. *IEEE Trans. Antennas Propagat.*, 56:371–380, 2008.

[2] D. A. Linebarger , R. D. DeGroat , E. M. Dowling , P.Stoica , G. L. Fudge. Incorporating a priori information into music-algorithms and analysis. *Signal Process.*, 46:84–105, 1995.

[3] G. Bouleux , P. Stoica , R. Boyer. An optimal prior knowledge-based doa estimation method. *17th European Signal Processing Conference(EUSIPCO 2009)*, pages 869–873, 2009.

[4] P. Wirfält , M. Jansson and G. Bouleux. Prior-exploiting direction-of-arrival algorithm for partially uncorrelated source signals. *IEEE Int. Conf. on Acoust., Speech and Signal Process.*, pages 3972–3976, 2013.

[5] S.U.Pillai , B.H.Kwon. Forward/backward spatial smoothing techniques for coherent signal identification. *IEEE Transactions on Acoustics, Speech and Signal Processing*, 37,(1):8–15, 1989.

[6] C. A. Balanis. *Antenna Theory: Analysis and Design*. Wiley, River Street, New Jersey, 1997.

[7] J. L. Allen , B. L. Diamond. Mutual coupling in array antennas. *Lincoln Laboratory, M.I.T., Lexington, MA, Tech. Rep. 424(ESD-TR-66-443)*, 1966.

[8] J. W. Wallace , M. A. Jensen. Mutual coupling in mimo wireless systems: A rigorous network theory analysis. *IEEE Transactions on Wireless Communications*, 3,(4):1317–1325, 2004.

[9] O. R. Schmidt. Multiple emitter location and signal parameters estimation. *IEEE Transactions on Antennas and Propagation*, 34:276–280, 1986.

[10] R.Roy , T. Kailath. Esprit-estimation of signal parameters via rotational invariance techniques. *IEEE Transactions on Acoustics, Speech, and Signal Processing*, 37(7):984–995, 1989.

[11] T. Filik , T. E. Tuncer. 2-d doa estimation in case of unknown mutual coupling for multipath signals. *Multidimensional Systems and Signal Processing*, 2014.

[12] Y. Li , M. H. Er. Theoretical analysis of gain and phase error calibration with optimal implementation for linear equispaced array. *IEEE Transactions on Signal Processing*, 54:712–723, 2006.

[13] C. Roller , W. Wasylkiwskyj. Effects of mutual coupling on superresolution df in linear arrays. *in Proc. IEEE Int. Conf. Acoustics, Speech, Signal Processing*, 5:257–260, 1992.

[14] A. J. Weiss , B. Friedlander. Mutual coupling effects on phase-only direction finding. *IEEE Trans. Antennas Propag.*, 40:535–541, 1992.

[15] T. Filik , T. E. Tuncer. A fast and automatically paired 2-dimensional direction-of-arrival estimation using arbitrary array geometry. *Signal Processing and Communications Applications Conference, SIU 2009*, page 556–559, 2009.

[16] M. Zhang , Z. Zhu. Compensation for unknown mutual coupling in bearing estimation. *Int. J. Electron.*, 75:965–971, 1993.

[17] B. C. Ng , C. M. S. See. Sensor-array calibration using a maximum-likelihood approach. *IEEE Trans. Antennas Propag.*, 44:827–835, 1996.

[18] I. S. D. Solomon , D. A. Gray , Y. I. Abramovich , S. J. Anderson. Receiver array calibration using disparate sources. *IEEE Trans. Antennas Propag.*, 47:496–505, 1999.

[19] S. Lundgren. A study of mutual coupling effects on the direction finding performance of esprit with a linear microstrip patch array using the method of moments. *Proc. Antennas and Propagation Society Int. Symp.*, 2:1372–1375, 1996.

[20] J. E. Fernandez del Rio , O. M. Conde-Portilla , M. F. Catedra. Estimating azimuth and elevation angles when mutual coupling is significant. *Proc. Antennas and Propagation Society Int. Symp.*, 1:215–218, 1998.

[21] T. E. Tuncer , B. Friedlander. *Classical and Modern Direction-of-Arrival Estimation*. Elsevier, Burlington, MA01803, USA, 2009.

[22] T. Filik , T. E. Tuncer. A fast and automatically paired 2-d direction-of-arrival estimation with and without estimating the mutual coupling coefficients. *Radio Science*, 45:1–14, 2010.

[23] M.Caliskan , T. E. Tuncer. Two dimensional doa estimation using uniform rectangular array with mutual coupling. *Signal Processing and Communications Applications Conference, SIU 2014*, pages 465–468, 2014.

[24] A. L. Swindlehurst , B. Ottersten , R. Roy and T. Kailath. Multiple invariance esprit. *IEEE Trans. Signal Process.*, 40:867–881, 1992.

[25] J. Liu , X. Liu. Joint 2-d doa tracking for multiple moving targets using adaptive frequency estimation. *IEEE Int. Conf. Acoust.,Speech Signal Process.*, 2:1113–1116, 2007.

[26] R. Goossens , H. Rogier. A hybrid uca-rare/root-music approach for 2-d direction of arrival estimation in uniform circular arrays in the presence of mutual coupling. *IEEE Trans. Antennas Propag.*, 55:841–849, 2007.

[27] B. Wang , Y. Wang and H. Chen. A robust doa estimation algorithm for uniform linear array in the presence of mutual coupling. *in Proc. IEEE Antennas Propag. Society Int. Symp.*, 3:924–927, 2003.

[28] A.P.-C. Ng. Direction-of-arrival estimates in the presence of wavelength. *IEEE Trans. Signal Process.*, pages 225–232, 1995.

[29] J. Dai , D. Zhao and Z. Ye. Doa estimation and self-calibration algorithm for nonuniform linear array. *International Symposium on Intelligent Signal Processing and Communication Systems(ISPACS 2010)*, pages 1–4, 2010.

[30] B. Friedlander , A. J. Weiss. Direction finding in the presence of mutual coupling. *IEEE Trans. Antennas Propag.*, 39:273–284, 1991.

[31] R. D. DeGroat , E. M. Dowling and D. A. Linebarger. The constrained music problem. *IEEE Trans. Signal Process.*, 41:1445–1449, 1993.

[32] P. Stoica , K. Sharman. Novel eigenanalysis method for direction estimation. *IEEE Proc. F,Radar Signal Process.*, 137,(1):19–26, 1990.

[33] P. Wirfält , G. Bouleux , M. Jansson and P.Stoica. Optimal prior knowledge-based direction of arrival estimation. *IET Signal Processing*, 6,(8):731–742, 2012.

[34] Z. Ye , C. Liu. 2-d doa estimation in the presence of mutual coupling. *Antennas and Propagation, IEEE Transactions on*, 56:3150–3158, 2008.

[35] H. V. Trees. *Optimum Array Processing: Part IV of Detection, Estimation, and Modulation Theory*. Wiley Interscience, New York, USA, 2002.

[36] Z. Chen , G. Gokeda , Y. Yu. *Introduction to Direction-of-Arrival Estimation*. Artech House, Boston, USA, 2010.

[37] H. Krim , M. Viberg. Two decades of array signal processing research. *IEEE Signal Processing Magazine*, 13,(4):67–94, 1996.

[38] F. B. Gross. *Smart Antennas for Wireless Communications With MATLAB*. 2005.

[39] M H. Moussa. *Direction of Arrival Estimation Using Maximum Likelihood Method and the Effect of Element Selection on System Performance*. M.S. Thesis in Concordia University, 2005.

[40] C. Liu , Z. Ye , Y. Zhang. Autocalibration algorithm for mutual coupling of planar array. *Signal Processing*, 90,(3):784–794, 2010.

[41] C. C. Yeh , M. L. Leou , D. R. Ucci. Bearing estimations with mutual coupling present. *IEEE Trans. Antennas Propagat.*, 37:1332–1335, 1989.

[42] B.D.Rao , K.V.S. Hari. Performance analysis of root-music. *IEEE Transactions on Acoustics, Speech and Signal Processing*, 37,(12):1939–1949, 1989.

[43] M.Viberg , B. Ottersen. Sensor array processing based on subspace fitting. *IEEE Transactions on Signal Processing*, 39,(5):1110–1121, 1991.

[44] B. Ottersen , P.Stoica and R.Roy. Covariance matching estimation techniques for array signal processing applications. *Digital Signal Process.*, 8,(3):185–210, 1998.

[45] M. Jansson , B. Göransson and B. Ottersten. A subspace method for direction of arrival estimation of uncorrelated emitter signals. *IEEE Trans. Signal Process.*, 47,(4):945–956, 1999.

[46] X. Xu , Z. Ye and Y. Zhang. Doa estimation for mixed signals in the presence of mutual coupling. *IEEE Trans. Signal Process.*, 57,(9):3523–3532, 2009.